Universidad Autónoma de Madrid

Faculty of Science
Department of Molecular Biology

Doctoral Thesis

Exploring the role of genomic instability in cancer and neurodegenerative disease through mouse models

Maria Nieto Soler

Madrid
2015

This work was entirely performed under the direction of Oscar Fernández-Capetillo in the Genomic instability lab, at the Spanish National Cancer Research Centre (CNIO), and was funded by "la Caixa" Foundation within the framework of "la Caixa"/CNIO international PhD programme.

CONTENTS

ABBREVIATIONS 9
PRESENTACIÓN 13
ABSTRACT 15
INTRODUCTION 17
1. Taking care of the genome 17
1.1. Damage sources 17
1.2. The DNA damage response (DDR) 18
1.3. Mechanisms of DNA damage repair 19
1.3.1. Double-stranded breaks (DSB) 20
Pathway choice in DSB repair 23
1.3.2. Replication stress (RS) 23
Sources of RS 24
The RS response (RSR) 25
Mechanisms of replication restart 26
Consequences of RS 27
Inducing RS 28
1.3.3. RS in cancer 28
2. FBH1: a molecule that promotes RS 31
3. Targeting RS in Ewing sarcoma 34
3.1. Ewing sarcoma: molecular pathogenesis 34
3.2. EWS protein: structure and function 35
3.3. EWS protein in disease 37
OBJECTIVES 39
MATERIALS AND METHODS 41
1. Mouse biology 41
1.1. Mouse models 41
1.2. Mouse genotyping 41
1.3. Survival curves 42
1.4. Xenograft assays 42
1.5. Inmunohistochemistry 43
2. Cellular biology 43

2.1. Generation of primary MEF cell cultures 43
2.2. Isolation of splenic B lymphocytes 43
2.3. Cell culture 44
2.4. Cell proliferation curves 44
2.5. Growth inhibition assay 44
2.6. Metaphase breakage analysis 44
2.7. Immunofluorescence 45
2.8. High throughput microscopy 45
3. Molecular biology 46
3.1. Southern blotting 46
3.2. Western blotting 46
3.3. Proteomic analysis 47
3.4. Quantitative RT-PCR 47
3.5. DRIP-qPCR 47
3.6. PCR Primers 48
3.7. RNA sequencing 49
3.8. Northern blotting 50
4. Antibodies 50
RESULTS 51
PART I: Reducing the toxicitity of RS in mice 51
1. Generation of an FBH1-deficient mouse strain 51
2. Phenotypical characterization of *Fbh1*$^{GT/GT}$ mouse cells 53
3. Impact of FBH1 deficiency on ATR mutant mice 54
4. Role of FBH1 in HR 55
PART II: Exploring the role of RS in cancer and age-related diseases 59
1. Targeting RS as a strategy to treat cancers 59
2. Ewing sarcoma-derived cell lines have RS and are sensitive to ATR inhibition 60
2.1. Ewing sarcoma cell lines have increased RS 60
2.2. ES cell lines are hypersensitive to ATR inhibition 61
2.3. ATRi impairs tumor growth in Ewing sarcoma xenografts 62
3. Expression of EWS/FLI1 leads to RS and ATRi hypersensitivity 63
4. EWS protein as a suppressor of RS 64
5. Generation of a mouse model for the deletion of *Ewsr1* 65
5.1. EWS deletion is embryonic lethal and results in embryonic RS 66

6. RS and sensitivity to ATRi in EWS-deficient cells ... 68
6.1. *Ewsr1*$^{GT/GT}$ MEF show increased levels of RS ... 68
6.2. *Ewsr1*$^{GT/GT}$ MEF have increased genomic instability ... 69
6.3. *Ewsr1*$^{GT/GT}$ MEF are hypersensitive to ATRi ... 70
6.4. The RSR is proficient in *Ewsr1*$^{GT/GT}$ MEF ... 71
7. R-Loops and RS ... 72
7.1. EWS is recruited to the nucleolus after nucleolar stress ... 74
7.2. *Ewsr1*$^{GT/GT}$ and EWS/FLI1-expressing cells have increased R-loops ... 75
7.3. R-loops persist into mitosiss ... 77
7.4. *Ewsr1*$^{GT/GT}$ MEF have increased genomic instability at NOR regions ... 78
7.5. Biogenesis of rRNA is unaltered in *Ewsr1*$^{GT/GT}$ and EWS/FLI1-expressing cells ... 79
7.6. RNA nuclear export is impaired in *Ewsr1*$^{GT/GT}$ and EWS/FLI1-expressing cells ... 81
8. Consequences of *Ewsr1* deletion in adult mice ... 83
8.1. Exploring a tumorigenic effect of *Ewsr1* deletion ... 84
8.2. *Ewsr1*$^{\Delta/\Delta}$ mice develop an ALS-like disease ... 84
DISCUSSION ... 89
PART I: Modest impact of FBH1 deficiency in mammals ... 89
PART II: New insights into Ewing sarcoma and EWS function ... 93
1. Exploiting tumor-associated RS for the treatment of Ewing sarcoma ... 93
2. Understanding Ewing sarcoma: R-loops are responsible for RS ... 93
3. Contributions of EWS deletion and EWS/FLI1 expression in tumorigenesis: molecular dissection ... 95
4. EWS contribution to preventing neurodegeneration ... 97
5. A mechanism for EWS protein ... 98
5.1. EWS is an R-loop suppressor ... 98
5.2. EWS is recruited to particular genomic sites ... 99
5.3. Self-aggregating properties of EWS ... 100
5.4. A model for EWS mechanism ... 101
6. A novel physiological role for R-loops? ... 104
CONCLUSIONS ... 107
CONCLUSIONES ... 109
BIBLIOGRAPHY ... 111

ABBREVIATIONS

4-OHT	4-hidroxy-tamoxifen
AT	ataxia telangiectasia
ATM	ataxia telangiectasia-mutated
ATR	ATM and Rad3-related
ATRi	ATR inhibitor
ATRIP	ATR-interacting protein
CDK	cyclin dependent kinase
CFS	common fragile site
CHK1	checkpoint kinase 1
CHK2	checkpoint kinase 2
CNV	copy number variation
CPT	camptothecin
CSR	class switching recombination
DAPI	4', 6-diamine-2-phenylindol
DDR	DNA damage response
DNA	deoxyribonucleic acid
dNTP	deoxynucleotide triphosphate
DSB	double-stranded break
dsDNA	double-stranded DNA
EdU	5-ethynyl-2'-deoxyuridine
ERFS	early replication fragile site
EU	5-ethynyl-2'-uridine
GT	gene-trapped (allele)
G1	gap1 (cell cycle phase)

G2	gap2 (cell cycle phase)
HR	homologous recombination
HTM	high throughput microscopy
HU	hydroxyurea
IF	immunofluorescence
IR	ionizing radiation
KI	knockin
KO	knockout
LOH	loss of heterozygosity
lox	floxed (allele)
MCM2-7	mini-chromosome maintenance 2-7 (complex)
MEF	mouse embryonic fibroblasts
MMR	mismatch repair
MMS	methyl methasulfonate
mRNA	messenger RNA
NHEJ	non-homologous end joining
nt	nucleotide(s)
PAR	poly(ADP-ribose)
PARP	PAR polymerase
PBS	phosphate buffered saline
PCR	polymerase chain reaction
PFA	paraformaldehyde
rDNA	ribosomal DNA

RNA	ribonucleic acid
RNAPI	RNA polymerase I
RNAPII	RNA polymerase II
ROS	reactive oxygen species
RPA	replication protein A
rRNA	ribosomal RNA
RS	replication stress
ssDNA	single-stranded DNA
T121	first 121 aminoacids of T-Large antigen within SV40 virus
TopBP1	topoisomerase II binding protein 1
TopoI	topoisomerase I
TopoII	topoisomerase II
UV	ultraviolet (radiation)
V(D)J	somatic recombination during lymphocyte maturation
WB	western blot
WT	wild type
$^{+/+}$	wild type
-/-	Knockout
γH2AX	phosphorylated form of histone H2A.X at ser139

PRESENTACIÓN

El estrés replicativo (RS) en el DNA está entre las formas más comunes y peligrosas de estrés genotóxico, que tiene lugar cuando la progresión de las horquillas de replicación se detiene a causa de lesiones endógenas o exógenas. Esto frecuentemente lleva a a la acumulación de DNA de cadena simple (ssDNA), el cual es altamente inestable. Si se da de forma persistente, el RS promueve roturas de doble cadena en el DNA (DSBs) y reordenamientos genómicos que pueden ser tóxicos para la célula. La cinasa ATR es uno de los componentes clave en la respuesta al RS, y promueve la activación del punto de control en G2/M del ciclo celular, a la vez que promueve la estabilización de las horquillas de replicación atascadas. La inhibición de ATR lleva a una acumulación de RS e impide la activación del punto de control G2/M, causando así un colapso celular debido a catástrofe mitótica.

El presente trabajo se ha centrado en la investigación de los mecanismos básicos de la toxicidad derivada de RS, y en la identificación y exploración de tumores especialmente sensibles a inhibidores de ATR. En la primera parte hemos estudiado el rol de FBH1, una helicasa de DNA que parece estar involucrada en el proceso de acumulación de ssDNA durante el RS así como en la regulación de la respuesta a los DSBs derivados de RS. Nuestro estudio nos ha llevado a concluir que en ratones, FBH1 tiene una contribución limitada en estos procesos y el impacto de su deleción es menor, tanto en fondos genéticos silvestres como en fondos con defectos en la función de reparación del DNA. La falta de un fenotipo puede ser debida a mecanismos compensatorios o factores redundantes presentes en mamíferos.

En la segunda parte del trabajo hemos explorado el papel del RS en el sarcoma de Ewing. Esta neoplasia se caracteriza por una translocación entre *EWSR1* y un factor de transcripción, siendo *FLI1* el más frecuente. La proteína de fusión resultante de la traslocación (EWS/FLI1) actúa como factor de transcripción oncogénico, lo cual se ha demostrado ampliamente, y es considerado el factor desencadenante de la tumorigénesis. Sin embargo no se ha puesto tanta atención en la función de EWS, la proteína producto de *EWSR1*, y en cómo una pérdida de función de EWS puede contribuir a la tumorigénesis en los sarcomas de Ewing. Nuestro trabajo demuestra en primer lugar que los sarcomas de Ewing estás sujetos a altos niveles de RS, y por lo tanto son candidatos susceptibles de ser tratados con inhibidores de ATR. Seguidamente demostramos que la fuente de RS en los sarcomas de Ewing son los bucles-R, y que su acumulación es debida a la pérdida de función de EWS. Especulamos que eso se podría deber a un efecto dominante-negativo de EWS/FLI1 sobre EWS. En base a ello proponemos un

modelo para la función de EWS en la supresión de bucles-R, por la cual la auto-agregación de EWS alrededor de los bucles-R promueve su eliminación. Finalmente describimos un fenotipo de neurodegeneración en ratones adultos en los que se ha deplecionado EWS, lo cual apunta a una función de EWS en la prevención de neurodegeneración asociada a esclerosis lateral amiotrófica.

ABSTRACT

DNA replication stress (RS) is one of the most common and dangerous forms of genotoxic stress, which occurs when the progression of replication forks is halted by endogenous or exogenous lesions. This frequently leads to the accumulation of highly unstable single-stranded DNA (ssDNA). If persistent, RS leads to DNA double-strand breaks (DSBs) and genomic rearrangements that are cell-toxic. The ATR kinase is one of the key players in the response to RS, and triggers the activation of the G2/M checkpoint while it promotes the stability of stalled replication forks. ATR inhibiton leads to an accumulation of RS and impairs checkpoint activation, thereby causing cells to collapse due to mitotic catastrophe.

Investigating the basic mechanisms of RS-driven toxicity and exploring tumors that are especially sensitive to ATR inhibitors constituted the core of the present work. On the first part we have studied the role of FBH1, a DNA helicase thought to mediate the accumulation of ssDNA during RS and to regulate the response to RS-derived breakage. Our study leads to conclude that in mice, the contribution of FBH1 in such processes has a minor impact either in physiological conditions or in a context of defective DNA damage repair. This might be due to compensatory mechanisms or redundant factors that evolved in mammals.

On the second part we explored the role of RS in Ewing sarcomas. These neoplasias bear a translocation between *EWSR1* and a transcription factor, most frequently *FLI1*. Evidence exists that the resulting fusion proteins (most commonly EWS/FLI1) act as oncogenic transcription factors and cause tumorigenesis. Less attention has been put on the actual role of EWS, the product of *EWSR1*, and how a loss of function of EWS can impact on tumorigenesis. Our work firstly demonstrates that Ewing sarcomas suffer a high degree of RS and therefore are suitable candidates for treatment with ATR inhibitors. Next we demonstrate that R-loops are responsible for RS in Ewing sarcomas, and that R-loop accumulation is caused by the absence of EWS activity. This might be due to a dominant-negative effect of EWS/FLI1 over EWS. Furthermore, we propose a model for EWS R-loop-suppressor function, by which self-aggregation around R-loops promotes R-loop removal. Finally we describe a phenotype of neurodegeneration in adult EWS-depleted mice, which reveals a role for EWS in preventing ALS-linked neurodegeneration.

INTRODUCTION

1. Taking care of the genome

The genome is the genetic material of an organism. In the vast majority of species, it consists of DNA molecules formed by two complementary nucleic acid strands. A copy of the genome is packed in the nucleus of every cell, and faithful duplication and transmission to daughter cells ensures perpetuation of the species. DNA mutations, deletions, translocations and a variety of genomic rearrangements can lead to malfunctioning of the cellular machinery, and this might translate into a range of outcomes, from mild disease to lethality (Ciccia and Elledge, 2010). To prevent this, organisms have evolved to incorporate several mechanisms to respond to and repair DNA damage.

1.1. Damage sources

A variety of conditions and insults can potentially damage DNA. UV light, ionizing radiations or reactive oxygen species (ROS) are exogenous insults that can generate DNA lesions: pirimidine dimers, double-stranded breaks (DSB) and oxidized DNA bases respectively. The endogenous metabolism of the cell is also a source of DNA damage: metabolic pathways that generate ROS and DNA metabolism constantly results in DNA alterations such as dNTP misincorporation or chemical modifications. For example, the rate of depurination for mammalian DNA corresponds to the loss of 9.000-10.000 bases per day, and transmethylation reactions of S-Adenosylmethionine with DNA result in the daily accumulation of 600 cytotoxic 3-methyladenine residues (Hoeijmakers, 2009; Lindahl and Barnes, 2000). A particularly interesting endogenous source of DNA damage is replication stress (RS), associated to the replication of the genome in cycling cells. RS generally leads to generation of long threads of single-strand DNA (ssDNA), which is toxic for the cell, and to replication fork stalling which, if not stabilized, might end up in fork collapse and DSB generation(Lecona and Fernandez-Capetillo, 2014; Lopez-Contreras and Fernandez-Capetillo, 2010; Zeman and Cimprich, 2014).

1.2. The DNA damage response (DDR)

The cell relies on a network of molecular pathways known as the DNA damage response (DDR) to repair DNA alterations and maintain genome integrity (Harper and Elledge, 2007; Jackson and Bartek, 2009). The DDR is organized hierarchically and is subjected to a precise spatiotemporal regulation. Early in the DDR, a variety of sensors work in detecting DNA lesions. The PIKK kinases (including ATM, ATR and DNA-PK) are then recruited to the sites of damage and orchestrate signaling cascades that are amplified by transducers, ultimately leading to the activation of effector proteins that promote a variety of cellular responses (Figure 1). At least two cellular responses are essential: one is the recruitment of repair factors to the DNA lesion in order to reestablish genome integrity, and the other is the regulation of cell cycle progression in order for the repair events to take place. One early and pivotal target of ATM and ATR is the phosphorylation of histone variant H2AX, known as γH2AX (Rogakou et al., 1998). This chromatin mark expands for up to 1-2 megabases around the site of damage and forms microscopically visible aggregates termed "foci". Foci serve as repair nodes for recruitment of multiple DNA repair factors and are important for amplification of the signaling in order to trigger cell cycle checkpoints (Fernandez-Capetillo et al., 2002; Harper and Elledge, 2007; Lukas et al., 2011). Additional regulatory mechanisms that mediate factor recruitment to foci include ubiquitilation and sumoylation (Chapman et al., 2012; Ciccia and Elledge, 2010). In parallel, the signaling is transmitted to Chk2 and Chk1, which subsequently activate cell cycle checkpoints and arrest or slow down cell cycle progression in order to give the cell time to repair DNA lesions before proceeding to DNA replication or mitosis. In this manner, the PIKKs orchestrate the repair of the DNA damage in coordination with cell cycle progression. The amount, nature

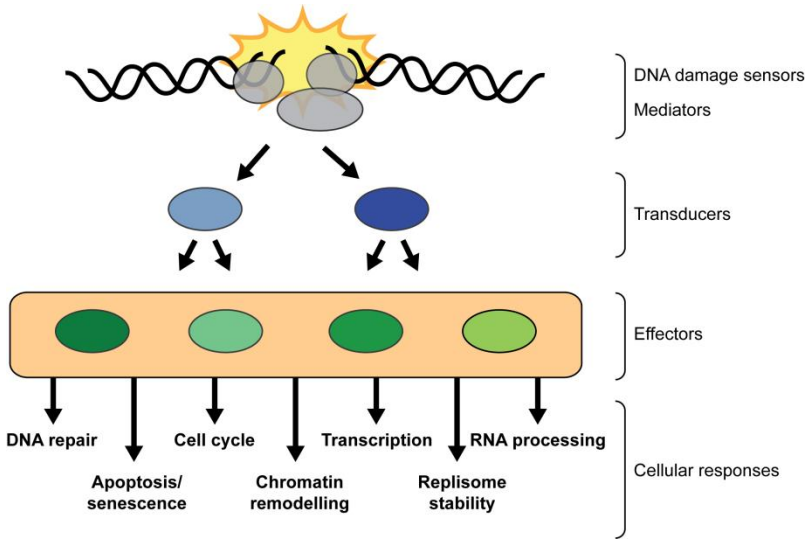

Figure 1
Model for the DDR. The DDR has a hierarchical organization. The presence of a lesion in the DNA is recognized by various sensor proteins. These initiate signaling pathways that are transduced to effector proteins, which in turn mediate a variety of cellular processes, including DNA repair, cell-cycle arrest, apoptosis or senescence, replication fork stability, chromatin remodeling, regulation of transcription and regulation of RNA processing.

or persistence of DNA damage can eventually lead to activation of pro-apoptotic or senescence pathways.

1.3. Mechanisms of DNA damage repair

Some types of simple lesions can be repaired through specific mechanisms that do not generally require an arrest of the cell cycle, such as the mismatch repair (MMR) pathway for mispaired DNA bases, or the base excision repair (BER) pathway for chemically altered bases (Jiricny, 2006; Lindahl and Barnes, 2000). However, more complex DNA lesions converge to the activation of common DDR pathways. On the one hand, some lesions evolve spontaneously or are actively processed into DSBs, which are amongst the most hazardous forms of DNA damage. On the other hand, RS can lead to fork stalling; reaching mitosis with under-replicated DNA can have catastrophic consequences for cells. Furthermore, stalled forks that are not stabilized can collapse and give rise to one-ended DSBs (Figure 2). In the following sections the main DDR pathways that respond to DSBs and RS are reviewed.

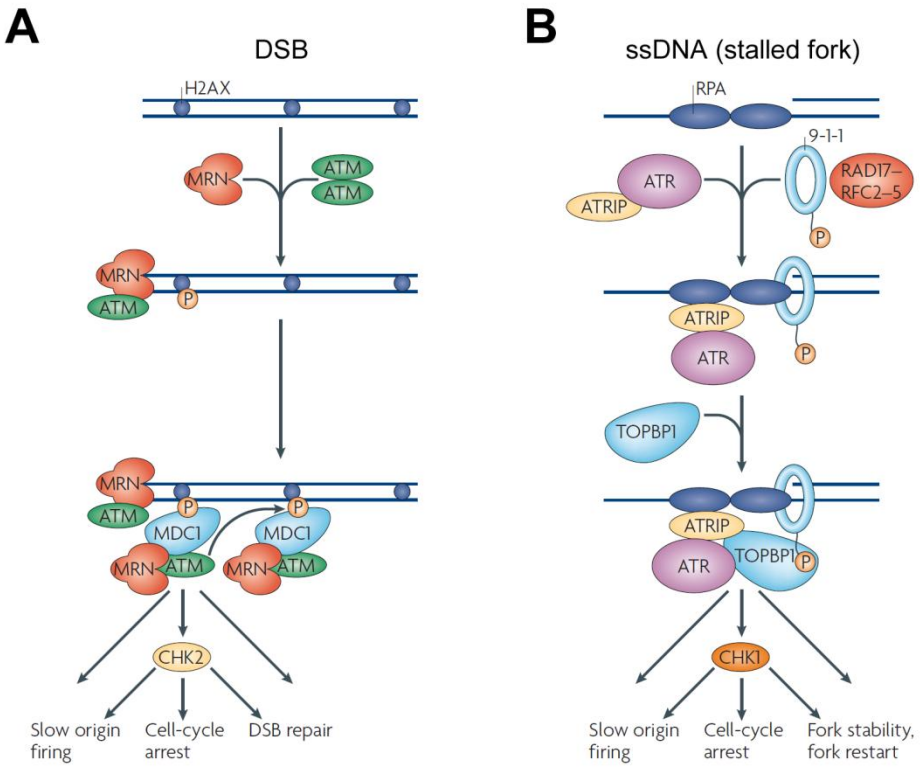

Figure 2
Models for ATM and ATR activation. (A) Formation of a DSB leads to the recruitment of the MRN complex and activation of ATM. This results in generation of γH2AX and downstream signaling to CHK2 – cell-cycle arrest and to local recruitment of repair factors for DSB repair. (B) A ssDNA-dsDNA junction at a stalled fork is coated with RPA, which leads to the recruitment of 9-1-1 and ATR-ATRIP. Activation of ATR leads to phosphorylation of downstream CHK1, which in turn activates cell-cycle arrest and promotes stabilization of the stalled fork. Adapted from (Cimprich and Cortez, 2008).

1.3.1. Double-stranded breaks (DSB)

DSBs are some of the most deleterious forms of DNA damage: if not properly processed they can give rise to chromosomal translocations and complex genomic rearrangements. In fact, defective DSB repair is associated with a variety of disorders, including developmental, neurological or immunological deficiencies and development of cancer (Jackson and Bartek, 2009). DSBs can be repaired through at least 4 different pathways: non-homologous end joining (NHEJ), alternative NHEJ (alt-NHEJ), homologous recombination (HR) or single-strand annealing (SSA) (Ciccia and Elledge, 2010). Following generation of a DSB, poly(ADP-ribose) polymerases (PARP), mainly PARP1/2, recognise the break and synthesize PAR chains on histones in the vicinity. This is one of the earliest events of the DDR and PAR chains serve as a transient platform for recruitment of repair factors (Schreiber et al., 2006).

The NHEJ pathway drives straight religation of two DNA ends, independently of sequence homology (Figure 3). As soon as a DSB arises, the sensor heterodimer Ku70/Ku80 (Ku) competes with PARP1/2 for binding of the double-stranded ends, where it keeps them in close proximity. Ku recruits and activates the DNA-PK catalytic subunit (DNA-PKcs) (Mahaney et al., 2009), which mediates limited DNA end processing (Meek et al., 2008). XRCC4/LIG4 is then recruited and promotes the religation of the DNA ends (Mahaney et al., 2009). A particular physiological process that elicits the NHEJ pathway is the genomic editing in B and T cells known as V(D)J recombination, that occurs during lymphocyte maturation. In this process, RAG1/2 cleaves DNA at defined sites and generates programmed DSBs. Segments of DNA are eliminated and the lasting DNA ends are religated (Market and Papavasiliou, 2003). Similarly, class-switch recombination (CSR) in activated B cells invokes NHEJ to edit DNA and generate new immunoglobulin isotypes (Stavnezer et al., 2008).

Alt-NHEJ operates as a backup to NHEJ and is triggered by PARP1/2 (Figure 3). Repair through Alt-NHEJ requires a limited end resection (around 5-25 nt) which serves to drive microhomology-directed end joining (You and Bailis, 2010; Yun and Hiom, 2009).

HR drives homology-directed repair of a DSB (Figure 3). PARylation of the break site by PARP1/2 facilitates the recruitment of repair factors, including the MRN (MRE11, RAD50 and NBS1) complex and ATM. RAD50 directly binds the DNA ends, while MRE11 interacts with RAD50 and contains endonuclease and exonuclease activities, important for the initial steps of DNA end resection (Williams et al., 2007). NBS1 is proposed to interact with MRE11 and facilitate the recruitment and activation of ATM (Kanaar and Wyman, 2008). ATM regulates

downstream signaling to cell cycle regulators through CHK2, and promotes DNA end resection, which consists on the degradation of the 5' strand and generation of 3' protruding ssDNA ends. End resection is carried out initially by CtIP in association with BRCA1 (Huen et al., 2010). Later, EXO1 and the BLM helicase take over to promote extensive resection (Bolderson et al., 2010). As ssDNA is generated it is rapidly coated by Replication Protein A (RPA; a heterotrimeric complex composed by RPA1, RPA2 and RPA3), which stabilizes ssDNA (Wold, 1997). RPA-ssDNA molecules recruit the ATR/ATRIP complex through direct interaction with ATRIP (Zou and Elledge, 2003). At the site of damage, ATR contributes to regulation of the repair process along with ATM. Phosphorylation of RPA by ATM/ATR facilitates replacement of RPA by RAD51, a rate-limiting process mediated by BRCA2 (West, 2003). The resulting RAD51-ssDNA nucleofilament then undergoes strand invasion and annealing to a homolog sequence (in somatic cells, usually the sister chromatid). This gives rise to a D-loop structure with two Holliday junctions (HJ; four-way DNA junction) that can be processed in different ways. It can undergo synthesis-dependent strand annealing (SDSA) mediated by RTEL (Barber et al., 2008), but the most common pathway is the generation of a double Holliday junction (dHJ) (West, 2003). dHJ can either be dissolved by the BLM/TOPOIIIa complex or resolved by MUS81/EME1, SLX1/SLX4 or GEN1 nucleases. Dissolution leads to the restoration of the two chromatids without a chance of crossover, while resolution implies that 50% of the events will end up with a crossover, that is, a chromatid exchange at each side of the cleavage point (Andersen et al., 2009; Ciccia et al., 2008; Fekairi et al., 2009; Ip et al., 2008; Munoz et al., 2009; Svendsen et al., 2009). HR responds not only to spontaneous breaks, but also to programmed DSBs in meiotic cells occurring at the first meiotic division, which serves to generate allelic combinations distinct from the ones at the parental germ line (Keeney and Neale, 2006).

In SSA, a DSB that occurs within or near a repetitive sequence is repaired through removal of a fragment of DNA and pseudo-homologous annealing between repeats (Figure 3). This process requires end resection, analogously to HR, but RAD52 works instead of RAD51 in forming the nucleoprotein filament at resected DNA ends. ERCC1 and XPF then mediate SSA (Hartlerode and Scully, 2009).

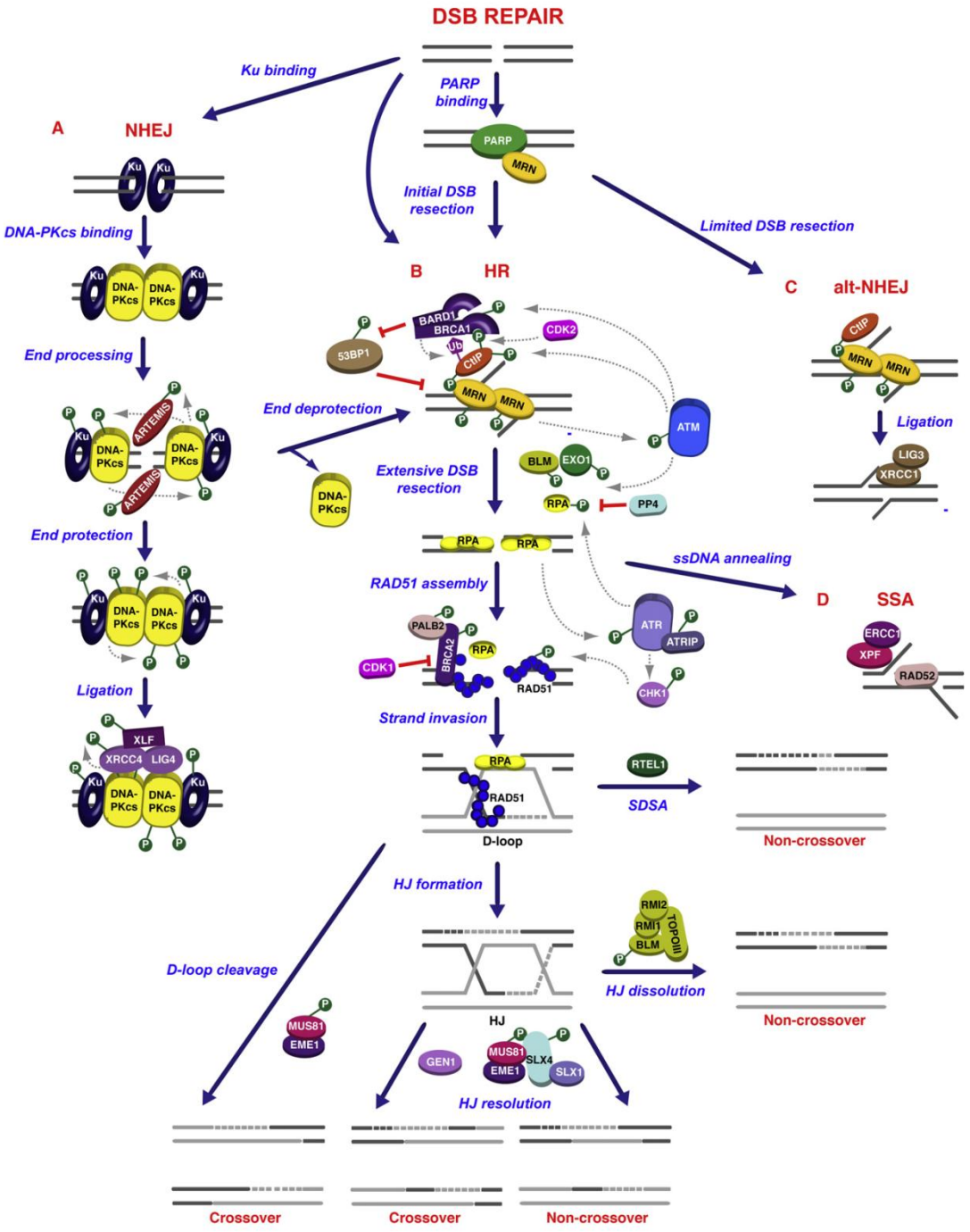

Figure 3
DNA repair pathways involved in the repair of DSB. A) Rapid association of Ku to DSBs promotes NHEJ by recruiting DNA-PKcs. Sequential autophosphorylation events on DNA-PKcs favor limited processing of DNA ends and DNA ligation. B) MRN complex, recruited to DSBs by PARP in competition with Ku, mediates initial DSB resection together with CtIP and BRCA1 to promote HR in S and G2. Extensive DSB resection and formation of RPA-coated ssDNA ends is induced by EXO1 and BLM. ATM plays a central role in the regulation of DSB resection. Displacement of RPA from the ssDNA ends and assembly of RAD51 nucleofilaments mediated by BRCA2 leads to strand invasion into homologous DNA sequences. Recruitment of RAD51 to ssDNA ends is regulated by the ATR pathway, which is activated following DSB resection. HJ structures formed after strand invasion can be cleaved by MUS81/EME1 or displaced by RTEL1 during SDSA to generate crossover or non-crossover events, respectively. Branch migration of the HJs results in the generation of a dHJ. Dissolution of dHJs by the BLM/TOPOIII generates noncrossovers, whereas dHJ resolution by the nucleases GEN1 and SLX1/SLX4, in association with MUS81/EME1, can generate both crossover and noncrossover events. C) limited DSB resection in G1 results in alt-NHEJ. D)Following DSB resection, ssDNA ends with homologous sequences can be directly annealed by RAD52. Figure adapted from (Ciccia and Elledge, 2010).

Pathway choice in DSB repair

NHEJ is an error-prone DSB repair mechanism as the direct ligation of two DNA ends frequently results in small nucleotide deletions, insertions or substitutions, or translocations if the two joined ends correspond to different loci within the genome. Conversely, HR is considered to be error-free because it uses a template strand (most frequently the sister chromatid) to accurately repair the break and restore sequence integrity. The repair pathway choice when a DSB occurs is conditioned by several determinants. In cycling cells, HR is highly favoured during S and G2 phases, where a sister chromatid is available. Actually, it is restricted to these phases, since unscheduled HR occurring in G1 can lead to HR-DSB repair based on pseudo-homologous sequences, which could translate into chromosomal translocations and loss of heterozigosity (LOH) events (Agarwal et al., 2006; Llorente et al., 2008). Instead, NHEJ is active throughout the cell cycle and is invoked during G1. 53BP1 and BRCA1 are two pivotal regulators of DSB repair pathway choice. 53BP1 promotes NHEJ by binding to DSB early in the DDR and inhibiting DSB resection (Chapman et al., 2012), and is active throughout the cell cycle, as assessed by its recruitment to IR-induced foci at any time. To counteract 53BP1 inhibitory effect on DSB resection and promote HR, BRCA1 antagonizes 53BP1 during S and G2 phases. BRCA1 deficiency is associated with genome instability and defective HR (Moynahan et al., 1999), and additional 53BP1 loss alleviates these effects by partially restoring HR (Bouwman et al., 2010; Bunting et al., 2010; Cao et al., 2009).

1.3.2. Replication stress (RS)

DNA replication must be fulfilled accurately and on time in order to reach mitosis with a fully duplicated genome and ensure faithful transmission of genetic information to the daughter cells. Slowing, stalling or eventual collapse of replication forks that impede faithful DNA replication is commonly referred to as replication stress (RS). Diverse exogenous and endogenous insults leading to unrepaired DNA damage, inter-strand crosslinks or dNTP pool depletion are sources of RS. Fork stalling poses one of the major threats to genome integrity, since entry into mitosis with under-replicated DNA can lead to genomic rearrangements, aneuploidy or mitotic catastrophe (Zeman and Cimprich, 2014). Moreover, single-stranded DNA (ssDNA) arises – frequently, but not always – during RS and is higly recombinogenic, potentially resulting into deleterious genomic rearrangements. ssDNA arises either due to uncoupling of the MCM helicase that continues to unwind DNA ahead of the stalled DNA polymerase (Byun et al.,

2005), due to ssDNA gaps left behind the polymerase, or through other unclear ssDNA-generating mechanisms.

Sources of RS

Replication *per se* poses a threat to genome integrity, as DNA molecules are subjected to intense manipulation; therefore it is an inherent source of RS. Cell types with high proliferative rates are more sensitive to RS, and some oncogenes increase the amount of RS by inducing premature entry into S-phase or by deregulating replication. In fact, expression of some oncogenes, including HRAS, MYC or cyclin E has been described as an important source of RS (Halazonetis et al., 2008; Jones et al., 2013; Srinivasan et al., 2013). Their possible mechanisms of action are an increase in replication initiation or in origin firing, which can lead to increased probability of collisions with transcriptional machinery or to dNTP pool depletion (Bester et al., 2011). dNTPs are the fuel for replication and their amount might be limiting, in which case fork progression is challenged. Depletion of dNTPs and subsequent RS can be originated due to impaired dNTP synthesis or excessive replication origin firing (Beck et al., 2012).

ssDNA Nicks and gaps are both sources and consequences of RS. They can arise as a result of DNA manipulation, for example during DNA repair or upon abortive topoisomerase I (TopoI) activity. As a source of RS, ssDNA nicks and gaps might result in passive generation of a one-ended DSB when replication forks encounter these lesions. As a consequence of RS, ssDNA nicks and gaps can arise if a stalled replication fork bypasses an unrepaired DNA lesion through DNA damage tolerance (DDT) pathways (Zeman and Cimprich, 2014).

Unrepaired DNA lesions, such as inter-strand crosslinks, thymidin dimers or DNA-protein crosslinks, become physical barriers to replication fork progression. These can be bypassed by the DDT pathways (Mailand et al., 2013). The agents that generate such DNA lesions include by-products of cellular metabolism, reactive aldehydes, UV light and chemical mutagens (Brooks and Theruvathu, 2005; Ciccia and Elledge, 2010). Misincorporation of rNTPs (ribonucleotides) also requires activation of the DDT pathways (Dalgaard, 2012; Nick McElhinny et al., 2010).

DNA sequences that are intrinsically difficult to replicate are a source of RS. These include trinucleotide repeats that can acquire secondary structures (Kim and Mirkin, 2013) and GC-rich areas that form G-quadruplexes (Bochman et al., 2012). The RS response reverses the formation of such secondary structures through activation of helicases that unwind them.

Because both replication and transcription use DNA molecules as a substrate, conflicts might arise between the two processes. Collisions between replication forks and transcriptional complexes travelling towards each other were shown to be a source of genomic instability (Bermejo et al., 2012). The recently described early-replicating fragile sites (ERFS) are genomic regions with a high transcription rate that are replicated early in S-phase. ERFS are especially prone to breakage, possibly owing to collisions between replication forks and transcriptional complexes (Barlow et al., 2013). Topoisomerases work to relieve topological stress generated in these scenarios (Tuduri et al., 2009), and deficient Topoisomerase activity leads to RS. Loss of RNA processing factors can also derive into RS. For example, slowing of the transcription rate or failure to release the transcriptional machinery from the DNA upon termination can promote collisions.

A particular source of RS associated to transcription-replication collisions is R-loop accumulation. Newly synthesized RNA can rehybridize to its template DNA to form a RNA:DNA hybrid and a displaced ssDNA strand, a structure termed R-loop (Aguilera and Garcia-Muse, 2012). While RNA:DNA hybrids have important functions in diverse physiological processes, from replication initiation in mitochondrial RNA to immunoglobulin class-switching (Chaudhuri and Alt, 2004; Pohjoismaki et al., 2010; Xu and Clayton, 1996), aberrant accumulation due to defective mRNA processing can be toxic. RNA:DNA helicases exist that unwind R-loops, such as SETX and PIF1 (Alzu et al., 2012; Boule and Zakian, 2007; Kim et al., 1999), while RNase H1 works to digest its RNA component (Huertas and Aguilera, 2003). Deficiencies in these and other factors for RNA metabolism can result in persistent R-loops, which are obstacles to replication fork progression and therefore sources of RS. In this regard, the lab of Andrés Aguilera made a valuable contribution in the field. The THO complex is a central player in RNA metabolism that couples transcription and RNA export. Aguilera and colleagues showed that yeast mutants of the THO complex accumulated R-loops and genomic instability, and this was due to impaired transcription elongation that lead to transcription-associated recombination. Together, they postulated R-loops as transcription-dependent structures with an impact on genomic integrity (Aguilera and Garcia-Muse, 2012; Huertas and Aguilera, 2003).

The RS response (RSR)

As part of the DDR, a series of pathways known as the RS response (RSR) are activated upon sensing RS in order to limit it and prevent further accumulation (Cimprich and Cortez, 2008;

Lopez-Contreras and Fernandez-Capetillo, 2010). During replication, newly generated, exposed ssDNA is rapidly coated by RPA. Upon fork stalling, ssDNA-RPA rapidly accumulates. The boundary of double-stranded DNA (dsDNA) with a 5' end adjacent to ssDNA-RPA generates a signaling platform for activation of the RSR and recruitment of repair factors (Byun et al., 2005). ATR/ATRIP is recruited through direct interaction of ATRIP with the RPA-ssDNA complex. RPA-ssDNA also stimulates the loading of 9-1-1 (RAD9-HUS1-RAD1) complex, which brings ATR-activating protein TOPBP1 close to the stalled fork. It is the proximity of TOPBP1 to ATR what stimulates ATR kinase activity. Downstream of this, ATR phosphorylates chromatin (generating the signaling mark γH2AX) and acts locally to perform three functions: stabilize the stalled fork, promote the restart of replication and initiate a signaling cascade transduced by CHK1. In turn, CHK1 collaborates in stabilizing the fork and triggers global responses including the activation of cell cycle checkpoints and the suppression of late origin firing, which gives the cell time to fulfill DNA replication (Figure 4) (Cimprich and Cortez, 2008; Lopez-Contreras and Fernandez-Capetillo, 2010).

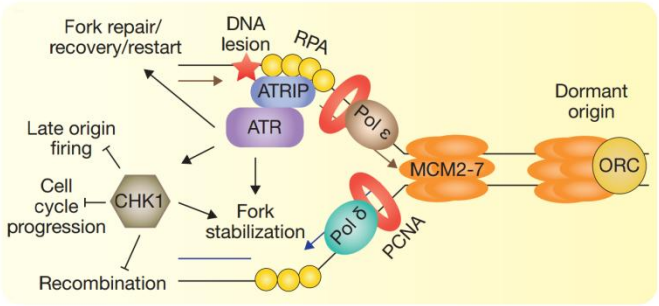

Figure 4
The ATR-mediated RSR. Parental DNA is unwound by the MCM complex and replicated by the DNA polymerases. When replication stalls at a DNA lesion (red star), DNA synthesis can resume downstream, generating a primer-template junction that is recognized by ATR-ATRIP. ATR activates CHK1, which promotes fork stabilization and restart while impairing cell cycle progression. Adapted from (Zeman and Cimprich, 2014).

Importantly, there exist obstacles that promote fork stalling without generation of ssDNA (i.e., without helicase-polymerase uncoupling). This is the case for protein-DNA complexes, ICLs, R-loops or other physical roadblocks ahead of the replication fork that impede fork progression (Lambert and Carr, 2013; Zeman and Cimprich, 2014). Under these circumstances, ATR might be activated by alternative, RPA-ssDNA-independent mechanisms yet to be understood (Zeman and Cimprich, 2014).

Mechanisms of replication restart

Once the source of stress is removed (for example, upon restoring of the dNTP pool) stalled replication forks can resume replication through at least three ATR-dependent mechanisms. First, a stalled fork might undergo remodeling, which enables straightforward restart. Second, the

fork might undergo regression by rewinding the parental DNA and extruding the newly synthesized strands, giving rise to a so-called "chicken-foot" structure, which resembles a HJ. HJ is then a substrate for nucleases and factors that mediate HR in a process in which the newly synthesized daughter strand is used as a template to proceed with replication. Third, the HJ is processed into a DSB and replication is resumed through break-induced replication (BIR). These cleavage mechanisms, although not ideal, would avoid permanent stalling of a replication fork (Petermann and Helleday, 2010). Of note, although BIR has been well established in yeast, there is weak evidence of conservation in higher eukaryotes (Ciccia and Elledge, 2010). On the other hand, the physiological role of the regressed forks or "chicken-foot" structures is under intense debate. Whereas they form and are subjected to nuclease cleavage more frequently in the absence of appropriate ATR signaling (Cotta-Ramusino et al., 2005; Couch et al., 2013; Hu et al., 2012; Sogo et al., 2002), evidence suggests that regression may actually protect the fork from being processed into a DSB (Betous et al., 2012). Thus, it is unclear whether fork regression is protective, pathological or both.

Besides the mechanisms of replication fork restart, the cellular machinery also has means to resume replication when the source of stress cannot be removed – for example, when facing unrepaired DNA lesions. One is the firing of dormant origins. Interestingly, an important number of the replication origins that are licensed before S-phase entry, are never actually fired in unperturbed conditions. These dormant origins might exist as a backup to resume replication in the case of global replication rate slowing due to fork stalling at DNA lesions (Ge et al., 2007; Ibarra et al., 2008). A second mechanism is the repriming of the template strand downstream of the DNA lesion to enable fork progression, which leaves a ssDNA gap behind (Elvers et al., 2011; Lopes et al., 2006). The gaps might be filled by template switch and usage of the newly synthesized complementary strand as a template, or by specialized translesion synthesis polymerases that act in the DNA damage tolerance (DDT) pathway. Translesion synthesis can occur after the fork has passed the DNA lesion, or in real-time, as the fork encounters the lesion (Zeman and Cimprich, 2014).

Consequences of RS

When mechanisms for fork stabilization and replication restart fail, a number of consequences of RS arise that have an impact on genome integrity. Common fragile sites (CFS) are late-replicating genomic regions especially prone to RS-induced DSB (Debatisse et al., 2012). Its biological significance is not well understood and the origin of their fragility is unclear. Several studies point

to a sequence-independent fragility. Instead, CFS appear to be devoid of replication origins, which would explain an inability to rescue replication through alternative origin firing (Debatisse et al., 2012; Le Tallec et al., 2013).

RS-derived breakage is also frequent at ERFS, regions that undergo replication early in S-phase. Because they host a high transcriptional rate, their fragility is probably due to collisions between replication and transcription (Barlow et al., 2013).

Copy-number variants (CNV) are another common outcome of unresolved RS. Stalled fork breakage and subsequent error-prone repair appear to be important mechanisms in the formation of CNVs with implications for developmental disorders and cancer (Arlt et al., 2009).

Inducing RS

A variety of RS-inducing chemical compounds and biological tools have been used in experimental settings to study the RSR. Hydroyurea (HU) blocks dNTP syhthesis by inhibiting the ribonucleotide reductase (RNR) which leads to dNTP pool depletion (Gagou et al., 2010), whereas ATR or CHK1 inhibitors suppress the RSR leading to fork stalling and collapse (Murga et al., 2011; Toledo et al., 2011). Camptothecin (CPT) inhibits Topoisomease I (TopoI), an enzyme that relieves torsional stress during transcription, and inhibition of TopoI leads to RS due to collision of replication forks with stalled transcriptional complexes (Tuduri et al., 2009). The so-called antimetabolites impede cell growth by interfering with essential processes required for replication. For example methotrexate and fluorouracil compete with intermediate metabolites to block *de novo* synthesis of thymidine and halt DNA replication, and are used as chemotherapeutics. In addition, many of the drugs initially used as chemotherapeutic agents, including doxorubicin, cisplatin or etoposide, do indeed block replication, and improved derivatives with reduced cytotoxicity are still in use in the clinics.

1.3.3. RS in cancer

RS is frequently related to cancer (Lecona and Fernandez-Capetillo, 2014). Certain oncogenes challenge DNA replication by altering the normal usage of replication origins (Bartkova et al., 2006; Di Micco et al., 2006; Ekholm-Reed et al., 2004), or by promoting collisions with transcription (Jones et al., 2013). These events generate high levels of RS (Halazonetis et al., 2008; Jones et al., 2013; Srinivasan et al., 2013), which has been shown to lead to genomic instability (Barlow et al., 2013; Burrell et al., 2013; Costantino et al., 2014; Dereli-Oz et al., 2011).

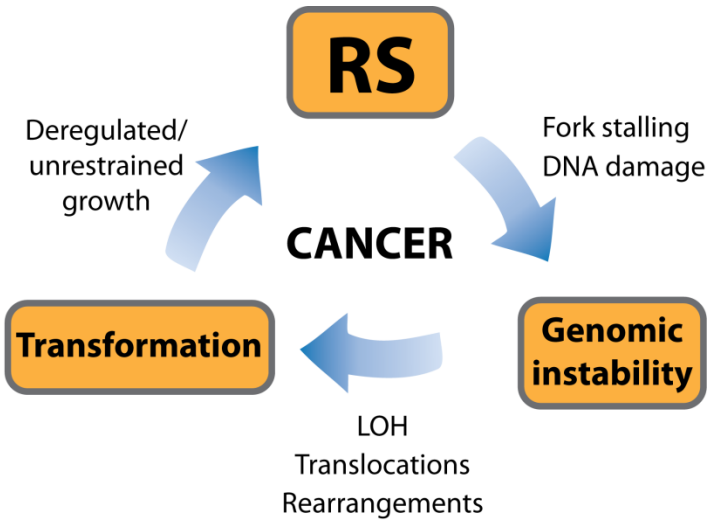

Figure 5
RS fuels cancer. Moderate amounts of RS favor genomic instability, which can lead to detrimental rearrangements such as LOH or gene translocations. These events are drivers of malignant transformation, which frequently promotes unrestrained cell-cycle progression and growth, leading to a further increase in RS. This positive feedback loop fuels cancer progression.

Chromosomal rearrangements, copy number alterations and other reorganizations can result into aberrancies such as translocations or LOH, which might contribute to malignant transformation. Finally, malignant transformation is frequently accompained by deficient cell cycle checkpoints and unrestrained growth. This contributes to further increase RS, thereby closing a positive feedback loop that fuels cancer (Figure 5). Similarly, mutations affecting DNA repair mechanisms predispose to tumorigenesis as deficient DNA repair can also lead to an accumulation of RS when forks encounter DNA lesions. For example, proteins of the Fanconi Anemia pathway promote repair of ICLs that block replication fork progress, and mutations in these proteins predispose to cancer (Clauson et al., 2013). The RECQ family of DNA helicases recognize and process specific toxic structures generated during replication, and mutations in these proteins result in syndromes that predispose carriers to tumorigenesis (Croteau et al., 2014).

Nonetheless, RS is a double-edged sword. Excessive amounts of RS do not predispose to cancer, but rather lead cells to collapse and death (Figure 6) (Murga et al., 2009; Schoppy et al., 2012). Such amounts of RS can be induced upon deletion or inhibition of ATR or CHK1, the primary response factors to RS. This has important clinical implications that are commented below.

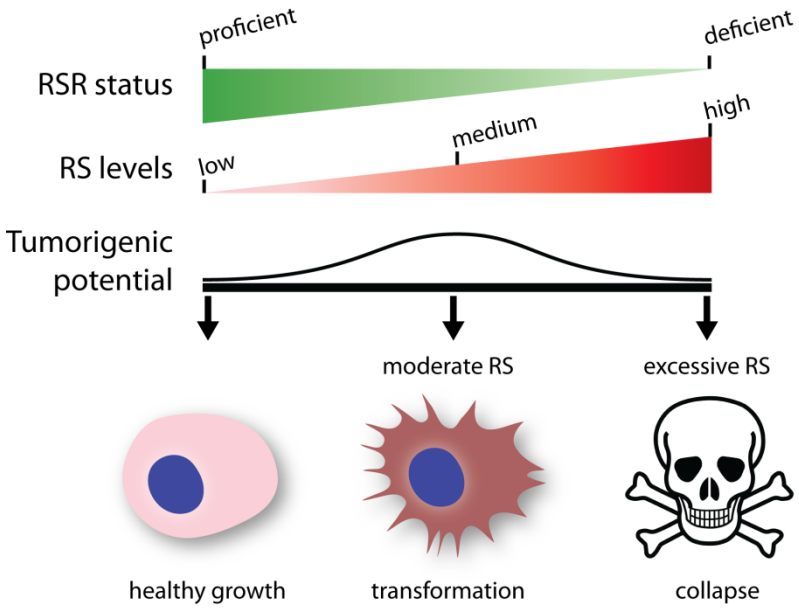

Figure 6
RS is a double-edged sword. A proficient RSR keeps RS levels low and prevents genomic instability in proliferating cells. Moderate RS levels, either due to exogenous sources of RS or to a partially deficient RSR, favor malignant transformation and tumorigenesis. A fully deficient RSR results in excessive RS levels that are incompatible with any kind of proliferation, and lead cells to collapse and death. This principle can be exploited as a strategy to selectively kill cancer cells (Murga et al., 2009; Schoppy et al., 2012).

2. FBH1: a molecule that promotes RS

ssDNA accumulates during RS and is toxic for the cell due to its highly recombinogenic nature, which might result in genomic instability (Lecona and Fernandez-Capetillo, 2014). One open question in the study of the molecular bases of RS is the identification of factors that mediate the accumulation of ssDNA. The depletion of such hypothetical factor should theoretically protect cells against RS-inducing agents, and would be of high relevance for clinical applications.

FBH1 is a member of the UvrD family of DNA helicases, first identified in S. pombe. It is conserved in fission yeast and higher eukaryotes, but not in budding yeast. FBH1 was initially identified as being stimulated by RPA, and 3'-5' directionality was determined (Park et al., 1997). It is a bifunctional protein containing a C-terminal domain with ATP-dependent DNA helicase activity and an N-terminal F-Box domain (Kim et al., 2002) (Figure 7A). F-box proteins act as substrate recognition factors whithin SCF complexes, which target proteins for ubiquitilation and degradation (Patton et al., 1998). The F-box of FBH1 contains an E3 ligase domain which provides ubiquitin ligase activity to its SCF complex (SKP1-CUL1-FBH1) (Kim et al., 2004). The roles of FBH1 have been a subject of controversy since its identification (Figure 7B).

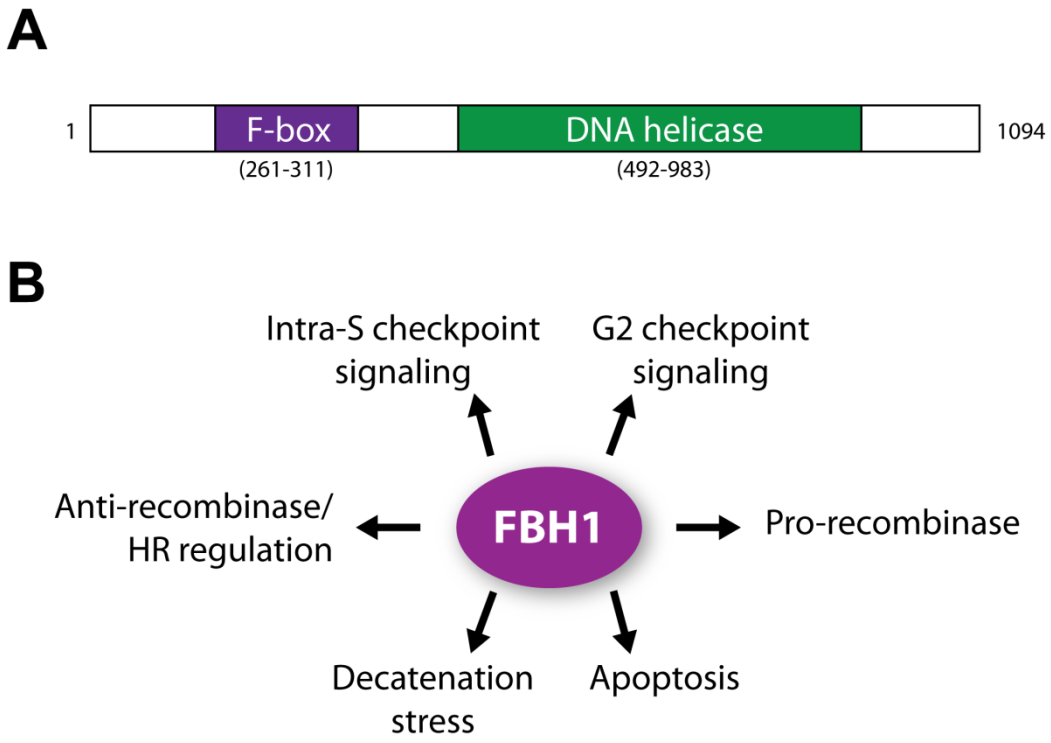

Figure 7
Structure and functions of FBH1. (A) FBH1 contains an N-terminal F-box domain with E3 ligase activity and a C-terminal DNA helicase domain with affinity for ssDNA and helicase-translocase activity. (B) Diverse functions have been described or proposed for FBH1: pro-recombinase, anti-recombinase, activation of pro-apoptotic signaling, survival to decatenation stress, and signaling of the intra-S and G2 checkpoints.

In regards to the identification of factors that mediate the accumulation of ssDNA, FBH1 emerged recently as a putative candidate. Fugger and colleagues showed that cells depleted from FBH1 failed to accumulate ssDNA upon exposure to HU, suggesting that FBH1 had an active role in promoting ssDNA accumulation. Based on the high recombinogenicity of ssDNA, they proposed a pro-recombinase role for FBH1 (Fugger et al., 2009).

Nonetheless, FBH1 had been previously described as a putative ortholog of Srs2, a canonical yeast anti-recombinase (Chiolo et al., 2007). In fact, hyperrecombinant phenotypes were observed in FBH1-deficient strains of S. pombe (Morishita et al., 2005; Osman et al., 2005), chicken (Kohzaki et al., 2007) and human cells (Fugger et al., 2009), which might be an outcome of unrestrained HR. Several studies support a role for FBH1 in HR, as it is recruited to RS- or damage-induced foci (Fugger et al., 2009) where it colocalizes with RAD51 (Osman et al., 2005). Furthermore, FBH1 directly interacts with Rad51 *in vitro* and disrupts the Rad51 nucleofilament by means of its ssDNA helicase-translocase activity, while it probably prevents Rad51 re-loading onto ssDNA by ubiquitylating it (Chu et al., 2015; Simandlova et al., 2013), consistent with an anti-recombinase role. Furthermore, codepletion of both FBH1 and Srs2 in fission yeast leads to a growth defect and hypersensitivity to RS-inducing agents, whereas codepletion of FBH1 and rqh1 (BLM homolog in fission yeast) is synthetic lethal (Osman et al., 2005; Roseaulin et al., 2008). Interestingly, these phenotypes are circumvented by inactivation of rad51 or rad51-related factors that initiate HR (Osman et al., 2005). A lot of interest in the field was raised around the identification of a bona-fide mammalian ortholog of Srs2 anti-recombinase; in this race, another candidate was RTEL1 (Barber et al., 2008). This helicase was described as a functional analog of Srs2 and was found to be required for genome stability and tumor avoidance. RTEL1 deletion in *C. elegans* lead to characteristic phenotypes shared with yeast Srs2 mutants, and HR was also limited by RTEL1 *in vitro*.

More recent works suggest that in mammals FBH1 has a minor role in regulating RS-derived HR. Instead, its main role would be to promote apoptosis in cells accumulating excessive RS. Breaks arising upon fork collapse can be subjected to HR-mediated repair, but this involves a risk of aberrant recombination and subsequent chromosomal rearrangements. In cells suffering from RS, FBH1 might counteract aberrant recombination at stalled forks by redirecting the cellular signaling network towards apoptosis. Mechanistically, FBH1 would promote nuclease-mediated DSB formation at stalled forks, which would serve as a molecular signal to trigger apoptosis (Fugger et al., 2013; Jeong et al., 2013b). This would represent a means for preventing perpetuation of aberrant genomic rearrangements and eventually tumoral transformation.

Supporting this idea, deleterious mutations at the *FBH1* gene have been found enriched in melanoma cell lines (Jeong et al., 2013a). Other studies have proposed additional roles for FBH1 in mitotic and meiotic chromosome seggregation (Laulier et al., 2010; Sun et al., 2011). Mitotic progression after decatenation stress by topoisomeraseII inhibition was largely abrogated in FBH1-deficient cells, and meiotic seggregation was deficient in fbh1 mutant yeast, correlating with increased recuritment of rad51 to break sites.

Alltogether, we aimed at exploring two main questions. First, whether FBH1 indeed promotes RS. If this were the case, deletion of FBH1 should be beneficial in a mouse model suffering from RS, such as the ATR-Seckel mouse previously developed in our lab (Murga et al., 2009). Second, we wanted to find whether FBH1 is an anti-recombinase. As such, deletion of FBH1 might rescue the phenotypes of a BRCA1 mutant mouse, a model with impaired recombination (Xu et al., 1999).

3. Targeting RS in Ewing sarcoma

Deficiencies in the repair of RS-inducing DNA damage can lead to a moderate accumulation of RS and favor tumorigenesis, as commented above (Figure 5). By contrast, inhibition of the primary response to RS - that is, ATR and Chk1 - leads to a massive accumulation of RS and does not favor tumorigenesis, but rather drives cells to death (Murga et al., 2009; Schoppy et al., 2012). ATR or CHK1 deletion/inhibition is incompatible with any form of cell proliferation; also – and especially – with tumoral proliferation. In fact, tumoral cells growing with RS are highly dependent on a proficient RSR (Figure 6). On this basis, targeting the RSR through ATR and Chk1 inhibition has proved to be a successful strategy for impairing tumoral growth in murine models of Eμ-myc lymphoma, H-Ras fibrosarcoma and MLL-ENL AML (Murga et al., 2011; Schoppy et al., 2012).

The success of targeting the RSR in cancers with high RS encouraged us to seek for other cancer types that might be susceptible to this strategy. In this regard, Ewing sarcomas display a high degree of genomic instability and rearrangements (Ferreira et al., 2008; Ohali et al., 2004) but, as pediatric cancers, very low frequency of single nucleotide polymorphisms (SNPs) and point mutations (Alexandrov et al., 2013), which are caused by a variety of mutagens and are a hallmark of other cancer types. These two conditions together are reminiscent of high RS.

3.1. Ewing sarcoma: molecular pathogenesis

Ewing sarcoma is the second most common bone tumor affecting children and adolescents (Ordonez et al., 2009). While current chemotherapy enables 75% survival for patients diagnosed with primary ES, metastasis still correlates with a bad prognosis. ES is a poorly differentiated tumor type of bone and soft tissues. It is a member of the Ewing sarcoma Family of Tumours (ESFT), which invariably present a reciprocal translocation involving a gene of the FET family of DNA and RNA-binding proteins (FUS/TLS, EWS and TAF15) and a transcription factor of the ETS family. All translocations involve the substitution of the C-terminal RNA/DNA binding domains of the FETprotein with a DNA binding domain contributed by the ETS transcription factor (Balamuth and Womer, 2010; Lessnick and Ladanyi, 2012; Ordonez et al., 2009; Paronetto, 2013). The most common translocation, accounting for 90% of the cases, is the t(11;22)(q24:q12) between the *EWSR1* gene and the *FLI1* gene, which generates the fusion protein EWS/FLI1 (Figure 8). Notably, FET/ETS translocations have also been found in other cancers, including malignant melanoma of soft parts (Zucman et al., 1993), extraskeletal myxoid

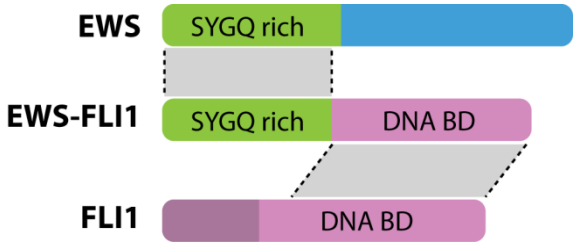

Figure 8
EWS/FLI1 translocation in Ewing sarcoma. The fusion protein resulting from the initiating translocation in Ewing sarcoma is composed of an N-terminal SYGQ-rich domain contributed by EWS and a C-terminal DNA-binding domain contributed by FLI1 or ETS family transcription factor.

chondrosarcoma (Labelle et al., 1995), myxoid liposarcoma (Panagopoulos et al., 1996) or desmoplastic small cell round tumours (Ladanyi and Gerald, 1994).

EWS/FLI1 chimeric protein has been a subject of intense study as the presumed initiating event in Ewing sarcoma (Kauer et al., 2009; Riggi et al., 2008). It behaves as an aberrant transcriptional regulator, and its expression in NIH-3T3 cells promotes transformation, revealing it as a bona-fide oncogene (May et al., 1993a; May et al., 1993b). Indeed, numerous EWS/FLI1-regulated genes have been identified (Bailly et al., 1994; Braun et al., 1995; Dauphinot et al., 2001; Fukuma et al., 2003; May et al., 1997; Nakatani et al., 2003; Thompson et al., 1996; Wai et al., 2002). Mouse models expressing EWS/FLI1 have been generated for the study of Ewing sarcoma and development of novel therapies (Lin et al., 2008). However, less attention has been put on the loss of EWS function upon translocation, and the actual contribution of EWS in preventing tumorigenesis remains largely unexplored.

3.2. EWS protein: structure and function

EWS is encoded by the *EWSR1* (Ewing Sarcoma breakpoint Region 1) gene, originally identified and termed after its translocation in Ewing sarcomas. All three members of the FET family of DNA and RNA-binding proteins (EWS, FUS and TAF15) share a very similar structure (Figure 9A). A SYGQ-rich N-terminal domain is followed by a C-terminal region with nucleic acid binding domains containing an RNA recognition motif (RRM), a zinc finger (ZF) and three arginine-glycine-glycine (RGG)-rich domains (Paronetto, 2013). Interestingly, EWS has been shown to bind diverse nucleic acid substrates, including DNA and RNA G-quadruplexes (via its RGG motifs) and ssDNA (Paronetto et al., 2011; Takahama et al., 2011). The three FET proteins are cointeractors (Pahlich et al., 2009; Spahn et al., 2003) and generally localize to the nucleus (Andersson et al., 2008).

EWS has been associated to a variety of cellular functions related to RNA metabolism (Figure 9B). A role in transcription was described based on its interaction with RNA polymerase II (RNAPII) (Bertolotti et al., 1996; Bertolotti et al., 1998), its association with TFIID (Bertolotti et

al., 1998), and with several transcriptional activators and repressors including OCT4, Brn3a, CBP and p300 (Araya et al., 2003; Fujimura et al., 2001; Gascoyne et al., 2004; Lee et al., 2005; Thomas and Latchman, 2002). It was also involved in RNA splicing; interaction of EWS with components of the spliceosome and splicing factors were described (Michaud and Reed, 1993; Yang et al., 2000), and a role for EWS in DNA damage-induced alternative splicing was proposed (Paronetto et al., 2014; Paronetto et al., 2011). Genome surveillance functions have also been associated to EWS (Figure 9B): it interacts with BARD1 which, together with BRCA1, promotes repair of DNA damage (Spahn et al., 2002), and it is required for resistance to CPT, an RS-inducing agent (O'Connell et al., 2010). Interestingly, all three FET proteins are recruited to laser microirradiation stripes in a PARP-dependent manner (Britton et al., 2014; Mastrocola et al., 2013; Rulten et al., 2014). While the contribution of these activities to physiological functions

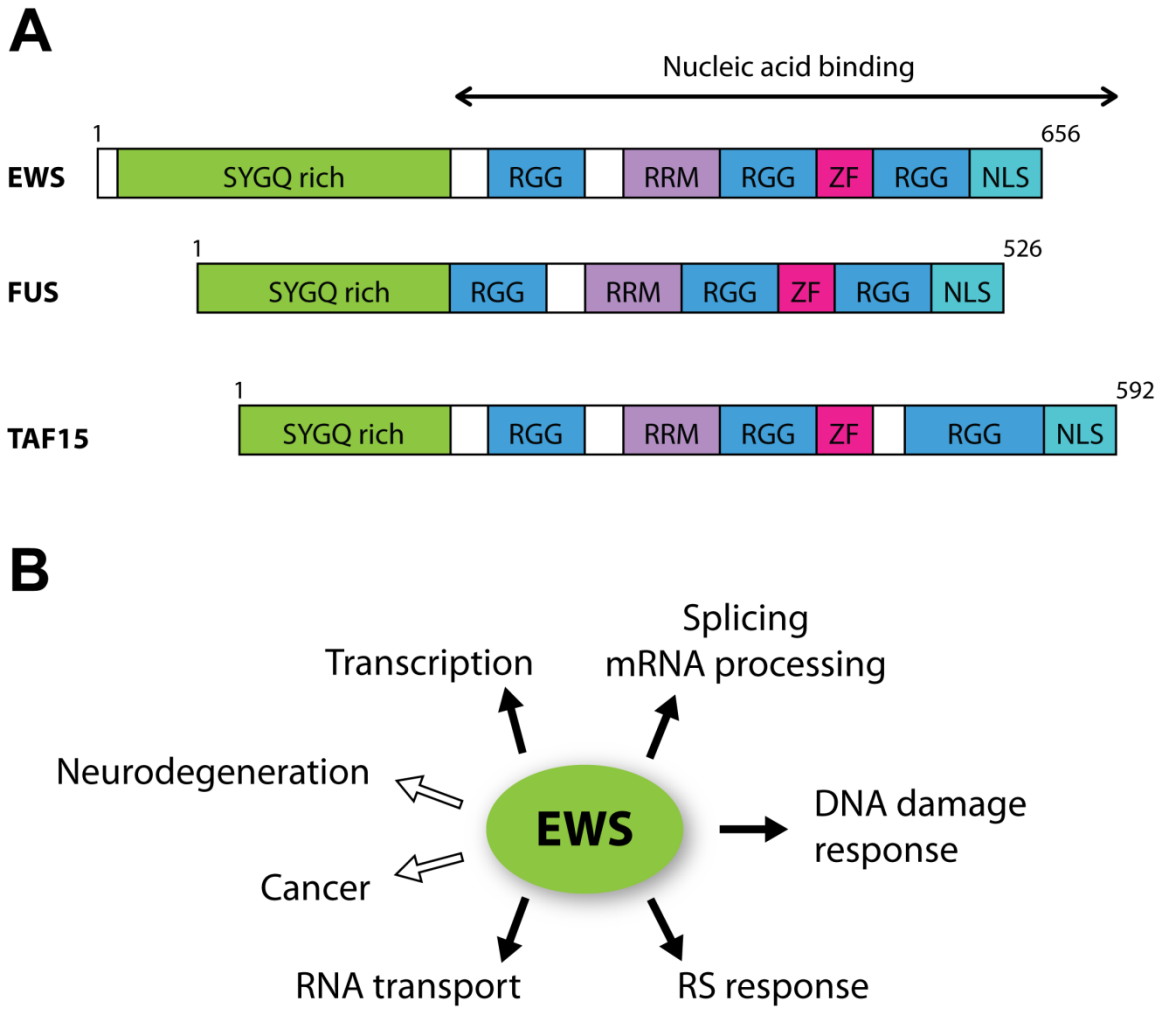

Figure 9
Structure and functions of EWS and related FET proteins. (A) EWS contains an N-terminus with SYGQ repeats and a C-terminus with nucleic acid binding domains containing an RNA recognition motif (RRM), a zinc finger (ZF) and three arginine-glycine-glycine (RGG)-rich domains. The structure is highly conserved across the FET family of DNA and RNA binding proteins formed by EWS, FUS and TAF15. (B) Several functions have been described for EWS in transcription, mRNA processing, RNA transport and genome surveillance (DNA damage response and RSR). EWS has been linked to cancer and neurodegeneration.

is not well understood, absence of EWS protein leads to a number of phenotypical traits at the organism level. A knockout mouse with constitutive deletion of EWS showed a high perinatal mortality, XY chromosome asynapsis at meiosis, defective B-cell development, hypersensitivity to ionizing radiation and an altered dynamics in hematopoietic stem cell population, all consistent with a role for EWS in preventing genomic alterations (Li et al., 2007). Similarly, a FUS-KO mouse showed embryonic lethality and genomic instability (Hicks et al., 2000).

3.3. EWS protein in disease

EWS protein has been linked to cancer mainly based on the known translocations leading to Ewing sarcoma. Nonetheless, its roles in genome surveillance suggest a putative function as a tumor suppressor, which has not been proven.

Defects in RNA metabolism have been linked to disease in the nervous system. Cytoplasmic aggregates of RNA binding proteins are frequent clinical hallmarks of neurodegenerative disease. In this regard, all three FET proteins are recruited in cytoplasmic aggregates in frontotemporal dementia (FTD) (Bosco et al., 2010; Huey et al., 2012; Kwiatkowski et al., 2009; Mackenzie and Neumann, 2012; Neumann et al., 2011; Takanashi and Yamaguchi, 2014). Furthermore, mutations in FUS are causative of familial cases of amyotrophic lateral sclerosis (ALS) (Bosco et al., 2010; Kwiatkowski et al., 2009). These findings suggest a neuroprotective role common for FET proteins.

In this project we aimed at assessing the suitability of Ewing sarcomas for treatment with ATR inhibitors and at unraveling the underlying causes of RS in this tumor type. At the molecular level we wanted to further understand the role of EWS and the impact of its deficiency in cancer and neurodegenerative disease.

OBJECTIVES

PART I

1. To evaluate the *in vivo* contribution of FBH1 to the maintenance of genome integrity

    - To understand the molecular mechanisms of FBH1 contribution to RS and HR

    - To assess the impact of FBH1 deletion in mouse models of high RS and defective HR

PART II

2. To assess the suitability of Ewing sarcomas to treatment with ATR inhibitors

3. To understand the underlying causes of RS in Ewing sarcomas

    - To dissect the molecular contributions of wild type EWS and EWS/FLI1 in RS

4. To explore the impact of EWS deficiency in disease

    - To understand the molecular role of EWS protein

    - To assess the tumorigenic potential of R-loop-driven RS.

    - To assess the contribution of EWS deletion in neurodegeneration.

MATERIALS AND METHODS

1. Mouse biology

1.1. Mouse models

Targeting constructs for the generation of the *Fbh1* and *Ewsr1* gene trapped alleles were obtained from the European Conditional Mouse Mutagenesis Program (EUCOMM) at the International Knockout Mouse Consortium (IKMC). Linearized vectors were electroporated into R1 (129X1/SvJ x 129S1) mouse embryonic stem cells. Neomycin-resistant colonies were screened by southern blotting for identification of recombinant clones, and selected clones were aggregated for generation of chimeras. *ATR*^{Seckel} (Murga et al., 2009) and *Brca1*$^{\Delta 11}$ (Xu et al., 1999) mice have been described. Mouse colonies were maintained under Specific Pathogen Free conditions with constant temperature and humidity, according to the institutional Spanish National Cancer Research Centre (CNIO) guidelines, in a mixed C57BL/6-129/Sv background. All mouse work was performed in accordance with the Guidelines for Humane Endpoints for Animals Used in Biomedical Research, and under the supervision of the Ethics Committee for Animal Research of the "Instituto de Salud Carlos III".

1.2. Mouse genotyping

Tail tissue fragments were used for genotyping mice. Tissue was digested overnight at 55°C with a lysis buffer containing NaCl 100 mM, Tris-HCl pH 8 20 mM, EDTA10 mM, SDS 0.5% and proteinase K (Roche) 400 µg/ml. Tissue lysates were deproteinized with a saturated NaCl solution and DNA in the supernatant was precipitated with isopropanol, washed with ethanol 70% and resuspended in distilled water. PCR reactions were prepared in a 10 µl final volume reaction containing 200 µM dNTPs, 1.5 mM MgCl2, 1 µl 10X reaction buffer (Invitrogen), 0.15 µl Taq polymerase (Platinum Taq, Invitrogen), 0,5 µM of each oligonucleotide primer and 100 ng genomic DNA. Taq polymerase was activated at 95ºC for 5' and PCR steps were as follows: denaturation at 95ºC 30" – annealing at 65ºC 30" – elongation at 72ºC 30", for 35 cycles.

The following table contains the primer sequences used and the band sizes generated by each allele.

Allele name	Primer name	Sequence (5'→3')	Band sizes
Ewsr1^{GT}	EW 5arm_2 FW	TGCTTCTCAAAGGCTTTACTTT	wt: 250 GT: 606 lox: 444 KO: 571
	EW neo FW	GCCATCACGAGATTTCGATT	
	EW exon RE	ATCCAAGATTCAGCCAGCAC	
	EW 3arm_2 RE	AGCAAACAGATGTGAAAACCAG	
Bmi1-CRE^{ERT2}	Bmi1CRE A	AAAGACCCCTAGGAATGCTC	wt: 421 KI: 365
	Bmi1CRE B	ACCAGCAACAGCCCCAGTGC	
	Bmi1CRE C	TAGGCATTAATTGAGATTAACAAACTA	
Fbh1^{GT}	FB2 5#arm Fw	GGCTGTGGTGGTTCATACCT	wt: 255 GT: 689
	FB2 exon Re	TCTGACCTCCACAAGCTCCT	
	FB2 neo Fw	GCCATCACGAGATTTCGATT	
ATR^{Seckel}	Seckel 3'E8	GGAATAAATCCATGGAAGTGAGAGCAT	wt: 300 KI: 500
	Seckel neo	TCCTCGTGCTTTACGGTATCGCC	
	Seckel 5'In7-8	CACTGGCCTCACAGACTTCAGCATG	
CRE	Cre1	CGATGCAACGAGTGATGAGGTTC	Tg: 350
	Cre2	GCACGTTCACCGGCATCAAC	
Brca1$^{\Delta 11}$	Brca Del11 B4	CTGGGTAGTTTGTAAGCATGC	wt: 480 d11: 650
	Brca Del11 B5	CAATAAACTGCTGGTCTCAGG	
	Brca Del11 B6	CTGCGAGCAGTCTTCAGAAAG	

1.3. Survival curves

At least 8 mice per genotype were maintained for each survival analysis. Age of death was recorded for each animal and reported on a Kaplan-Meyer curve with GraphPad (Prism software).

1.4. Xenograft assays

8-10 week-old CB17/lcr-Prkdc scid/Crl mice were used. $1x10^6$ A4573 cells were inoculated subcutaneously in the right flank of mice. The growing tumor masses were measured with the aid of a Vernier caliper, and tumor volumes were calculated using the formula: (width x (length) ^{2}) /2. When tumor volume reached about 100 mm^3 mice were randomized into two groups and treatment started. 7 mice per group were used. Compound or vehicle was administered via oral gavage 5 days per week at a dose of 50 mg/Kg. ATRi was dissolved in 10%NMP (443778; Sigma-Aldrich), 50% PEG-300 (202371; Sigma-Aldrich) and 40% H2O.

1.5. Inmunohistochemistry

Tissues were fixed in formalin and embedded in paraffin for subsequent processing. 2.5 μm sections were treated with citrate for antigenic recovery and processed for immunohistochemistry with the indicated antibodies or for histological staining with cresyl violet. Slides were scanned and digitalized with a MIRAX system (Zeiss) for analysis.

2. Cellular biology

2.1. Generation of primary MEF cell cultures

Females were mated with males until vaginal plugs were detected. At day 13.5 post-coitum females were sacrificed and embryos were extracted. In a laminar airflow hood, the fetal liver was discarded for each embryo and a fragment of tissue was extracted for genotyping (see Mouse genotyping). The remaining embryo tissue was chopped with a sterile blade and incubated for 10' with 1ml trypsin 0,25%, EDTA (Gibco). The resulting mixture was disaggregated by pipeting and trypsin was neutralized with 9ml DMEM 15% FBS. Cell suspension was incubated at 37ºC in 5% oxygen atmosphere and medium was changed on the following day.

2.2. Isolation of splenic B lymphocytes

Splenectomy was performed in 8 to 12-week-old mice. Whole spleens were disaggregated in washing buffer containing 1% bovine seroalbumin (BSA Fraction V, Roche) in PBS. After centrifugation, cellular pellets were treated with a hypotonic solution (ACK Lysing Buffer, Lonza) for 5' and solution was inactivated by adding washing buffer. Cellular aggregates were eliminated through a 40um filter and suspension was centrifuged 5' at 350g. Cellular pellet was suspended in 900ul of washing solution and 80ul of anti-CD143-conjugated magnetic beads (Miltenyi Biotech) were added. The mix was incubated at 4°C for 15'. Cells were washed, suspended in 1ml washing solution and transferred to a magnetic separation column (MS Columns, Miltenyi Biotech) attached to a magnetic scaffold (OctoMACS separator, Miltenyi). The eluted fraction, containing a pool enriched in B cells, was maintained in culture as indicated in the Cell culture section.

2.3. Cell culture

Human Ewing sarcoma, osteaosarcoma and 293T cell lines were grown in Dulbecco's Minimum Essential Media (DMEM, Invitrogen) supplemented with 10% FBS (Lonza) and 1% penicillin/streptomycin (Gibco, Invitrogen). MEF were grown in DMEM supplemented with 15% FBS and 1% penicillin/streptomycin, in a 5% oxygen atmosphere to minimize exposure to ROS. For all experiments, MEF were used at a low passage (<3) or after immortalization through T121 expression. B cells were cultured in RPMI medium (Euroclone) supplemented with 10% FBS, 1% penicillin/streptomycin, glutamine 2mM (Gibco, Invitrogen), non-essential aminoacids (Lonza), sodium pyruvate (Gibco, Invitrogen), β-mercaptoethanol 50 mM (Gibco, Invitrogen) and HEPES 10 mM (Lonza). 25mg/ml LPS (Sigma-Aldrich) were added to stimulate B-cell proliferation and 5 ng/ml IL4 (Gibco) was used to induce immunoglobulin class-switching recombination.

2.4. Cell proliferation curves

1,25 x 10^5 cells were plated in a 35mm plate. 2 days later cells were collected, counted, and 1,25 x10^5 cells were again plated. The operation was repeated for several passages. The increase in population doublings (PDLs) per passage was calculated applying the formula PDLs = log (nf / n0) / log2, where n0 is the initial cell number and nf is the final cell number in each passage.

2.5. Growth inhibition assay

Cells were grown on clear bottom 96-well plates and treated for 36h with increasing concentrations of compounds. Cell Proliferation Kit II-XTT (Roche) was used for assessing metabolic activity as a reporter of growth inhibition. The colorimetric reaction product was measured with a Wallac 1420 VICTOR^2 multilabel plate reader (Perkin Elmer). Dose-response curves were generated with Prism software (GraphPad Software) to calculate LD50 values for each compound.

2.6. Metaphase breakage analysis

Cultured cells were arrested at mitosis with Colcemid (GIBCO/BRL) and fixed with methanol-acetic acid (3:1). Metaphase spreads were hybridized with a Cy3-labeled telomere-repeat PNA probe (Panagene) and stained with DAPI. For immuno-FISH, slides were stained with antibody S9.6 after hybridization with telomere-repeat probe following standard immunofluorescence

techniques (see Immunofluorescence). Breaks and chromosomal aberrations were quantified manually using a Zeiss Imager Z1 fluorescence microscope with an ORCA 1394 camera (Hamamatsu) and 40x or 63x objectives (Leica and Zeiss).

2.7. Immunofluorescence

Cells were grown on coverslips, fixed with 4% PFA and permeabilized with 0.1% Triton-X100. For R-loop detection with S9.6, cells were pre-extracted before fixation as previously described (Celeste et al., 2003). Briefly, cells were treated for 5' with with ice-cold cytoskeleton (CSK) buffer containing 10mM PIPES mH6.8, 100mM NaCl, 300mM sucrose, 3mM MgCl2, 1mM EGTA, 0.5% Triton X-100. CSK was washed off 3 times with PBS and cells were incubated for 30' at room temperature in mSTF fixing solution containing 150mM 2-bromo-2-nitro-1,3-propanediol, 108mM diazolidinyl-urea, 10mM sodium citrate, 50mM EDTA pH 5.7. Cells were washed off 3 times with PBS and blocked with blocking solution containing 2.5% BSA, 0.1% goat serum, 0.1% Tween-20 for 30' at room temperature. Primary antibodies were incubated in blocking solution for 1h at room temperature or overnight at 4ºC. Cells were washed 3 times with PBS and incubated in blocking solution with secondary antibodies (Alexa Fluor, Invitrogen) for 45'. Cells were washed 3 times with PBS, incubated in DAPI for 1', and mounted on a glass slide in Mowiol mounting solution (Sigma-Aldrich). Images were acquired in a Zeiss Imager Z1 fluorescence microscope with an ORCA 1394 camera (Hamamatsu) and 40x or 63x objectives (Leica and Zeiss).

2.8. High throughput microscopy

Cells were grown on μClear® bottom 96-well plates (Greiner Bio-One). Immunofluorescence was performed using standard procedures (see Immunofluorescence) with the indicated antibodies. Analysis of DNA replication by EdU incorporation was done using Click-it reaction Kit (Invitrogen) following manufacturer's instructions. Cell viability assay using HTM has been described before (Eguren et al., 2014). Briefly, cells were incubated 1μM TO-PRO®-3 and 5 ug/ml Hoechst 33342 (Invitrogen) for 30' and subsequently analyzed *in vivo*. For all assays, images were automatically acquired from each well using an Opera High-Content Screening System (Perkin Elmer). A 20x or 40x magnification lens was used and images were taken at non-saturating conditions. Images were segmented using DAPI or Hoechst 33342 signals to generate masks matching cell nuclei, from which mean intensity signals for the used markers were

calculated with the Acapella Imaging software (Perkin Elmer). Data were represented with the use of the Prism software (GraphPad Software).

3. Molecular biology

3.1. Southern blotting

15ug of DNA per sample were digested with an appropriate restriction enzyme for 12h at 37°C in a solution containing digestion buffer, BSA 0,1mg/ml and spermidine 2,5mM. Digested DNA was separated by electrophoresis in a 0,8% agarose gel at 40V for 12h. The gel was incubated in a 0,25M HCl solution for 15', washed with distilled water and incubated in denaturing solution containing NaOH 0,4M and 0,6M NaCl for 45'. Following a wash with distilled water it was incubated in 0,5M Tris-HCl pH 7,5, 1,5M NaCl neutralizing solution for 30'. DNA was transferred by diffusion in SSC10x to a Hybond N+ nylon membrane (Hybond-XL, GE Healthcare) during at least 12 hours. UV light (Stratalinker, Stratagene, Agilent Technologies) was used to crosslink DNA to the membrane. Membrane was incubated for 2h at 65ºC in hybridizing solution (0,25m sodic phosphate pH7,2, 1mM EDTA, 1% BSA, 7% SDS, 0,05 mg/ml salmon sperm (Invitrogen)). Radioactive labeling of the probe was performed as follows: 20ng of DNA probe were dissolved in a final volume of 45ul TE buffer and the probe was denatured at 99°C. [α-32P] dCTP incorporation reaction was performed with the Random Prime System Kit (Stratagene) following manufacturer's instructions, and radiolabeled probe was purified in a Sephadex G-50 Column (ProbeQuant, GE Healthcare). Probe was added to the hybridizing solution with the membrane, and incubated overnight at 65°C. The membrane was washed twice in SSC 2x 1% SDS for 20' and once in SSC 0,2x, 0,1% SDS for 20'. Phosphor screens were exposed to membranes for 2 to 24h and scanned with a Phosphorimager (Storm 820; Molecular Dynamics).

3.2. Western blotting

For total protein extracts, cells were washed once with PBS and lysed with RIPA buffer (Tris-HCl 50 mM, pH 7.4, NP-40 1%, Na-deoxycholate 0.25%, NaCl: 150 mM, EDTA 1 mM) containing protease and phosphatase inhibitors (Sigma) or with a buffer containing 50 mM Tris (pH 7.5), 8 M urea, and 1% 3-[(3-cholamidopropyl)-dimethylammonio]-1-propanesulfonate (CHAPS). Sub-cellular fractionation extracts were obtained as follows: harvested cells were washed twice with ice-cold PBS, resuspended in 180 µl of ice-cold hypotonic lysis buffer

(HEPES 10 mM pH 7.9, KCl 10 mM, EDTA 0.1 mM containing protease and phosphatase inhibitors), and incubated on ice for 10', followed by addition of 20 µl of Nonidet P-40; after 3' at room temperature, cells were vortexed and the cytosolic fraction was obtained by centrifugation for 5' at 2,500 × g and collection of the supernatant. The nuclear pellet was resuspended in 60 µl of high-salt-concentration extraction buffer (20 mM HEPES, pH 7.9, 0.4 M NaCl, 1 mM EDTA containing protease and phosphatase inhibitors) and incubated with shaking at 4°C for 1 h. The nuclear extract was centrifuged for 5' at 16,000 × g and the supernatant (nuclear soluble fraction) stored at −80°C. A volume of (Tris 50mM pH 7.9, urea 8M, Chaps 1%) was added to the pellet and incubated with shaking at 4ºC for 30' . Chromatin-bound fraction was obtained by centrifuging for 5' at 16,000 × g and collecting the supernatant. Samples were resolved by SDS-PAGE and analyzed by standard Western blotting techniques. Protein blot analyses were performed on the LICOR platform (Biosciences).

3.3. Proteomic analysis

Cell pellets were extracted and proteins were digested using the FASP protocol (Wisniewski et al., 2009). Peptides were labelled with 8-plex iTRAQ reagents and samples were pooled. The complex mixture was subjected to IEF fractionation and separation by on-line nano-LC, and fractions were analyzed by electrospray MS/MS using a LTQ Orbitrap Velos mass spectrometer (Thermo Scientific). Raw files were searched against SwissProt mouse database (23993 entries) using Sequest-HT as the search engine through the Proteome Discoverer 1.4 (Thermo Scientific) software. Peptides were filtered by Percolator at 1% FDR using the target-decoy strategy.

3.4. Quantitative RT-PCR

Total RNA was extracted with Absolutely RNA Miniprep Kit (Agilent) and quantitative RT-PCR was performed with Superscript III Platinum One Step qRT-PCR system (Invitrogen) following manufacturer's instructions.

3.5. DRIP-qPCR

DRIP analysis was performed as described (Ginno et al., 2012). In brief, 5×10^6 cells were collected, washed with PBS, resuspended in 1.6ml of Tris-EDTA (TE) buffer and treated overnight with 41.5µl of 20% SDS and 5µl of proteinase K (Roche). DNA was extracted gently with phenol–chloroform. Precipitated DNA was spooled on a glass rod, washed with 70%

ethanol, resuspended gently in TE and digested overnight with 50U of HindIII, EcoRI, BsrGI, XbaI and SspI, 2mM spermidine and BSA. As negative control, half of the DNA was treated overnight with 3µl of RNase H (M0297; New England BioLabs). Digested DNA (5µg) was bound overnight to 10µl of S9.6 antibody (1mg/ml) in 500µl of binding buffer (10mM NaPO4, 140mM NaCl, 0.05% Triton X-100) at 4°C. DNA–antibody complexes were immunoprecipitated for 2h with Dynabeads Protein A (Invitrogen) at 4°C and washed three times with binding buffer. DNA was eluted with 50mM Tris-HCl pH8.0, 10mM EDTA, 0.5% SDS, then treated for 45' with 7µl of proteinase K at 55°C and cleaned with phenol–chloroform. qPCR was performed at the indicated regions (APOE, RPL13A, ERG1 and SNRPN genes on human cells, and AIRN gene on mouse cells). Primer sequences are indicated at the PCR primer table. The signal intensity plotted is the relative abundance of DNA–RNA hybrid immunoprecipitated in each region, normalized to input values and to the signal at the SNRPN negative control region (in human cells). All experiments were performed in triplicate and average and standard deviation of results are provided.

3.6. PCR Primers

Primer name	Sequence (5'→3')
Pre-GT –forward	ATGGGCTTCTTGGAATGTTG
Pre-GT – reverse	TGACAGCCTGCTCTTCATTG
Post-GT –forward	AATGCCAATGTGTTTGACGA
Post-GT – reverse	GCAATCTTCGCTTCCAGTTC
GAPDH – forward	GCCACCCAGAAGACTGTGGATGGC
GAPDH – reverse	CATGATGGCCATGAGGTCCACCAC
45S-forward	GAACGGTGGTGTGTCGTT
45S-reverse	GCGTCTCGTCTCGTCTCACT
18S-5'-jucntion- forward	GCCGCGCTCTACCTTACCTACCT
18S-5'-jucntion- reverse	CAGACATGCATGGCTTAATCTTTG
18S-3'-jucntion- forward	AGTCGTAACAAGGTTTCCGTAGGT
18S-3'-jucntion- reverse	CCTCCGGGCTCCGTTAAT
5.8S-5'-jucntion- forward	TACGACTCTTAGCGGTGGATCA
5.8S-5'-jucntion- reverse	TCACATTAATTCTCGCAGCTAGCT
5.8S-3'-jucntion- forward	GAATTGCAGGACACATTGATCATC
5.8S-3'-jucntion- reverse	GGCAAGCGACGCTCAGA

28S-5'-jucntion- forward	CCGAGACGCGACCTCAGAT
28S-5'-jucntion- reverse	TCCGCTGACTAATATGCTTAAATTCA
18S- forward	GATGGTAGTCGCCGTGCC
18S- reverse	GCCTGCTGCCTTCCTTGG
5.8S- forward	ACTCGGCTCGTGCGTC
5.8S- reverse	GCGACGCTCAGACAGG
28S- forward	GTGACGCGCATGAATGGA
28S- reverse	TGTGGTTTCGCTGGATAGTAGGT
APOE- forward	CCGGTGAGAAGCGCAGTCGG
APOE- reverse	CCCAAGCCCGACCCCGAGTA
RPL13A- forward	GCTTCCAGCACAGGACAGGTAT
RPL13A- reverse	CACCCACTACCCGAGTTCAAG
EGR1- forward	TTCGGATTCCCGCAGTGT
EGR1- reverse	TCACTTTCCCCCCTTTATCCA
SNRPN- forward	TGCCAGGAAGCCAAATGAGT
SNRPN- reverse	TCCCTCTTGGCAACATCCA
AIRN1- forward	GCTGCCTGGCTGATAGACTGTT
AIRN1- reverse	TGCCCACTGCTCTTCAGGTT
AIRN2- forward	TGTGGTTGCTGGGAATTGAA
AIRN2- reverse	GCTCAGCGGTTAAGAGCATTG

3.7. RNA sequencing

RNA integrity numbers were in the range 9.1-10 when assayed on an Agilent 2100 Bioanalyzer. PolyA-positive fraction was purified and randomly fragmented, converted to double stranded cDNA and processed through subsequent enzymatic treatments of end-repair, dA-tailing, and ligation to adapters as in Illumina's "TruSeq Stranded mRNA Sample Preparation Part # 15031047 Rev. D". Adapter-ligated library was completed by PCR with Illumina paired-end primers (8 cycles). The resulting purified cDNA library was applied to an Illumina flow cell for cluster generation and sequenced on an Illumina HiSeq2500 instrument by following manufacturer's protocols. For the generation of UCSC gene expression tracks, sequencing reads were aligned to human reference transcriptome build mm9 from UCSC using TopHat (v 2.0.10) (Trapnell, Pachter e Salzberg, 2009). Mapped transcripts were uploaded into UCSC genome browser for visualization. For this purpose the corresponding "accepted_hits.bam" result files were pretreated with SAMtools sort and index scripts.

3.8. Northern blotting

Total RNA was extracted with Absolutely RNA Miniprep Kit (Agilent). RNA extracts (5 μg/well) were separated on a 1% agarose gel prepared with NorthernMax® Denaturing Gel Buffer (Ambion) containing 1.2% formaldehyde and run in NorthernMax® Running Buffer (Ambion) at 90 V. RNAs were transferred to a Hybond N+ nylon membrane (GE Healthcare) and fixed by UV cross-linking. Membranes were prehybridized for 1 h at 45°C in hybridization buffer containing 6× SSC, 5× Denhardt's solution, 0.5% SDS and 1μg/ml salmon sperm DNA. The oligodeoxynucleotide probe was labeled with [γ-32P] ATP and incubated overnight on the membrane with hybridization buffer at 45°C. After hybridization, membranes were washed twice for 10' at room temperature in 2× SSC with 0.1% SDS and once in 1× SSC with 0.1% SDS. Phosphor screens were exposed to membranes and scanned with a phosphorimager (Storm 820; Molecular Dynamics). Hybridization probe sequences were P1 (5'-acgccgccgctcctccacagtctcccgtt-3') and P2 (5'-acccaccgcagcgggtgacgcgattgatcg-3'), described in (Wang et al., 2014).

4. Antibodies

Antibodies against Chk1 (NCL, Novocastra), phospho-S345-Chk1 (2348S, Cell Signaling), Rpa32 (2208, Cell Signaling), phospho-S4/8-Rpa32 (A300-245A, Bethyl), γH2AX (05-636, Millipore), Rad51 (sc-8349, Santa Cruz), H2A (#3636, Cell Signaling), IgG1 (553401, BD Pharmingen), EWS (sc-6533 and sc-28327; Santa Cruz), FLI1 (sc-356, Santa Cruz), Nucleophosmin (3542, Cell Signaling), Fibrillarin (2639, Cell Signaling), S9.6 (kind gift from D. Koshland), α-actin (Sigma) and Cdk2 (sc-163, Santa Cruz) were used.

RESULTS

PART I: Reducing the toxicitity of RS in mice

One focus of interest in our lab is the molecular basis of RS, and we aim at understanding how different factors mediate a cellular response when fork stalling is induced. One of the first symptoms of RS upon exposure to HU is the accumulation of ssDNA-RPA at stalled replication forks, which is used by the cell machinery as a signaling platform to trigger the RSR (Byun et al., 2005; Zeman and Cimprich, 2014).

RS is toxic for cells, one of its outcomes being cell death. In the lab we were interested in identifying RS mediator proteins. In this regard, work at the lab of Claus Sorensen suggested a possible candidate. They showed that cells depleted from FBH1 failed to accumulate ssDNA-RPA after HU treatment (Fugger et al., 2009). However, cell proliferation was largely unaffected, indicating that absence of ssDNA was not a mere reflection of proliferation arrest, and that FBH1 is not required for normal proliferation. Furthermore, FBH1-depleted cells showed a better survival and reduced cell death in response to HU (Fugger et al., 2013; Jeong et al., 2013b). Consistently, deleterious mutations in the *FBH1* gene were enriched in melanoma cell lines (Jeong et al., 2013a).

Provided that RS leads to cancer and ageing (Lecona and Fernandez-Capetillo, 2014), an organism with reduced RS levels should be protected from tumorigenesis and/or ageing. This rationale has been demonstrated *in vivo* by the use of transgenic alleles for overexpression of RS-protective factors in mice. An extra Chk1 allele prolongs the survival of *ATR*^{seckel} mice, which suffer from RS (Lopez-Contreras et al., 2012). Similarly, extra Rrm2 gene dosage (a rate-limiting component of the RNR complex, responsible for nucleotide synthesis) extends the lifespan of *ATR*^{seckel} mice and limits CFS breakage (Lopez-Contreras et al., 2015). We hypothesized that if FBH1 is a bona-fide promoter of RS, mice suffering from RS might benefit from lacking FBH1.

1. Generation of an FBH1-deficient mouse strain

To evaluate the *in vivo* function of FBH1 we generated an *Fbh1* gene-trapped allele (*Fbh1*^{GT}; Figure 10A). A construct carrying a gene-trapping cassette was used to target the endogenous

Fbh1 locus in mouse embryonic stem cells and neomycin-resistant clones were screened by southern blotting to search for recombinant clones (Figure 10B). Selected clones were used for embryonic stem cell aggregation and generation of chimeras, from which a mouse colony was established. The efficiency of the gene trapping was assessed by measuring expression levels of FBH1 mRNA in primary mouse embryonic fibroblasts (MEF) and in B-cells (Figure 10C). Depletion of mRNA was almost complete downstream of the gene trapping cassette as assessed by the corresponding primer set pair ("Post-GT"), showing a down regulation of around 98-99%. Remarkably, a primer set pair upstream of the gene trapping ("Pre-GT") detected decreased mRNA content in the *Fbh1*$^{GT/GT}$ samples, which might be explained by instability of the truncated mRNA.

Birth ratios showed the expected mendelian distribution (Figure 10D). Adult *Fbh1*$^{GT/GT}$ mice showed a mild decrease in weight that did not reach statistical significance (p value=0.052; n=8 *Fbh1*$^{+/+}$ and 15 *Fbh1*$^{GT/GT}$ mice; Figure 10E). Both males and females were fertile, looked healthy overall, and their lifespan was unaffected (Figure 10F).

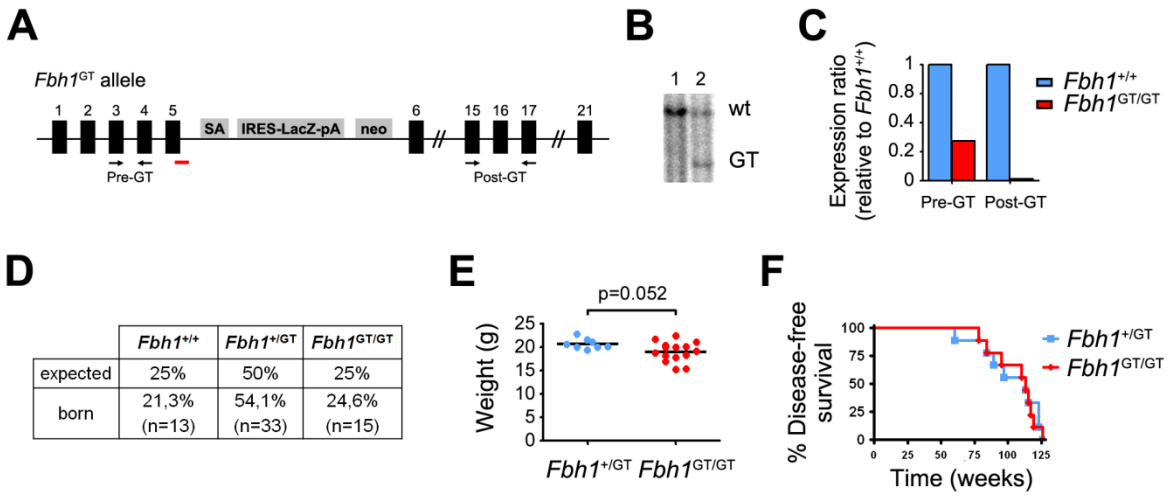

Figure 10
Fbh1 deletion results in viable mice. (A) The *Fbh1* gene-trapped allele is depicted. A splice acceptor (SA) cassette followed by a polyadenilation signal (pA) interrupt the expression of FBH1 protein at the mRNA level. (B) Southern blot for detection of recombinant ES cell colonies after electroporation with the targeting construct. A probe against the 5' homology arm, mapping to the red-labelled locus in (A) was used. Lane 1, wild-type clone; lane 2, recombinant heterozygous clone. (C) Efficacy of the gene trapping was evaluated by quantitative RT-PCR with a primer set upstream of the gene-trapping cassette and a primer set downstream (Pre-GT and Post-GT; primers depicted as black arrows in (A)) Data is representative of three independent analyses. (D) Expected and obtained birth ratios of *Fbh1*$^{+/+}$, *Fbh1*$^{+/GT}$ and *Fbh1*$^{GT/GT}$ mice. (E) Weights of *Fbh1*$^{+/+}$ (n=8) and *Fbh1*$^{GT/GT}$ (n=15) mice. (F) Kaplan-Meyer representation of the lifespan of *Fbh1*$^{+/GT}$ (n=7) and *Fbh1*$^{GT/GT}$ (n=8) mice.

2. Phenotypical characterization of *Fbh1*$^{GT/GT}$ mouse cells

Next we characterized the mouse strain at the cellular level. Previous studies using human cell lines showed attenuated signalling in FBH1-depleted cells in response to RS, including reduced RPA phosphorylation and γH2AX, along with an increased survival after RS (Fugger et al., 2013; Fugger et al., 2009; Jeong et al., 2013b). We cultured mouse-derived primary cells and subjected them to HU treatment. Both RPA phosphorylation (Figure 11A) and γH2AX (Figure 11B) were reduced in *Fbh1*$^{GT/GT}$ cells. However, we did not observe an increase in cell survival or any alteration in cell-cycle phase distribution in untreated, HU-treated or ATR inhibitor-treated *Fbh1*$^{GT/GT}$ cells (Figure 11C). Response to ionizing radiation (IR) was also unaltered (Figure 11C).

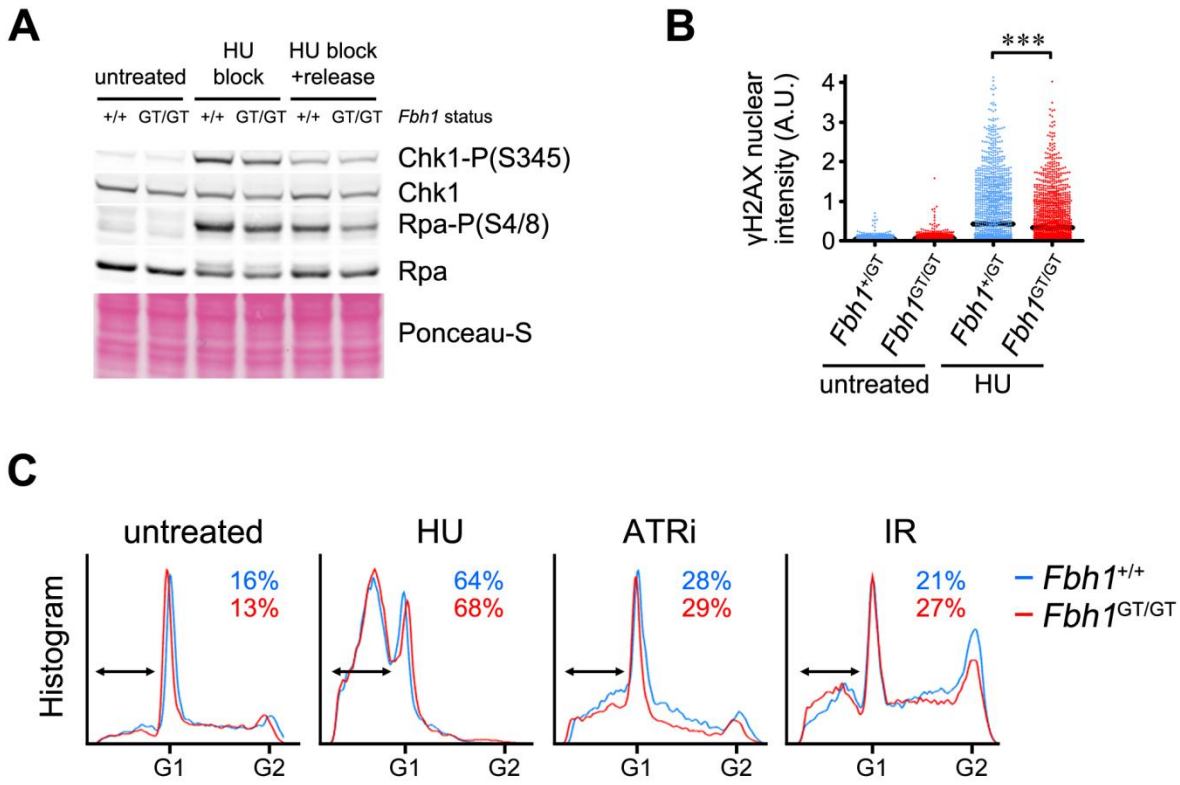

Figure 11
FBH1 contributes to signaling RS. (A) *Fbh1*$^{+/+}$ and *Fbh1*$^{GT/GT}$ embryonic stem cells were cultured and treated with HU 1mM for 4 hours and collected immediately or after a release into fresh media for 2-hour recovery. Cell extracts were immunoblotted with the indicated antibodies. (B)) *Fbh1*$^{+/+}$ and *Fbh1*$^{GT/GT}$ MEF derived from littermate embryos were treated with HU 2mM for 4 hours, stained with anti-γH2AX and quantified by high-throughput microscopy (HTM). (C) Primary B cells from) *Fbh1*$^{+/+}$ and *Fbh1*$^{GT/GT}$ 8 week-old male littermates were stimulated with LPS and CD180. 24 hours after stimulation cells were treated with HU 0.5 mM or ATR inhibitor (ATRi) 0.5 μM for 24 additional hours, or subjected to 4 Gy ionizing radiation (IR) and left in culture for 24 hours. Cells were fixed and stained with propidium iodide (PI) and cell cycle profiles were analyzed. Percentage values of sub-G1 populations, corresponding to cell death (regions labeled by arrows), are indicated. Data are representative of two independent experiments.

Altogether, whereas we observed lower HU-induced γH2AX and RPA phosphorylation in *Fbh1*$^{GT/GT}$ MEF and ES cells, B cells showed no alterations in sensitivity towards HU, ATRi or IR. We speculated that *Fbh1*$^{GT/GT}$ mice might have a subtle phenotype which could be unmasked upon conditions of high RS. Similarly to rescue of the lifespan of *ATR*$^{S/S}$ mice by overexpression of RS-protective factors Chk1 or Rrm2 (Lopez-Contreras et al., 2012; Lopez-Contreras et al., 2015), we wondered wether deletion of FBH1 might rescue the phenotypes of *ATR*$^{S/S}$ mice to some extent.

3. Impact of FBH1 deficiency on ATR mutant mice

To investigate whether *Fbh1* deletion could have a more profound impact in the presence of RS, we took advantage of a mouse model of *ATR*^{Seckel} previously developed at our lab (Murga et al., 2009). This model has hypomorphic levels of ATR and suffers from extensive RS and apoptosis during embryonary development, which translates into sublethality at birth, a growth defect and premature ageing. Following the hypothesis exposed above, if FBH1 mediates accumulation of RS, deletion of *Fbh1* in *ATR*$^{S/S}$ mice might rescue its lethality and phenotypes.

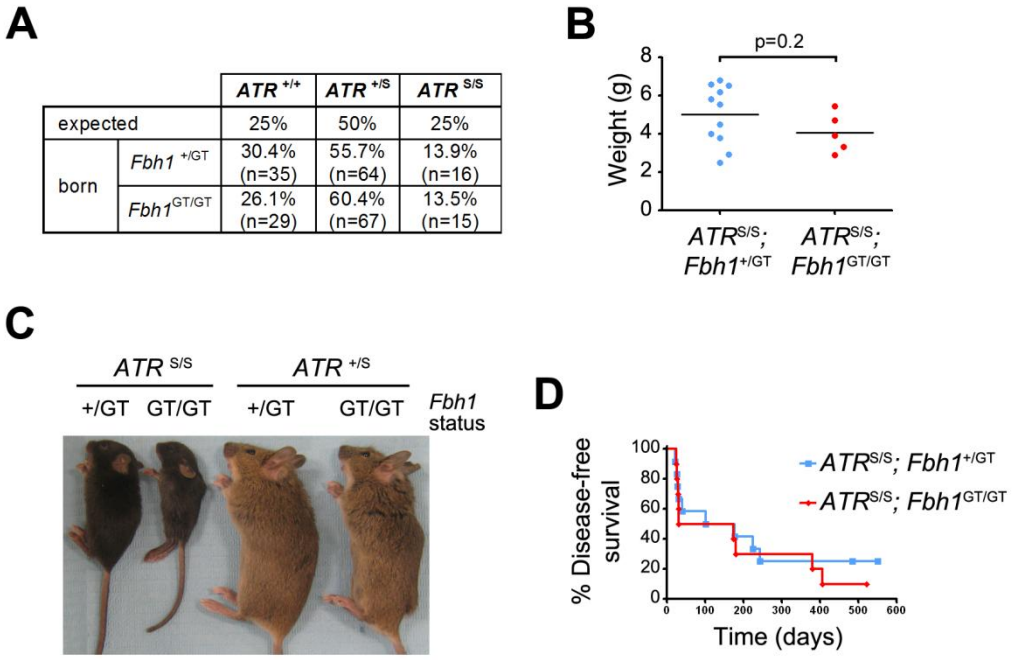

		ATR +/+	ATR +/S	ATR S/S
expected		25%	50%	25%
born	Fbh1 +/GT	30.4% (n=35)	55.7% (n=64)	13.9% (n=16)
	Fbh1 GT/GT	26.1% (n=29)	60.4% (n=67)	13.5% (n=15)

Figure 12
Fbh1 deletion further aggravates the phenotypes derived from excessive RS in *ATR*$^{S/S}$ mice. (A) Expected and obtained birth ratios of *ATR*$^{+/+}$, *ATR*$^{+/s}$ and *ATR*$^{s/s}$ mice in *Fbh1*$^{+/GT}$ or *Fbh1*$^{GT/GT}$ backgrounds. (B) Weights of *Fbh1*$^{+/GT}$ (n=11) and *Fbh1*$^{GT/GT}$ (n=5), *ATR*$^{s/s}$ 8-week-old mice. (C) Representative picture of four 4-week-old female littermates. (D) Kaplan-Meyer representation of the lifespan of *Fbh1*$^{+/GT}$ (n = 12) and *Fbh1*$^{GT/GT}$ (n = 10), *ATR*$^{s/s}$ mice.

We generated a cohort of *Fbh1*$^{+/GT}$; *ATR*$^{S/S}$ and *Fbh1*$^{GT/GT}$; *ATR*$^{S/S}$ mice and analyzed their phenotypes. Submendelian birth ratios characterystical of *ATR*$^{S/S}$ mice were not rescued by deletion of *Fbh1* (Figure 12A). Instead, if anything, dwarfism was further aggravated: *Fbh1*$^{GT/GT}$; *ATR*$^{S/S}$ mice were 20% smaller than their *Fbh1*$^{+/GT}$; *ATR*$^{S/S}$ counterparts (Figure 12B) although this did not reach statistical significance (p value=0.2). Figure 12C shows a representative litter with 4 female littermates at the age of 4 weeks. In spite of that, mean lifespan of *Fbh1*$^{GT/GT}$; *ATR*$^{S/S}$ mice was unaltered compared to corresponding counterparts (Figure 12D).

Together, we conclude that deletion of *Fbh1* does not have an overall contribution to suppress RS-derived toxicity; on the contrary, if anything, it seems to aggravate the phenotype of *ATR*$^{S/S}$ mice, suggesting that FBH1 might act in signaling a response downstream of RS, rather than promoting RS itself.

4. Role of FBH1 in HR

FBH1 was proposed as an ortholog of canonical yeast anti-recombinase Srs2 (Chiolo et al., 2007), and several works in the field support an anti-recombinase role for FBH1 at collapsed forks (Chiolo et al., 2007; Fugger et al., 2009; Kohzaki et al., 2007; Lorenz et al., 2009; Morishita et al., 2005; Osman et al., 2005). Furthermore, recent work by Ian Hickson and colleagues revealed a direct interaction between RAD51 and FBH1. RAD51 binds ssDNA in competition with RPA (Liu et al., 2010) and forms a nucleoprotein filament that has a central role in HR-mediated DSB repair. Hickson and colleagues showed that FBH1 negatively regulates RAD51 by displacing it from ssDNA through its helicase-translocase activity, which in FBH1-mutant cells results into an increase of chromatin-bound RAD51 (Simandlova et al., 2013). To assess the degree of RAD51 binding to chromatin in our model we subjected proliferating B-cells to sub-cellular fractionation. However, chromatin-bound level of RAD51 in *Fbh1*$^{GT/GT}$ cells was not altered, either in untreated cells or in cells treated with Mitomycin C (a potent DNA crosslinker that induces fork stalling and DSB generation) (Figure 13A). It has also been proposed that FBH1 ubiquitylates RAD51 by means of its E3 ligase activity, and promotes RAD51 degradation as a regulatory mechanism. However, *Fbh1*$^{GT/GT}$ cells did not show increased RAD51 total levels in 3 different cell types or tissues (Figure 13B).

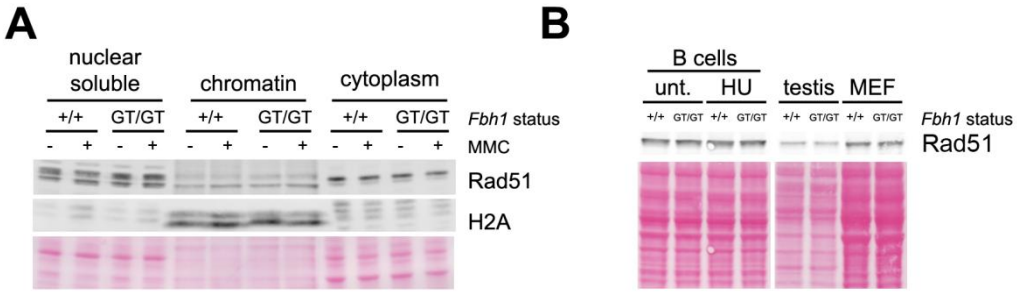

Figure 13
Rad51 binding to chromatin or total levels are unaltered in *Fbh1*$^{GT/GT}$ cells. (A) Sub-cellular fractionation and immunoblotting of primary B cell extracts from *Fbh1*$^{+/+}$ and *Fbh1*$^{GT/GT}$ 8 week-old male littermates, 48 hours after stimulation. Cells were left untreated or subjected to 250 nM mitomycin C (MMC) for 4 hours before processing. Antibodies used are indicated. (B) Total protein extracts of primary B cells, mouse testis and primary MEF were immunoblotted for Rad51 total levels.

In spite of these results we aimed at testing the putative anti-recombinase function of FBH1 *in vivo*. We speculated that depletion of FBH1 might alleviate phenotypes of mice that have a deficient HR. For this we used a mouse model with mutant BRCA1. BRCA1 is a pro-recombinase factor; the *Brca1*$^{\Delta 11}$ allele lacks exon 11, and deficient BRCA1 activity leads to impaired HR which causes embryonic lethality and severe cellular phenotypes, including premature senescence and chromosomal instability. These deficiencies are suppressed by deletion of 53BP1 (Bouwman et al., 2010; Bunting et al., 2010; Cao et al., 2009), and based on this 53BP1 was initially proposed to be an anti-recombinase. In our aim to prove an anti-recombinase role for FBH1, we wondered wether deletion of *Fbh1* would mimick 53BP1 in rescuing the *Brca1*$^{\Delta 11/\Delta 11}$ mouse phenotypes.

Brca1$^{\Delta 11/\Delta 11}$ mice succumb at a late stage of embryogenesis and very rarely reach birth. We expected that a rescue by *Fbh1* deletion might translate into an increase in birth rate of *Brca1*$^{\Delta 11/\Delta 11}$; *Fbh1*$^{GT/GT}$ mice. However we did not observe this, as embryo lethality was not significantly altered (Figure 14A). Next we assessed the proliferative potential of *Brca1*$^{\Delta 11/\Delta 11}$; *Fbh1*$^{GT/GT}$ MEF compared to that of *Brca1*$^{\Delta 11/\Delta 11}$; *Fbh1*$^{+/GT}$ counterparts. However, and consistent with the previous result, premature senescence of *Brca1*$^{\Delta 11/\Delta 11}$ MEF was not rescued by deletion of *Fbh1* (Figure 14B). Finally we looked at the status of genomic instability in our model by analyzing rates of breakage and chromosomal aberrancies in metaphase spreads, but again, *Fbh1* deletion did not alter the degree of genomic instability characteristic of *Brca1*$^{\Delta 11/\Delta 11}$ cells (Figure 14C).

The actual mechanism by which 53BP1 competes with BRCA1 and limits HR is not by directly impairing HR, but instead it acts in deviating the repair of a DSB towards the NHEJ pathway before the DSB is committed to HR (Bouwman et al., 2010; Bunting et al., 2010; Cao et al.,

2009). This is evidenced by a repair defect in 53BP1$^{-/-}$ B-cells during immunoglobulin class-switching (CSR), a process that relies on NHEJ to join distant DSB ends and generate new immunoglobulin classes. Analogously to 53BP1, we wanted to test whether FBH1 actually had a pro-NHEJ function. To assess this we subjected proliferating B-cells to stimulation with IL4 and measured rates of class-switching to IgG1. However, no class-switching defect was observed in *Fbh1*$^{GT/GT}$ cells (Figure 14D). Taken together, FBH1 *in vivo* does not negatively regulate Rad51 levels or binding to chromatin, and it does not oppose an HR-promoting factor such as BRCA1 at the organism level.

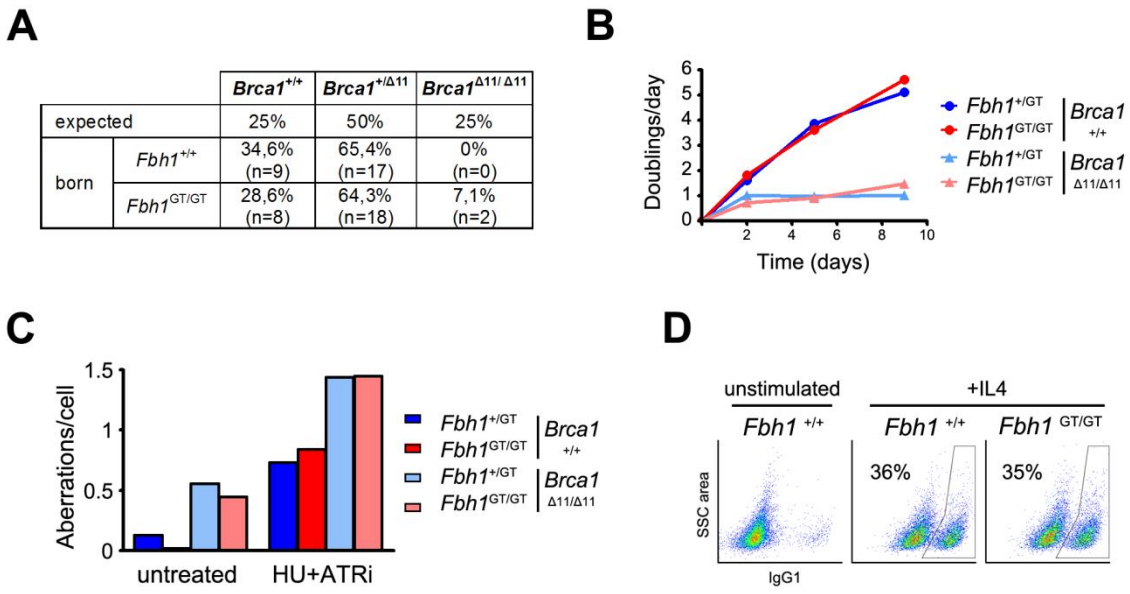

		Brca1$^{+/+}$	Brca1$^{+/\Delta 11}$	Brca1$^{\Delta 11/\Delta 11}$
expected		25%	50%	25%
born	Fbh1$^{+/+}$	34,6% (n=9)	65,4% (n=17)	0% (n=0)
	Fbh1$^{GT/GT}$	28,6% (n=8)	64,3% (n=18)	7,1% (n=2)

Figure 14
FBH1 does not show an anti-recombinase role. (A) Expected and obtained birth ratios of *Brca1*$^{+/+}$, *Brca1*$^{+/\Delta 11}$ and *Brca1*$^{\Delta 11/\Delta 11}$ mice in *Fbh1*$^{+/+}$ or *Fbh1*$^{GT/GT}$ backgrounds. (B) Growth curves of *Fbh1*$^{+/GT}$ and *Fbh1*$^{GT/GT}$ MEF in *Brca1*$^{+/+}$ *or Brca1*$^{\Delta 11/\Delta 11}$ backgrounds. (C) Analysis of breakage and aberrations in *Fbh1*$^{+/GT}$ and *Fbh1*$^{GT/GT}$ MEF metaphases in a *Brca1*$^{+/+}$ *or Brca1*$^{\Delta 11/\Delta 11}$ background. Data are representative of 2 independent experiments. (D) Class-swithching to IgG1 in primary B cells from *Fbh1*$^{+/+}$ and *Fbh1*$^{GT/GT}$ 8 week-old male littermates after stimulation with IL4 during 96 hours. Percentages of IgG1-positive populations are indicated. Data are representative of 2 independent experiments.

Overall, we could not demonstrate an RS-promoting role for FBH1, as its deletion did not protect cells or mice from RS. As opposed to previous results by other groups, the effects of *Fbh1* deletion *in vivo* are very mild. In regards to an HR-regulatory role, no impact of *Fbh1* deletion on the regulation of RS-derived HR was observed either. Therefore, the contribution of murine FBH1 to the RSR at the organism level remains elusive.

PART II: Exploring the role of RS in cancer and age-related diseases

1. Targeting RS as a strategy to treat cancers

We have previously reported that tumor types with high RS are specially dependent on a proficient RSR, and inhibiting ATR or CHK1 in these tumors efficiently abrogates tumoral growth (Murga et al., 2011; Schoppy et al., 2012).

Work in our lab demonstrated that the process of tumoral transformation generates RS, and that an extra allele of CHK1 reduces RS levels during this process, thereby facilitating transformation (Lopez-Contreras et al., 2012; Schulze et al., 2014). Accordingly, tumors tend to gain CHK1 expression levels in order to protect themselves from the RS arising during transformation and tumoral growth (Bartek et al., 2012; Sarmento et al., 2014). Based on this, we used CHK1 expression levels as a surrogate marker for RS, and interrogated the Cancer Cell Line Encyclopedia (CCLE) on CHK1 expression levels across different human tumoral cell lines as a means to identify new tumor types that might be suitable to our strategy (Figure 15).

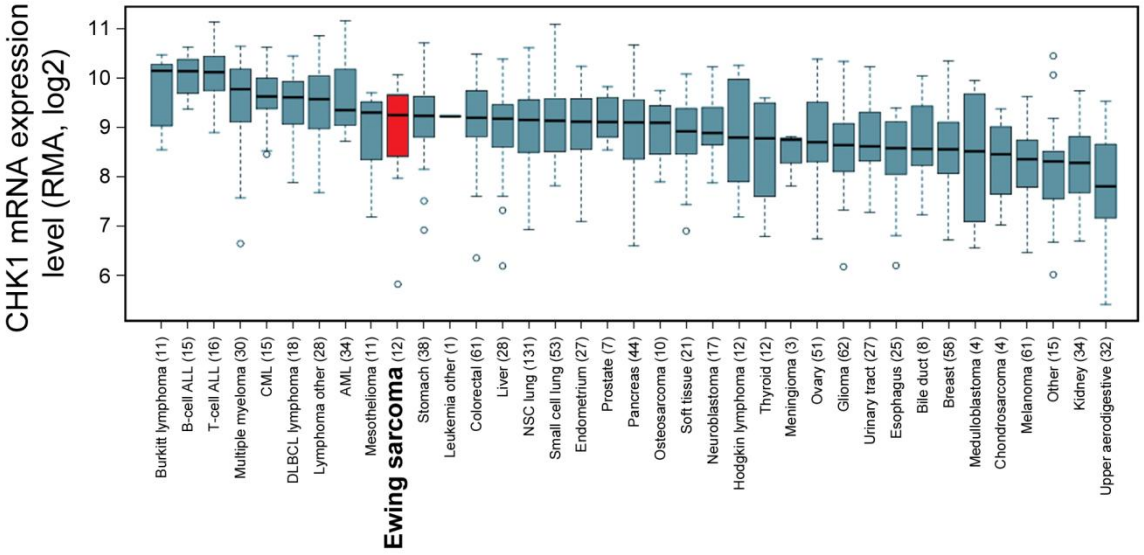

Figure 15
CHK1 expression levels across human tumoral cell lines. Ewing sarcoma is the second solid tumor with highest CHK1 expression levels, below mesothelioma. Above them, 8 hematologic tumors occupy the highest places in CHK1 expression across all human tumors. Gene expression data extracted from the Cancer Cell Line Encyclopedia (http://www.broadinstitute.org/ccle)

Expectedly, the tumor types with highest CHK1 levels were lymphomas and leukemias, which have been demonstrated to have high RS levels and hypersensitivity to inhibition of the RSR (Murga et al., 2011; Schoppy et al., 2012). Hematologic cancers aside, Ewing sarcoma is the second solid tumor type with highest RS (below mesothelioma). This matched our initial observation that the high degree genomic instability in Ewing sarcoma but low SNP and point mutation rate described for pediatric cancers were reminiscent of RS in Ewing sarcoma (Alexandrov et al., 2013; Ferreira et al., 2008; Ohali et al., 2004).

2. Ewing sarcoma-derived cell lines have RS and are sensitive to ATR inhibition

2.1. Ewing sarcoma cell lines have increased RS

To verify a signature of RS in Ewing sarcomas we used a panel of Ewing sarcoma cell lines (ES cell lines) and non-ES, osteosarcoma cell lines, as well as human primary cells. Consistent with CCLE data (Figure 15), ES cell lines present increased levels of CHK1 protein, and these correlate with increased γH2AX levels (Figure 16A). Whereas γH2AX is a common mark signalling different types of DNA damage, a specific pattern with pannuclear staining is characteristical of RS (Syljuasen et al., 2005; Toledo et al., 2011). To assess this we used a tissue

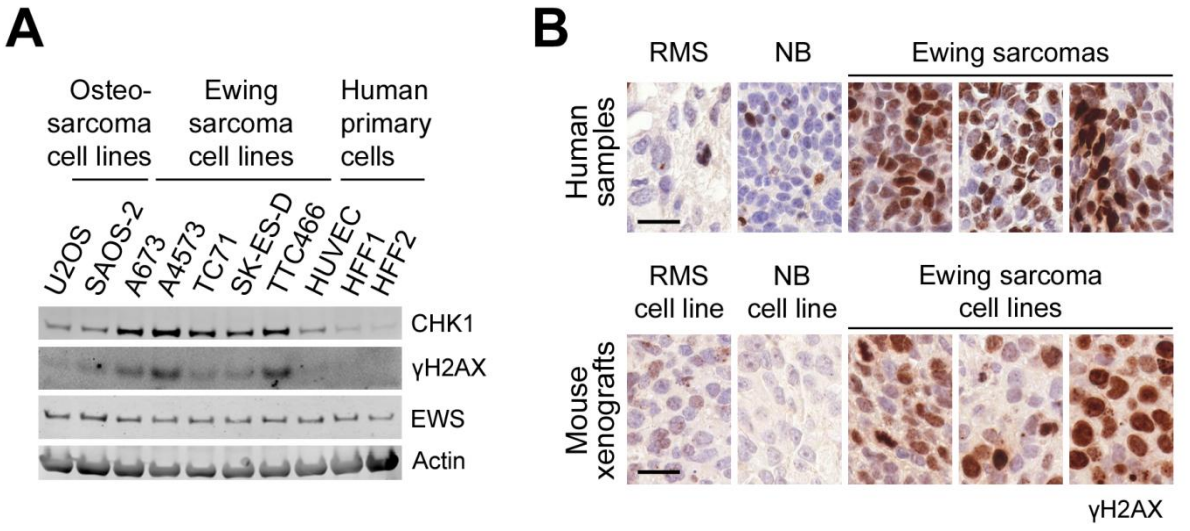

Figure 16
ES cell lines have increased RS. (A) Protein extracts from osteosarcoma cell lines, ES cell lines and human primary cells were immunoblotted with the indicated antibodies. (B) Immunohistochemistry for γH2AX staining was performed on human tumoral samples of rhabdomyosarcoma (RMS), neuroblastoma (NB) and Ewing sarcoma (upper panels); and on mouse xenografts generated with cell lines derived from human RMS (cell line SJRH), NB (cell line SKNAS) and Ewing sarcomas (cell lines A673, TC71, A4573) (lower panels). Scale bars, 20 μM.

microarray containing samples from Ewing sarcoma and non-Ewing sarcoma primary tumors, and a tissue microarray containing murine xenograft samples generated from ES and non-ES cell lines (Figure 16B). We observed not only an abundant γH2AX signal, but also a strong pannuclear staining pattern both in Ewing sarcoma primary tumors and in ES cell line-derived xenografts, consistent with RS. Because ES cell lines consistently showed a particular signature of RS, we wondered whether targeting the RSR in Ewing sarcomas could serve to selectively kill tumoral cells.

2.2. ES cell lines are hypersensitive to ATR inhibition

To test the efficacy of ATR inhibition in Ewing sarcoma we subjected ES cell lines and osteosarcoma cell lines to a prolonged treatment with vehicle or ETP-46464 (an ATR inhibitor developed in our lab in collaboration with the Experimental Therapeutics Unit at CNIO (Toledo et al., 2011); from now on, ATRi). Analysis of the cell cycle profiles showed a specific toxicity towards ES cell lines, which presented significative sub-G1 populations indicative of cell death, whereas osteosarcoma cell lines remained largely unaffected (Figure 17A).

Next we assessed the *in vitro* sensitivity of ES cell lines and control cells to ATR inhibition. Importantly, we assayed two independent ATR inhibitors: ATRi and AZ-20 (Astra Zeneca). We also assayed sensitivity to temozolomide (TMZ), one chemotherapeutic agent currently used in Ewing sarcomas, and to Olaparib (a PARP1 inhibitor), as ES cell lines were recently identified as being sensitive to PARP inhibition (Garnett et al., 2012) and Olaparib is now being explored as an alternative to TMZ (Brenner et al., 2012). We determined the 50% lethal dose (LD50) values for a panel of ES and non-ES sarcoma cell lines, as well as for primary cells, subjected to treatment with ATR inhibitors, Olaparib or TMZ (Figure 17B and C). Both ATR inhibitors were highly toxic to ES cells. ATRi showed LD50 values to ES cell lines more than 10-fold lower than to non-ES cell lines, and close to 1000-fold lower compared to primary human cells. LD50 for AZ-20 was over 4-fold lower in ES cells than in non-ES cancer cells, and around 10-fold lower compared to primary cells. Remarkably, whereas Olaparib was also toxic to ES cells, it was so within the micromolar scale. In contrast, both ATR inhibitors were effective at the nanomolar scale. Finally, for all cell lines, LD50 values to TMZ were out of the assayed dose range (3nM to 100μM) and above that, and we could only state LD50s being above 100μM for all cell lines. Therefore, we could not determine whether a preferential toxicity of TMZ exists towards ES cells.

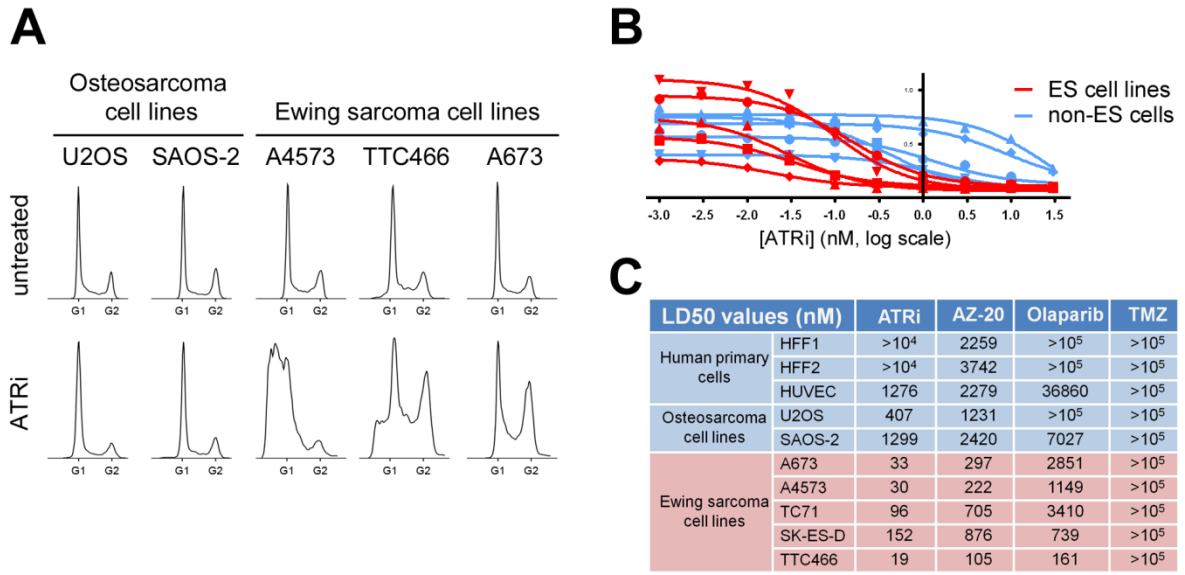

C

LD50 values (nM)		ATRi	AZ-20	Olaparib	TMZ
Human primary cells	HFF1	>10^4	2259	>10^5	>10^5
	HFF2	>10^4	3742	>10^5	>10^5
	HUVEC	1276	2279	36860	>10^5
Osteosarcoma cell lines	U2OS	407	1231	>10^5	>10^5
	SAOS-2	1299	2420	7027	>10^5
Ewing sarcoma cell lines	A673	33	297	2851	>10^5
	A4573	30	222	1149	>10^5
	TC71	96	705	3410	>10^5
	SK-ES-D	152	876	739	>10^5
	TTC466	19	105	161	>10^5

Figure 17
ES cell lines are hypersensitive to ATR inhibition. (A) ES cell lines and osteosarcoma cell lines were subjected to 150 nM ATR inhibitor (ATRi) treatment for 72h or left untreated. Cells were collected and processed for flow cytometry using propidium iodide as an indicator of DNA content. Cell cycle profiles are displayed. (B) Human primary cells (HuVEC, HFF1, HFF2; blue), osteosarcoma cell lines (U2OS, SAOS-2; blue) and ES cell lines (A673, A4573, TC71, SK-ES-D, TTC466; red) were treated with increasing concentrations of ATRi for 24h. A viability colorimetric assay based on cellular metabolic activity was used to calculate LD50 values for each cell line. Absorbance, proportional to cell viability, is plotted against ATRi concentration for each cell line. (C) The assay was repeated for AZ-20 (an independent ATR inhibitor), Olaparib (a PARP-1 inhibitor) and temozolomide (TMZ). LD50 values for all compounds are listed.

2.3. ATRi impairs tumor growth in Ewing sarcoma xenografts

Next we asked whether ATR inhibition would have an impact on tumoral growth *in vivo*. For this we injected A4573 ES cells subcutaneously to immunodeficient mice to generate ES xenografts, and treated mice with ATR inhibitors or vehicle. We used two independent ATR inhibitors: AZ-20 and MSC253, an *in vivo* derivative of ETP-46464 that has been licensed to Merck for clinical developments. Xenograft growth was greatly abrogated upon treatment with ATR inhibitors, most strikingly with MSC253, as depicted in Figure 18A. Representative tumours at day 11 after treatment initiation are shown (Figure 18B). Importantly, tumours treated with ATR inhibitors undergo massive accumulation of RS as evidenced by pannuclear γH2AX staining, which was evident in xenograft tissue sections taken 48 hours after treatment initiation (Figure 18C). Of note, chemotherapeutic treatments frequently consist of multiple drug combinations, and clinical/pre-clinical trials are addressed accordingly. The fact that ATR inhibitors (especially MSC253) efficiently abrogate tumoral growth as monotherapy suggests a great potential for an eventual translation into the clinics.

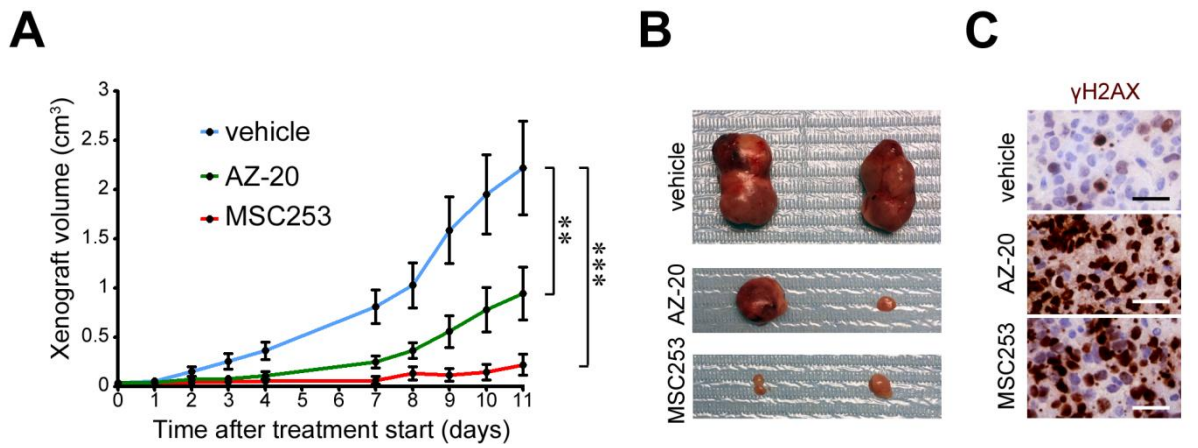

Figure 18
ATR inhibition abrogates tumoral growth of ES cell line-derived xenografts. (A) 1x10^6 cells from A4573 ES cell line were subcutaneously injected into immunodeficient (SCID) mice. As soon as tumors were palpable (around 50 mm^3) treatments with ATR inhibitors AZ20, MSC253, or vehicle were started. 50 mg/Kg of compound were administered 5 days per week (Monday to Friday) with an intragastric probe. Tumor sizes were measured daily with a caliper, and tumor volume was inferred through the formula (width*(length)^2)/2. Mean tumoral growth is plotted for each treatment group. Vehicle, n=7; AZ20, n=7; MSC253, n=7. (B) representative tumors from each group at day 11 after treatment start. (C) Tumoral tissue samples extracted at day 2 after treatment start and processed for IHC with anti-γH2AX. Scale bars, 30 μM.

Taken together, in sections 1 and 2 we learned that Ewing sarcomas suffer from high RS levels. Consistently, ES cell lines presented *in vitro* and *in vivo* sensitivity towards ATR inhibition. In the following sections we asked about the origin of RS in Ewing sarcomas.

3. Expression of EWS/FLI1 leads to RS and ATRi hypersensitivity

To verify that ATRi sensitivity was not a particularity of the ES cell lines in use, we asked whether expression of the translocation product EWS/FLI1 is sufficient to drive accumulation of RS and sensitization towards ATR inhibition. In a work mainly developed by Isabel Morgado at our lab, we used a transgenic mouse model for conditional expression of the EWS/FLI1 fusion protein (Figure 19A) (Lin et al., 2008), and we cultured wild-type (WT) and CRE-inducible *EWS/FLI1* (*EWS/FLI1*^{ind}) MEF, both expressing a CRE^{ERT2} recombinase dependent on hydroxytamoxifen (OHT) (Figure 19B). After induction with OHT, cell cycle profiles were analyzed. EWS/FLI1-expressing MEF showed an increase in the sub-G1 population compared to WT MEF, which evidenced a sensitization towards ATR inhibition, consistent with increased RS levels (Figure 19C). Interestingly, for other RS-inducing oncogenes such as MYC or H-RAS, acceleration of the replication rate has been described as the source of RS. Conversely, EWS/FLI1 expression did not promote acceleration of replication, rather the contrary (Figure 19D), thereby suggesting that EWS/FLI1 induces RS by other means different than acceleration of replication.

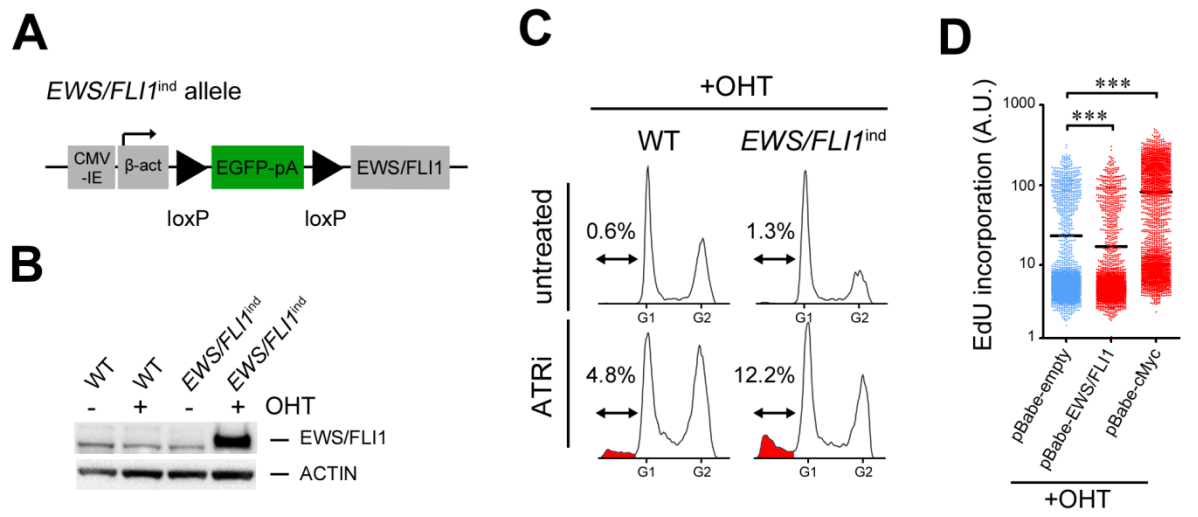

Figure 19
Expression of EWS/FLI1 leads to accumulation of RS and sensitizes to ATR inhibition. (A) Transgenic allele for inducible expression of EWS/FLI1. Adapted from (Lin et al., 2008). A chicken β-actin promoter and a CMV enhancer control expression of the transgene. An EGFP-polyA cassette prevents expression of EWS/FLI1. Upon CRE-mediated excision of the EGFP-polyA cassette, EWS/FLI1 expression is enabled. (B) Wild-type (WT) and transgenic (*EWS/FLI1*^{ind}) MEF, both expressing CRE^{ERT2}, where generated. Protein extracts with and without a 48h-induction with OHT were blotted for detection of EWS/FLI1 expression. (C) OHT-induced, WT and EWS/FLI1ind MEF were untreated or treated with ATRi 1μM for 48h. Cells were collected and processed for flow cytometry with propidium iodide staining. Cell cycle profiles are displayed and relative percentages of Sub-G1 populations (red) are indicated. (D) Wild-type MEF were infected with an empty vector(pBabe-empty), a vector for EWS/FLI1 expression (pBabe-EWS/FLI1) or a vector for c-Myc expression. 48h after infection cells were incubated with EdU for 30min and processed for HTM-mediated quantitative detection of EdU incorporation. All experiments were performed by Isabel Morgado. Data in B and C are representative of three independent experiments. In D, center lines indicate mean values. *, P < 0.05; **, P < 0.01; ***, P < 0.001.

4. EWS protein as a suppressor of RS

The EWS/ETS translocation event and its fusion product were postulated as drivers of tumorigenesis, based on the oncogenic activity described for EWS/FLI1 (May et al., 1993a; May et al., 1993b) and its direct alteration of the cellular expression pattern (Kauer et al., 2009; Riggi et al., 2008). Nonetheless, genetically, the translocation event also implies the truncation of *EWSR1* gene at the affected allele. Therefore two genetic modifications occur upon translocation: a) the generation of a novel fusion product and b) the loss of one copy of *EWSR1*. Because the latter might imply a loss of function of EWS, we wondered whether this has an actual contribution to the pathology of Ewing sarcoma. Furthermore, loss of function could be enhanced if considering a hypothetical dominant-negative effect of EWS/FLI1 over the remaining wild-type EWS protein, an idea that has already been suggested (Spahn et al., 2003).

In this context we wondered whether loss of EWS function, analogously to expression of EWS/FLI1, also results in accumulation of RS and sensitization to ATR inhibition; that is, if EWS has a protective role against RS (Figure 20). In fact, several evidence in the literature point to a role for EWS in genome surveillance; first, a knockout mouse model for *Ewsr1* phenotypically resembles the $ATR^{S/S}$ mouse (a mouse model of RS) in that both present craneofacial abnormalities, sub-lethality, reduced body weight and reduced lifespan (Li et al., 2007). Second, EWS depletion in germinal cells drives XY asynapsis, which is prevented by ATR. Third, EWS interacts with BARD1 which, in complex with BRCA1, is involved in the repair of broken replication forks to promote replication restart (Spahn et al., 2002). Fourth, EWS is required for resistance to CPT, a TopoI inhibitor that generates RS (O'Connell et al., 2010). To dissect the relative contributions of the two genetic contidions present in Ewing sarcoma, namely the EWS/ETS fusion product and EWS loss of function (Figure 20), we decided to generate a mouse model for the genetic deletion of *Ewsr1* gene.

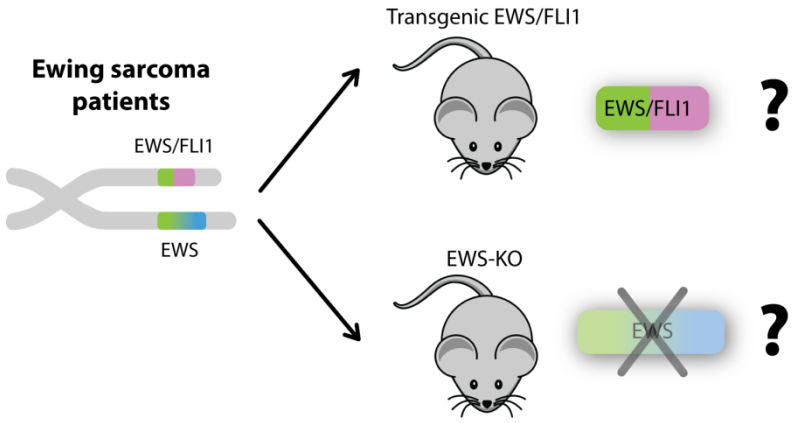

Figure 20
Dissecting the genetic contributions of EWS/FLI1 and EWS loss of function to Ewing sarcoma. Ewing sarcoma patients suffer a translocation between EWS and an ETS transcription factor (most frequently FLI1), resulting in two genetic conditions: gain of EWS/FLI1 fusion product and loss of EWS. We have used mouse models for expression of EWS/FLI1 and for deletion of EWS protein in order to dissect the contributions of the two genetic conditions to the phenotypes observed in Ewing sarcomas and in ES cell lines.

5. Generation of a mouse model for the deletion of *Ewsr1*

We used a "gene-trap first" construct from the European Consortium targeting the *Ewsr1* locus. The construct contained a floxed promoter-driven neo cassette and an IRES:lacZ trapping cassette inserted into intron 3 (Figure 21A). The splice acceptor (SA) and the IRES:LacZ-polyA disrupts gene function and promotes early termination or gene trapping of the transcript (*Ewsr1*^{GT} allele). Exon 4 is floxed. FLP recombination mediates excision of the neo and IRES:LacZ cassette and converts the "gene-trap first" allele to a conditional allele, restoring gene activity (*Ewsr1*^{lox} allele). CRE recombination results in excision of the floxed exon 4 to generate a frameshift mutation that triggers nonsense mediated decay of the resulting transcript.

Mouse embryonic stem cells were electroporated with the targeting construct and neomycin-resistant clones were screened by southern blotting to search for recombinant clones (Figure 21B). Selected clones were used for embryonic stem cell aggregation and generation of chimeras, from which a mouse colony was established in a B6-129Sv mixed genetic background. Efficacy of the gene-trapping was validated by western blotting on MEF culture protein extracts with an antibody against EWS protein (Figure 21C).

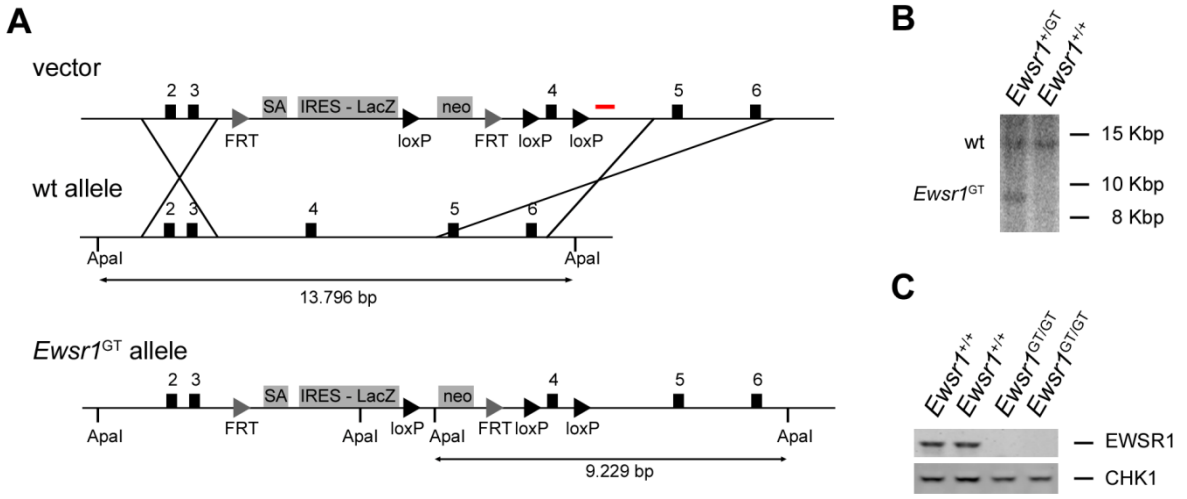

Figure 21
Description of the *Ewsr1* "gene-trap first" allele. (A) A construct targeting the *Ewsr1* endogenous locus was provided by the Euroean Consortium. The construct contains an IRES-LacZ gene-trapping cassette and a promoter-driven neo cassette inserted in intron 3 and flanked by FRT sites, and two loxP sites flanking exon 4. An allele bearing the full construct works as a gene-trap, and leads to constitutive deletion of EWS protein. FLP-mediated recombination of the FRT sites promotes excision of the LacZ and neo cassettes, thereby converting the genetrap allele to a conditional allele and restoring gene activity. Subsequent CRE-mediated excision of exon 4 generates a frameshift mutation, knocking out *Ewsr1* gene. The full construct (vector) was electroporated into embryonic stem cells. (B) Neo-resistant clones were screened by southern blot to identify recombinants, and a probe hybridizing to the 3' homology arm was used (labeled in red in panel A). (C) Deletion of EWS protein in homozygous *Ewsr1*$^{GT/GT}$ MEF was validated by western blotting.

5.1. EWS deletion is embryonic lethal and results in embryonic RS

The previously reported *Ewsr1*-knockout mouse model presented mendelian birth ratios and a high rate of postnatal lethality prior to weaning (Li et al., 2007) In our model, maybe due to a more restrictive genetic background, homozygous deletion of the *Ewsr1* gene was lethal already at the late embryonic stage. Whereas at day E13.5 post-coitum the ratios of homozygous and heterozygous embryos matched the expected mendelian ratios, few *Ewsr1*$^{GT/GT}$ pups were born and they were all invariably dead within few hours after birth. We next analyzed late-stage embryos in order to look for alterations that could explain the embryonic lethality of *Ewsr1*$^{GT/GT}$ mice.

The highly proliferative erythropoietic compartment is especially sensitive to RS; a number of mouse models that suffer from RS present an activated DDR in this cellular population, and suffer from anemia due to depetion of erythropoietic progenitors (Murga et al., 2009; Shima et al., 2007). Strikingly, some *Ewsr1*$^{GT/GT}$ E18.5 embryos presented a pale appearance suggestive of anemia, and a smaller size (Figure 22A). EWS deletion in all tissues was validated by full-embryo IHC (Figure 22B). Consistent with anemia, blood analyses of the embryos revealed a defect in erythropoiesis with decreased red blood cell counts, but unaltered white blood cell counts (Figure 22C). Pannuclear γH2AX-positive cells were detected in all tissues in *Ewsr1*$^{GT/GT}$ embryos (Figure 22D), and were particularly high at the embryonic liver, where embryonic erythropoiesis takes place (Figure 22E, F). Together, absence of EWS promotes the accumulation of RS during embryonic development. This is particularly abundant at the erythropoietic compartment and is the probable cause of anemia in *Ewsr1*$^{GT/GT}$ embryos, which in turn is likely to cause late-stage embryo lethality.

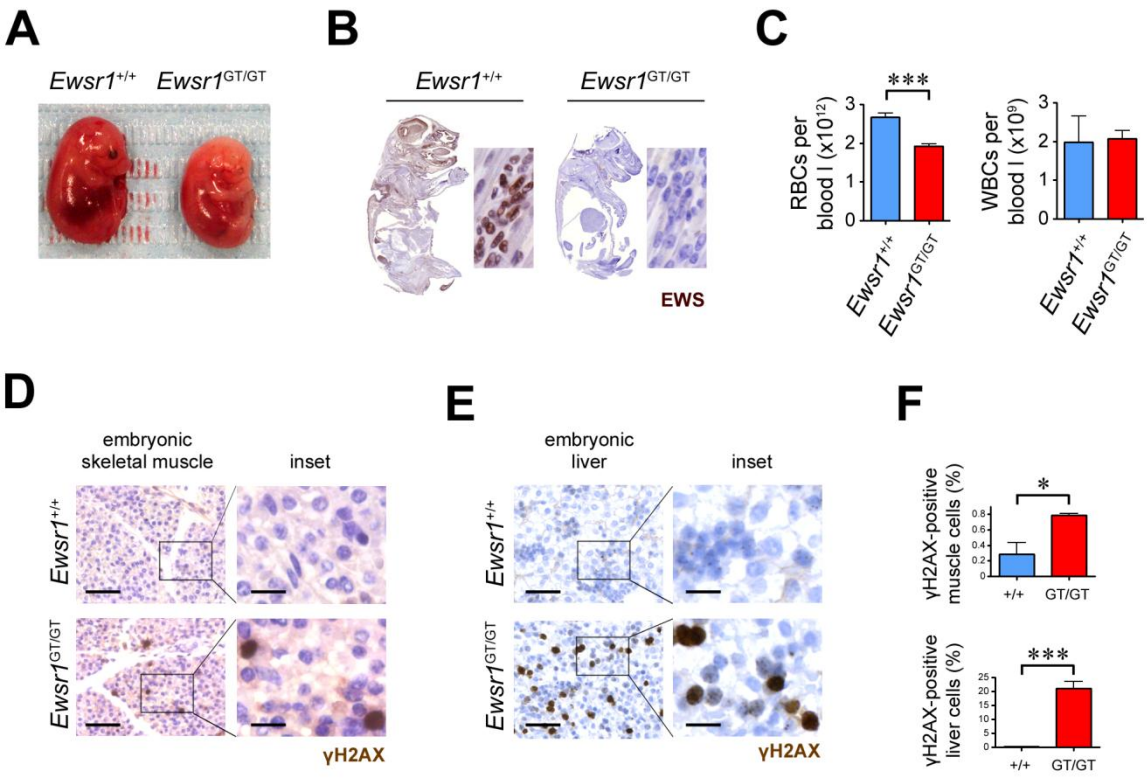

Figure 22
Deletion of EWS leads to accumulation of RS and anemia at the late-embryo stage. (A) Representative picture of E18.5, *Ewsr1*$^{+/+}$ and *Ewsr1*$^{GT/GT}$ littermate embryos. (B) IHC on *Ewsr1*$^{+/+}$ and *Ewsr1*$^{GT/GT}$ E18.5 embryos for detection of EWS. (C) Blood analyses of *Ewsr1*$^{+/+}$ and *Ewsr1*$^{GT/GT}$ E18.5 embryos including red blood cell (WBC) counts and white blood cell (WBC) counts. Data are representative of 5 independent analyses. (D and E) IHC for γH2AX detection at skeletal muscle (D) and liver (E) tissues of E18.5 *Ewsr1*$^{+/+}$ and *Ewsr1*$^{GT/GT}$ littermate embryos. Scale bars, 40 μM. Insets (squares) are provided at high magnification to illustrate the nature of the signal. Scale bars, 12 μM. (F) Quantification of γH2AX-positive cells in D and E. Data in D, E and F are representative of 3 independent experiments.

6. RS and sensitivity to ATRi in EWS-deficient cells

To further explore the role of EWS in RS, we cultured MEF derived from *Ewsr1*$^{+/+}$ and *Ewsr1*$^{GT/GT}$ E13.5 littermate embryos. Notably, *Ewsr1*$^{GT/GT}$ MEF proliferated significantly slower and reached senescence prematurely (Figure 23A, B).

6.1. *Ewsr1*$^{GT/GT}$ MEF show increased levels of RS

We looked at RS levels on MEF. Untreated *Ewsr1*$^{GT/GT}$ cells presented a moderate increase in γH2AX compared to wild-type counterparts (Figure 23C, D). As exposed above, ATR responds

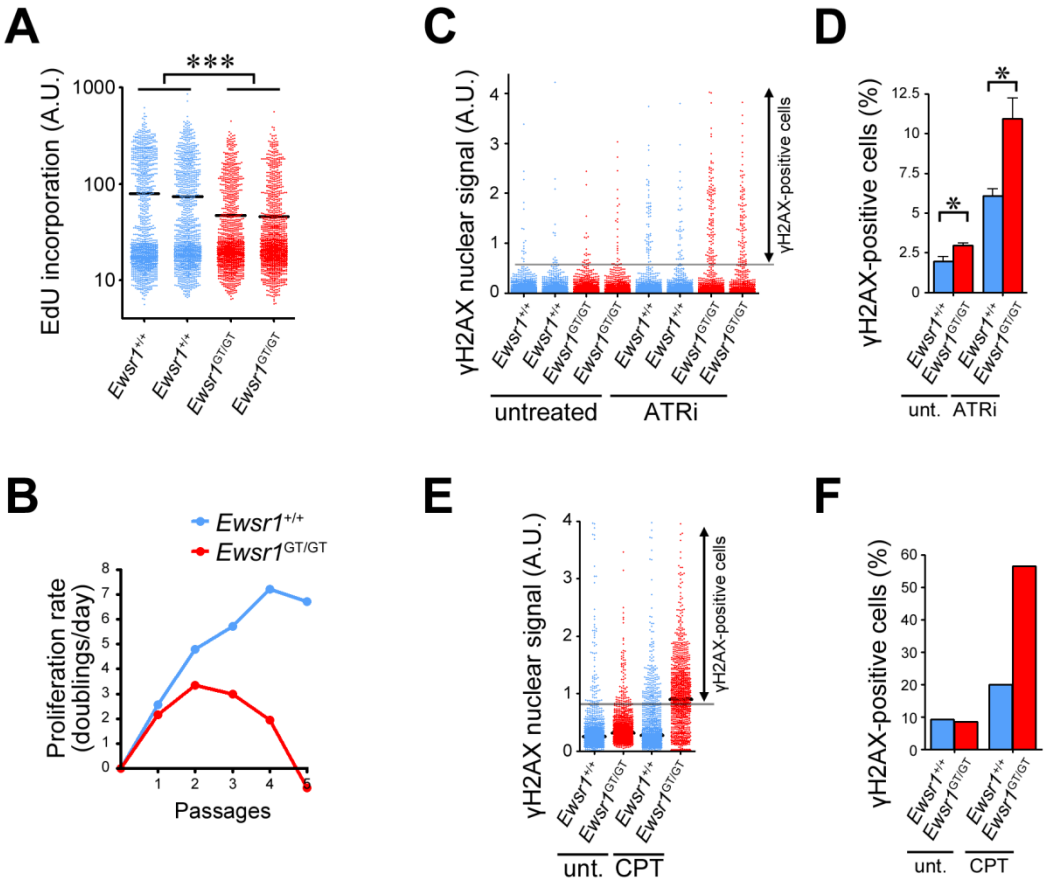

Figure 23
Absence of EWS in MEF leads to RS and premature senescence. (B) *Ewsr1*$^{+/+}$ and *Ewsr1*$^{GT/GT}$ primary MEF were incubated with EdU for 30min and processed for HTM-mediated quantitative detection of EdU incorporation. Data are representative of 5 independent experiments. (C) Growth curves of *Ewsr1*$^{+/+}$ and *Ewsr1*$^{GT/GT}$ primary MEF. (D) *Ewsr1*$^{+/+}$ and *Ewsr1*$^{GT/GT}$ primary MEF were untreated or treated with ATRi 5 μM for 4h and processed for HTM-mediated quantification of γH2AX. A threshold (grey horizontal line) was set to define subpopulations of ^{γH2AX}-positive cells. (E) Graphic representation of γH2AX-positive cells in D. (F) *Ewsr1*$^{+/+}$ and *Ewsr1*$^{GT/GT}$ MEF were untreated or treated with CPT 100nM for 16h and processed for HTM-mediated quantification of γH2AX. A threshold (grey horizontal line) was set to define subpopulations of γH2AX-positive cells. (G) Graphic representation of γH2AX-positive cells in F. Data in D and E are representative of 3 independent experiments.

to and limits RS; therefore, a mechanism to highlight an underlying RS in growing cells is to inhibit ATR. Based on this we challenged cells with ATRi. *Ewsr1*$^{GT/GT}$ cells presented a remarkable accumulation of γH2AX in response to ATRi, indicative of increased RS (Figure 23C, D). ES cell lines were identified as sensitive to topotecan and irinotecan (clinical derivatives of CPT) (Barretina et al., 2012), and drug combinations involving these compounds are currently being explored for chemotherapy (Kurucu et al., 2015). Because of its clinical relevance, we challenged cells with CPT and, again, *Ewsr1*$^{GT/GT}$ showed a significative increase in γH2AX (Figure 23E, F). This was consistent with the previously described requirement of EWS for resistance to CPT (O'Connell et al., 2010), and further supports the hypothetical dominant-negative effect of EWS/FLI1 over EWS, as Ewing sarcomas are also sensitive to CPT.

Importantly, the decreased proliferation rate of *Ewsr1*$^{GT/GT}$ cells (Figure 23A, B) suggests that we might be underestimating the levels of RS detected in these cells; considering this, the increase in γH2AX in *Ewsr1*$^{GT/GT}$ cells is even more significant than what observed values suggest. In the same line, the decreased proliferation rate of *Ewsr1*$^{GT/GT}$ cells might contribute to mask any further increase in γH2AX when these cells are growing in basal conditions.

6.2. *Ewsr1*$^{GT/GT}$ MEF have increased genomic instability

Since RS leads to genomic instability (Barlow et al., 2013; Burrell et al., 2013; Costantino et al., 2014; Dereli-Oz et al., 2011), we wondered whether this took place in *Ewsr1*$^{GT/GT}$ MEF. We prepared *Ewsr1*$^{+/+}$ and *Ewsr1*$^{GT/GT}$ metaphase spreads and quantified breaks and other chromosomal aberrations. Although not reaching statistical significance, the breakage ratio in *Ewsr1*$^{GT/GT}$ MEF was increased (Figure 24A, B). Genomic instability frequently results in chromosomal segregation problems during mitosis and subsequent accumulation of micronuclei, DNA bridges and other nuclear aberrations that are visible in interphasic nuclei. We quantified micronuclei and DNA bridges and found increased nuclear aberrations in *Ewsr1*$^{GT/GT}$ MEF (Figure 24C). In Figure 24D cells with micronuclei (left panel) and DNA bridges (right panel) are shown to illustrate the nature of this kind of aberrations. These observations suggested that an EWS loss of function in Ewing sarcomas might contribute to the described pattern of genomic instability in Ewing sarcomas.

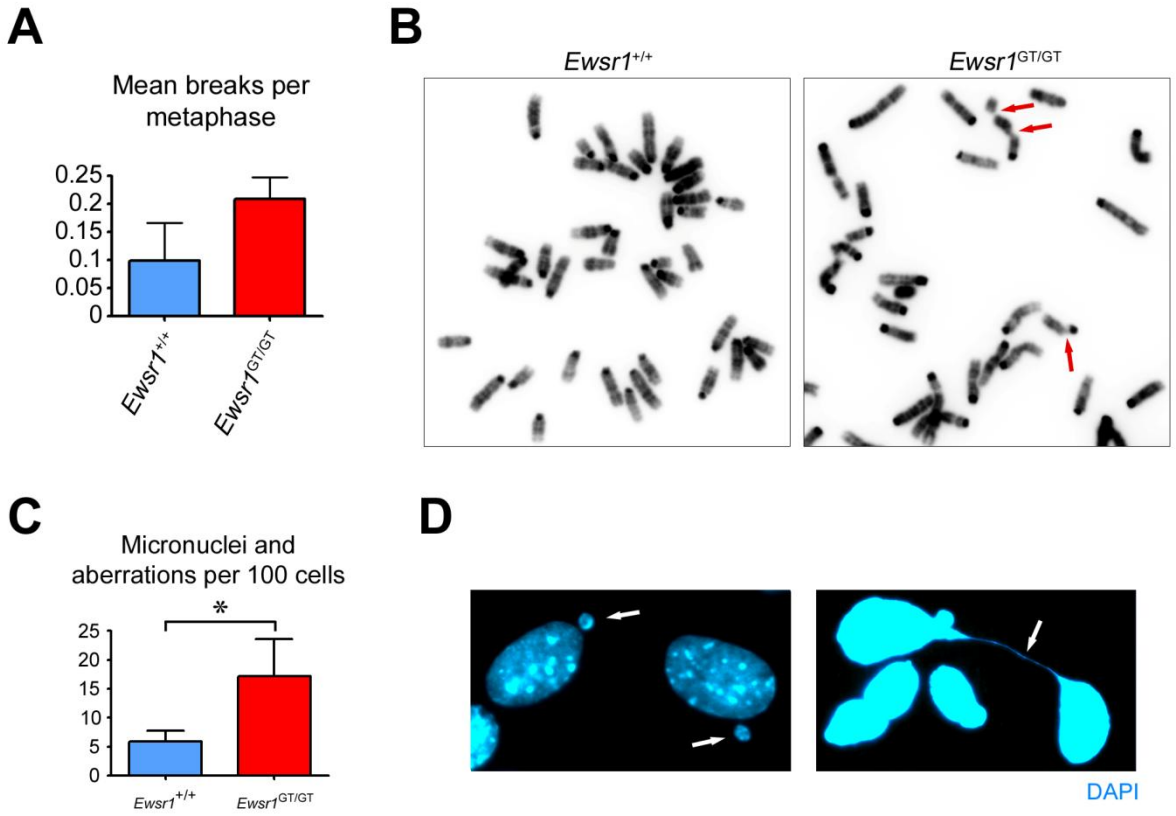

Figure 24
Ewsr1$^{GT/GT}$ MEF have increased genomic instability. (A) *Ewsr1*$^{+/+}$ and *Ewsr1*$^{GT/GT}$ MEF metaphases were spreaded on glass slides and stained with DAPI. Quantification of chromosomal breaks and aberrations is plotted. (B) Example *Ewsr1*$^{+/+}$ and *Ewsr1*$^{GT/GT}$ metaphases are shown. Red arrows indicate chromatid breaks. (C) Untreated *Ewsr1*$^{+/+}$ and *Ewsr1*$^{GT/GT}$ MEF cultures were fixed and stained with DAPI. Quantification of micronuclei, DNA bridges and other nuclear aberrations is plotted. (D) Example interphasic nuclei with aberrations are shown. White arrows indicate micronuclei (left panel) and DNA bridges (right panel).

6.3. *Ewsr1*$^{GT/GT}$ MEF are hypersensitive to ATRi

Based on the increased RS and genomic instability detected in *Ewsr1*$^{GT/GT}$ MEF, we wanted to assess whether EWS deletion sensitized cells to ATR inhibition. Analogously to EWS/FLI1-expressing MEF, cell cycle profiling revealed an increased sub-G1 population in *Ewsr1*$^{GT/GT}$ MEF after ATR inhibition, indicating increased cell death and hypersensitivity to ATRi (Figure 25A). We further characterized hypersensitivity by measuring the uptake of intravital stain ToPRO3 on live cell cultures. The percentage of ToPRO3-positive cells, reflecting dead cells, was significantly higher in *Ewsr1*$^{GT/GT}$ cells both in untreated and in ATRi-treated conditions (Figure 25B and C).

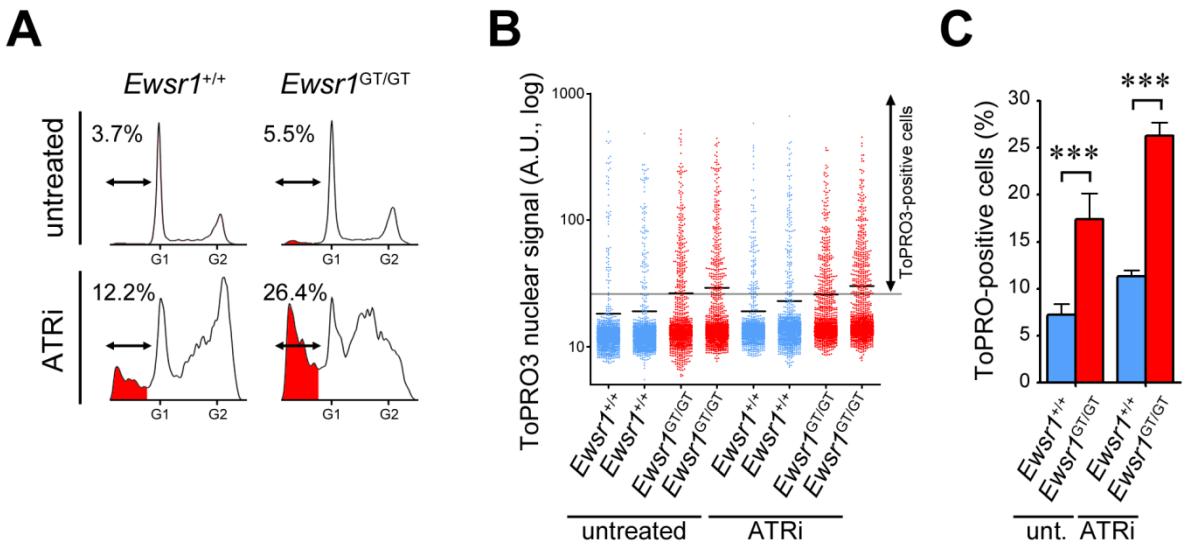

Figure 25
Ewsr1$^{GT/GT}$ MEF are hypersensitive to ATR inhibition. (A) *Ewsr1*$^{+/+}$ and *Ewsr1*$^{GT/GT}$ primary MEF were untreated or exposed to ATRi 5μM for 48h and processed for flow cytometry with propidium iodide as a marker of DNA content. Cell cycle profiles are depicted, and sub-G1 relative populations (labeled in red) are quantified. (B) *Ewsr1*$^{+/+}$ and *Ewsr1*$^{GT/GT}$ primary MEF were untreated or exposed to ATRi 2.5μM for 8h. ToPRO3 intravital stain was added before *in vivo* HTM-mediated analysis of ToPRO3 incorporation in cells. A threshold (grey horizontal line) was set to define subpopulations of ToPRO3-positive cells. (C) Quantification of ToPRO3-positive, dead cells in experiment B. Data in A, B and C are representative of 3 independent experiments.

Taken together, we showed that both the expression of EWS/FLI1 and the deletion of EWS generate RS and genomic instability, and sensitize cells to ATR inhibition, phenotypes that are observed in Ewing sarcomas (section 2). Given that both conditions lead to decreased replication (Figures 19D and 23A), the reasons by which loss of EWS function leads to RS remained unexplained and demanded further investigation.

6.4. The RSR is proficient in *Ewsr1*$^{GT/GT}$ MEF

One of the proposed roles of EWS is in splicing. Paronetto and colleagues described a splicing defect in EWS-deficient cells that affected alternative splicing of DDR genes in response to DNA damage (Paronetto et al., 2011). To test whether *Ewsr1*$^{GT/GT}$ MEF sensitivity to RS-inducing agents was due to a deficient RSR we treated MEF with HU and analyzed markers of RSR activation. *Ewsr1*$^{GT/GT}$ MEF presented a proficient RSR, as demonstrated by efficient phosphorylation of RPA and CHK1 (Figure 23A). We next performed RNA sequencing of *Ewsr1*$^{+/+}$ and *Ewsr1*$^{GT/GT}$ MEF. As a validation of the sequencing process, Ewsr1 mRNA appeared decreased in *Ewsr1*$^{GT/GT}$ MEF (Figure 26B, upper panel). We looked at distinct DDR and RSR genes and found no significant variations in exon usage between *Ewsr1*$^{+/+}$ and *Ewsr1*$^{GT/GT}$ MEF (Figure 26B, lower panel), suggesting that the hypersensitivity of *Ewsr1*$^{GT/GT}$ MEF is not due to splicing defects.

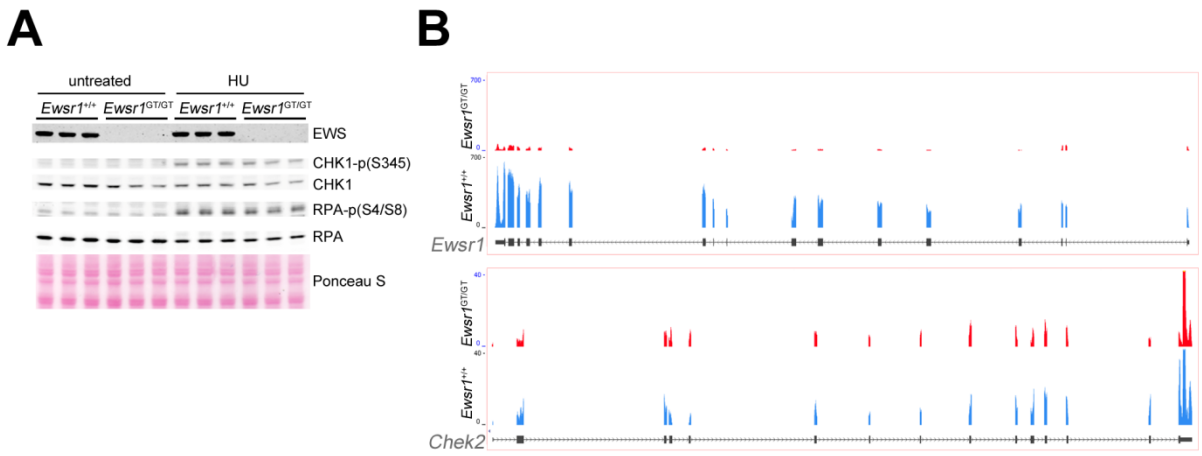

Figure 26
Ewsr1$^{GT/GT}$ MEF do not show deficiencies in the RSR or alterations in splicing. (A) *Ewsr1*$^{+/+}$ and *Ewsr1*$^{GT/GT}$ primary MEF were untreated or treated with HU 2mM for 4h, and subsequently processed for protein extraction. Western blotting was performed with the indicated antibodies. (B) Exon usage at *Chek2* gene is not affected in *Ewsr1*$^{GT/GT}$ MEFs. RNA from *Ewsr1*$^{+/+}$ and *Ewsr1*$^{GT/GT}$ MEF was used for RNA sequencing. Expression tracks were generated and uploaded to the UCSC browser. Expression levels for *Ewsr1* and *Chek2* in *Ewsr1*$^{+/+}$ and *Ewsr1*$^{GT/GT}$ MEF are shown. Upper panel, *Ewsr1*; lower panel, *Chek2*.Cristina mayor performed the sequencing analysis and expression track generation.

7. R-Loops and RS

Frequently, RS leads to replication fork stalling and helicase-polymerase uncoupling which generates long threads of ssDNA (Byun et al., 2005). A common marker used to define the presence RS is the detection of ssDNA itself, or RPA foci accumulation, which form on ssDNA. However, even though we observed increased ATRi sensitivity and high pan-nuclear γH2AX levels, we were unable to detect increased RPA foci formation in *Ewsr1*$^{GT/GT}$ or in EWS/FLI1-expressing cells either in untreated or in RS-challenging conditions (data not shown). Taking into account the proliferative defect in these cells (Figure 19D and Figure 23A), we considered sources of RS that do not involve fork uncoupling (and therefore would not promote RPA foci accumulation) and that are not necessarily dependent on a deregulation of the cell cycle progression. This is the case for R-loops.

R-loops are three-stranded nucleic acid structures composed of an RNA:DNA hybrid and a displaced DNA strand (Aguilera and Garcia-Muse, 2012). These structures arise when newly synthesized RNA re-hybridizes with its template DNA (Figure 27A). Collisions of replication forks with persistent R-loops are a source of RS (Figure 27B) (Aguilera and Garcia-Muse, 2012). R-loop formation occurs with special frequency at sites with high transcription rates such as the nucleolus (El Hage et al., 2010). The nucleolus, which is composed of ribosomal DNA (rDNA),

hosts the transcription of the highly abundant ribosomal RNA (rRNA), accounting for 80% of cellular transcription. Nucleoli accumulate R-loops, as observed in cultured wild-type U2OS cells stained with S9.6, an antibody that specifically recongnizes RNA:DNA hybrids (Figure 27C). This accumulation is dependent on active transcription as evidenced by loss of S9.6 signal upon inhibition of RNA polymerase I (RNAPI) by treatment with a low dose of actinomycin D (5nM), which selectively inhibits RNAPI but not RNAPII (Figure 27D). Importantly, R-loops are not restricted to nucleoli, as they have also been described to occur at sites of RNAPII transcription (Ginno et al., 2012; Wongsurawat et al., 2012).

R-loops pose a threat to replication as they are physical obstacles to fork progression, and active mechanisms exist to prevent collisions. RNase H removes R-loops by endonucleolytical cleavage of the RNA fraction (Huertas and Aguilera, 2003) and several helicases, including Pif1, DHX9 and Senataxin can unwind the RNA:DNA hybrids (Alzu et al., 2012; Boule and Zakian, 2007; Chakraborty and Grosse, 2011; Kim et al., 1999; Yuce and West, 2013).

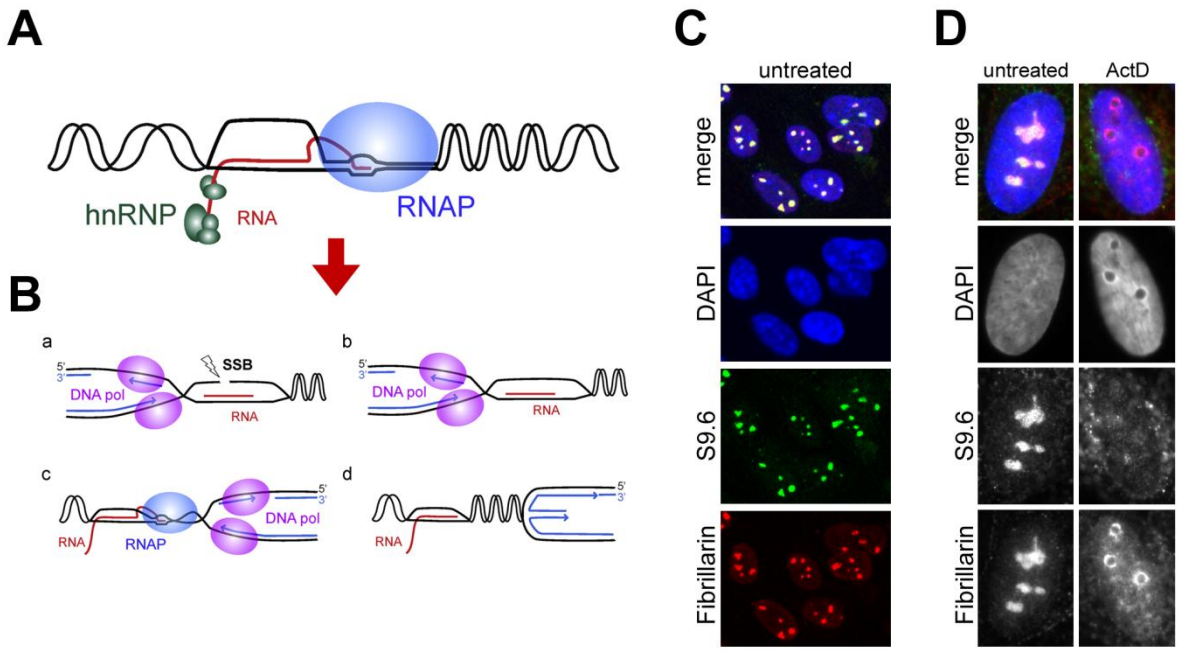

Figure 27
R-loops are transcription-associated RNA:DNA hybrid structures that interfere with replication and generate RS. (A) RNA:DNA hybrids termed R-loops arise as newly-synthesized transcripts anneal to template DNA. (B) A series of conflicts invoving R-loops can occur that generate RS upon collision of an approaching replication fork with (a) unrepaired DNA lesions in the ssDNA displaced strand, (b) the RNA:DNA hybrid itself, (c) an RNAP putatively trapped at the transcription site by the R loop, (d) R loop-mediated torsional stress. Panels A and B are adapted from (Aguilera and Garcia-Muse, 2012). (C) S9.6 antibody specifically recognizes RNA:DNA hybrids and labels R-loops, which are enriched at the nucleoli. (D) Inhibition of transcription with ActD 5nM for 2h abrogates R-loop accumulation.

The structural determinants and described functions of EWS are compatible with a role in R-loop metabolism. First, EWS was originally described as an RNA and DNA binding protein, and interaction with several partners is dependent on the presence of RNA (Pahlich et al., 2009). Second, as demonstrated by its interaction with RNAPII and TFIID, EWS has roles in transcription (Bertolotti et al., 1996; Bertolotti et al., 1998), a major source of R-loops. Third, a role for EWS has also been proposed in RNA splicing (Michaud and Reed, 1993; Paronetto et al., 2011), and there is indirect evidence that defective splicing promotes R-loop accumulation (Li and Manley, 2005a; Li and Manley, 2005b; Paulsen et al., 2009).

7.1. EWS is recruited to the nucleolus after nucleolar stress

As previously published (Rossow and Janknecht, 2001), immunostaining of wild-type cultured MEF showed a widespread nuclear localization of EWS (Figure 28A). As already mentioned, TopoI relieves torsional stress during transcription. Importantly, R-loops forming at the rDNA region in yeast cells are significantly increased in top1Δ mutant strains (El Hage et al., 2010). Consistent with a role for EWS in R-loop metabolism, inhibition of TopoI by treatment with CPT promoted EWS nucleolar localization (Figure 28A). Recruitment to nucleoli was very fast, occurring within 10' after CPT addition in 100% of the cells, and dispersal from the nucleolus

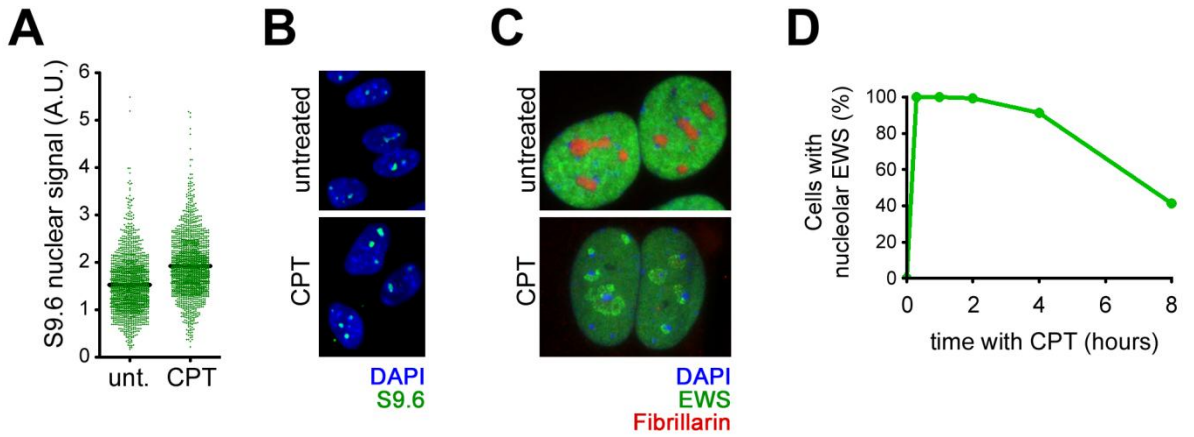

Figure 28
EWS protein is recruited to the nucleolus after nucleolar RS. (A) R-loop levels are increased in nucleoli after CPT treatment. Plot shows HTM-mediated quantification of nuclear S9.6 signal in untreated or 10nM CPT-treated wild-type MEF. (B) Representative images from A. (C) EWS is recruited to the nucleolus after CPT treatment. Immunofluorescent co-staining of EWS and Fibrillarin in wild-type MEF before and after treatment with CPT 10μM for 20'. (D) Wild-type MEF were treated with CPT 10μM for different times and immunostained as in C. Percentage of cells with nucleolar localization of EWS was quantified for each timepoint.

happened progressively within the following 8 hours (Figure 28B). Based on this evidence, we wondered whether the cause of RS in EWS-deficient and EWS/FLI1-expressing cells was an accumulation of R-loops.

7.2. *Ewsr1*$^{GT/GT}$ and EWS/FLI1-expressing cells have increased R-loops

We measured total levels of R-loops in *Ewsr1*$^{GT/GT}$ and EWS/FLI1-expressing MEF by HTM-mediated quantification of S9.6 signal. Strikingly, both *Ewsr1*$^{GT/GT}$ and EWS/FLI1-expressing MEF had increased R-loops compared to their corresponding counterparts (Figure 29A and B). Representative pictures of *Ewsr1*$^{+/+}$ and *Ewsr1*$^{GT/GT}$ MEF are shown (Figure 29C). Next we asked about R-loop levels at RNAPII-transcribed genes. To explore this, we collaborated with the lab of Andrés Aguilera, with renowned knowledge and expertise in R-loop biology. In collaboration with María García Rubio we performed DRIP-qPCR to assess R-loop levels at particular sites. The *Airn* gene was defined as an R-loop hotspot site in mouse cells (Ginno et al., 2012). Measurement at two different regions of the gene (*Airn*1 and *Airn*2) showed that both *Ewsr1*$^{GT/GT}$ and EWS/FLI1-expressing MEF had significantly increased R-loop levels, which were abolished upon RNAseH sample treatment as expected (Figure 29D and E). Next, we wondered whether ES cell lines had increased R-loops as well. For this we assessed R-loop levels in APOE, RPL13A and ERG1, described as R-loop hotspot sites in human cells (Ginno et al., 2012). Strikingly, R-loops were increased in all ES cell lines compared to a control cell line (Figure 29F). Hence, increased R-loop levels appear to be the cause of RS in EWS-depleted and EWS/FLI1-expressing cells, as well as in ES cell lines.

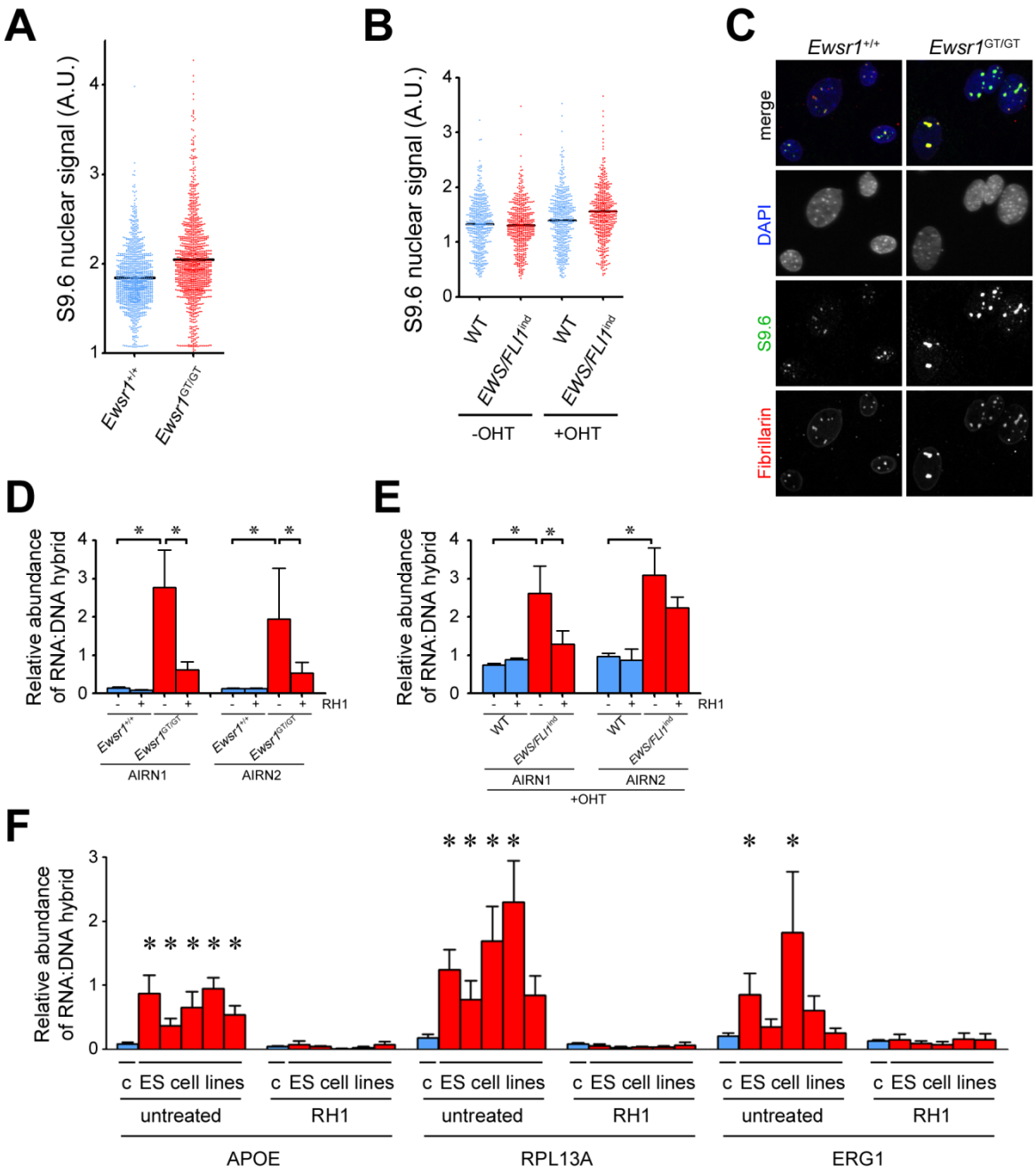

Figure 29
EWS-depleted, EWS/FLI1-expressing and ES cell lines accumulate R-loops in the nucleolus and in RNAPII-expressed genes. (A) *Ewsr1*$^{+/+}$ and *Ewsr1*$^{GT/GT}$ MEF were stained with S9.6 and nuclear signal was quantified by HTM. (B) WT and EWS/FLI1-expressing MEF were stained with S9.6 and nuclear signal was quantified by HTM. (C), representative pictures of (A). (D, E and F) Quantification of R-loops at RNAPII-transcribed genes by DRIP-qRT-PCR in *Ewsr1*$^{+/+}$ and *Ewsr1*$^{GT/GT}$ MEF (D), WT and EWS/FLI1-expressing MEF (E), and ES cell lines and control cell lines (F). Extracted DNA was mock-digested or digested with RNAseH1 and immunoprecipitation with S9.6 was performed. qRT-PCR on the indicated genes was used as a measure of R-loop acumulation. Data in D, E and F were produced in a collaboration with Andrés Aguilera and María García Rubio. All data are representative of at least 3 independent experiments.

7.3. R-loops persist into mitosiss

rDNA genes are organized in tandem repeats at the so-called nucleolar organizer regions (NOR), and account for around 80% of total RNA synthesis in eukaryotic cells. The repetitive and highly transcribed rDNA has a propensity to breakage (Butler, 1992; Huang et al., 2012). Provided that R-loops accumulate constitutively at NOR regions (Figure 27C), we inferred that R-loops might be the cause of such instability. In this regard, we wondered whether R-loops persist into mitosis, where chromosomal segregation of underreplicated DNA frequently results in chromosomal breakage. In mice and humans, NORs are localized at subcentromeric regions (Babu and Verma, 1985; Goodpasture and Bloom, 1975) in a variable number of chromosomes, depending on the species, and ranging from 5 to 8 (Heliot et al., 1997). NORs can be specifically identified on metaphases by either in situ hybridization with an rDNA probe or by immunolabeling with NOR-specific proteins such as RNAPI or UBF, which remain associated to rDNA genes during mitosis (Roussel et al., 1996; Weisenberger and Scheer, 1995). We prepared metaphase spreads of wild-type MEF and U2OS cells and stained them with S9.6. Surprisingly, all metaphases systematically presented an S9.6 staining pattern matching that of NOR regions. S9.6 signals were subcentromeric, as evidenced by their localization below the

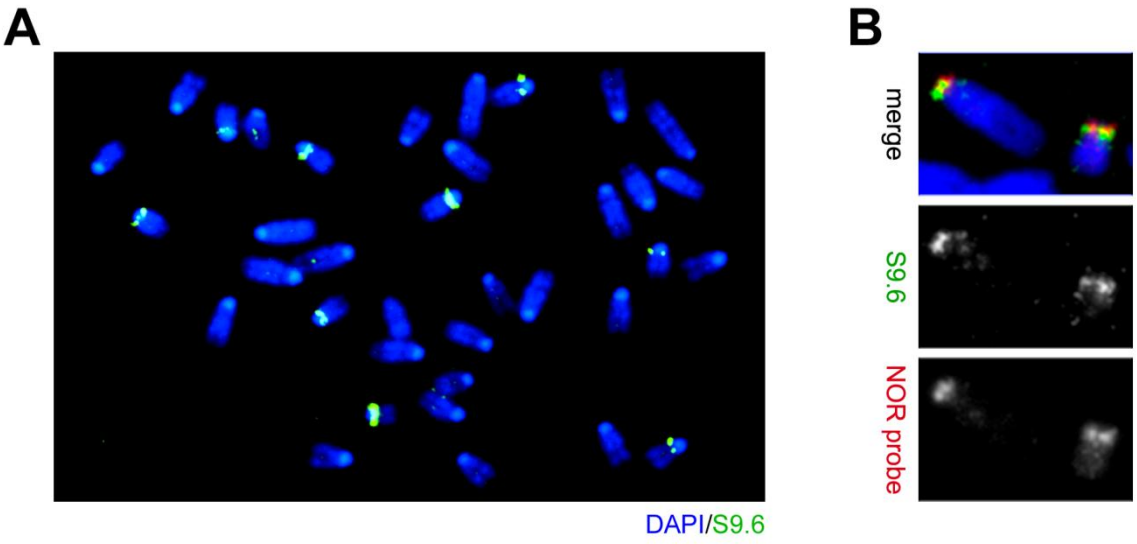

Figure 30
R-loops are detected at NOR regions in metaphasic chromosomes. (A) A wild-type MEF metaphase spread immunostained with S9.6 antibody. (B) U2OS metaphase spreads with Immuno-FISH for s9.6 staining and a hybridization probe for NOR regions. The two signals colocalize at subcentromeric regions.

high density regions that correspond to centromeres (Figure 30A). A total of 6 to 8 chromosomes within a metaphase presented an S9.6 signal. Immuno-FISH with a NOR-specific probe demonstrated S9.6 colocalization to NOR regions (Figure 30B). This novel finding opens new interrogants regarding the persistence of R-loops into mitosis, which, to our knowledge, has not been described to date. For the scope of this work, S9.6 antibody proved to be a bona fide marker of NOR regions.

7.4. *Ewsr1*$^{GT/GT}$ MEF have increased genomic instability at NOR regions

Next we asked about the consequences of having increased R-loops in EWS-deficient cells. In section 6 we detected RS-derived genomic instability in *Ewsr1*$^{GT/GT}$ MEF (Figure 24), consistent with several works reporting genomic instability as a consequence of RS. We now speculated that R-loop-derived RS might have a preferential impact on genomic instability at highly transcribed regions, such as NORs. To assess this we focused our metaphase breakage analysis on NOR regions. We stained *Ewsr1*$^{+/+}$ and *Ewsr1*$^{GT/GT}$ MEF metaphase spreads with S9.6 and a telomeric probe (Figure 31A) and quantified the fraction of breaks and aberrations occurring specifically at NOR regions. Strikingly, the ratio of NOR-specific breaks over total breaks was increased in *Ewsr1*$^{GT/GT}$ cells (Figure 31B). Examples of NOR-specific chromosomal breaks (Figure 31A, white arrows) and chromatid breaks (Figure 31C) are shown. Of note, the mean ratios of NOR-specific breaks range from 5% to 16%. Therefore, the increased breakage at NOR regions cannot account for global breakage differences between *Ewsr1*$^{+/+}$ and *Ewsr1*$^{GT/GT}$ cells (Figure 24). Altogether, data indicates that EWS-deficient cells have an increased fragility both globally throughout the genome and specifically at NOR regions.

We repeated the breakage analyses on EWS/FLI1-expressing cells. However, these did not follow the tendency of *Ewsr1*$^{GT/GT}$ cells; instead, instability was rather decreased upon expression of EWS/FLI1. A parsimonious explanation is that the decrease in the proliferation rate upon expression of EWS/FLI1 (Figure 19D) prevents replication-driven genomic instability. Because RS-derived fragility is dependent on replication, a reduced replication rate might mask fragility at EWS/FLI1-expressing cells.

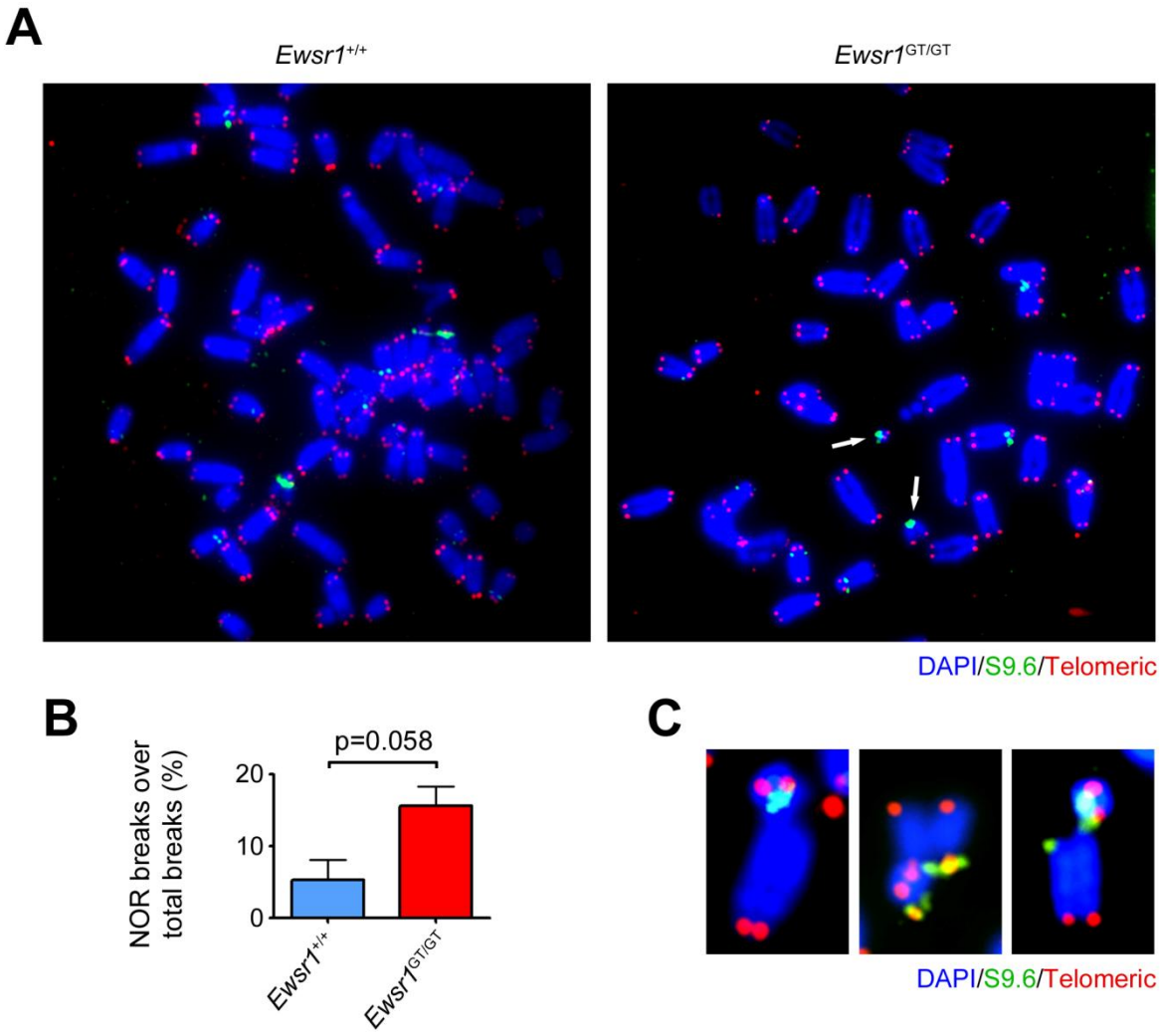

Figure 31
Genome instability is specifically increased at NOR regions in *Ewsr1*$^{GT/GT}$ MEF. (A) Representative pictures of *Ewsr1*$^{+/+}$ and *Ewsr1*$^{GT/GT}$ MEF metaphase spreads. White arrows point the two chromosome fragments resulting from a chomosomal break that occurred at a NOR region. (B) Quantification of chromosomal aberrations occuring at NOR regions relative to total aberrations in *Ewsr1*$^{+/+}$ and *Ewsr1*$^{GT/GT}$ MEF. (C) Examples of chromatid breaks occurring at NOR regions. Data B are representative of 3 independent experiments.

7.5. Biogenesis of rRNA is unaltered in *Ewsr1*$^{GT/GT}$ and EWS/FLI1-expressing cells

Next we wondered about the causes of R-loop accumulation in EWS-deficient cells. Since EWS had been previously linked to RNA splicing and processing (Paronetto, 2013; Paronetto et al., 2011), and because R-loops indeed accumulate preferentially at nucleoli, we speculated whether R-loop accumulation in *Ewsr1*$^{GT/GT}$ and EWS/FLI1-expressing MEF might be the result of an

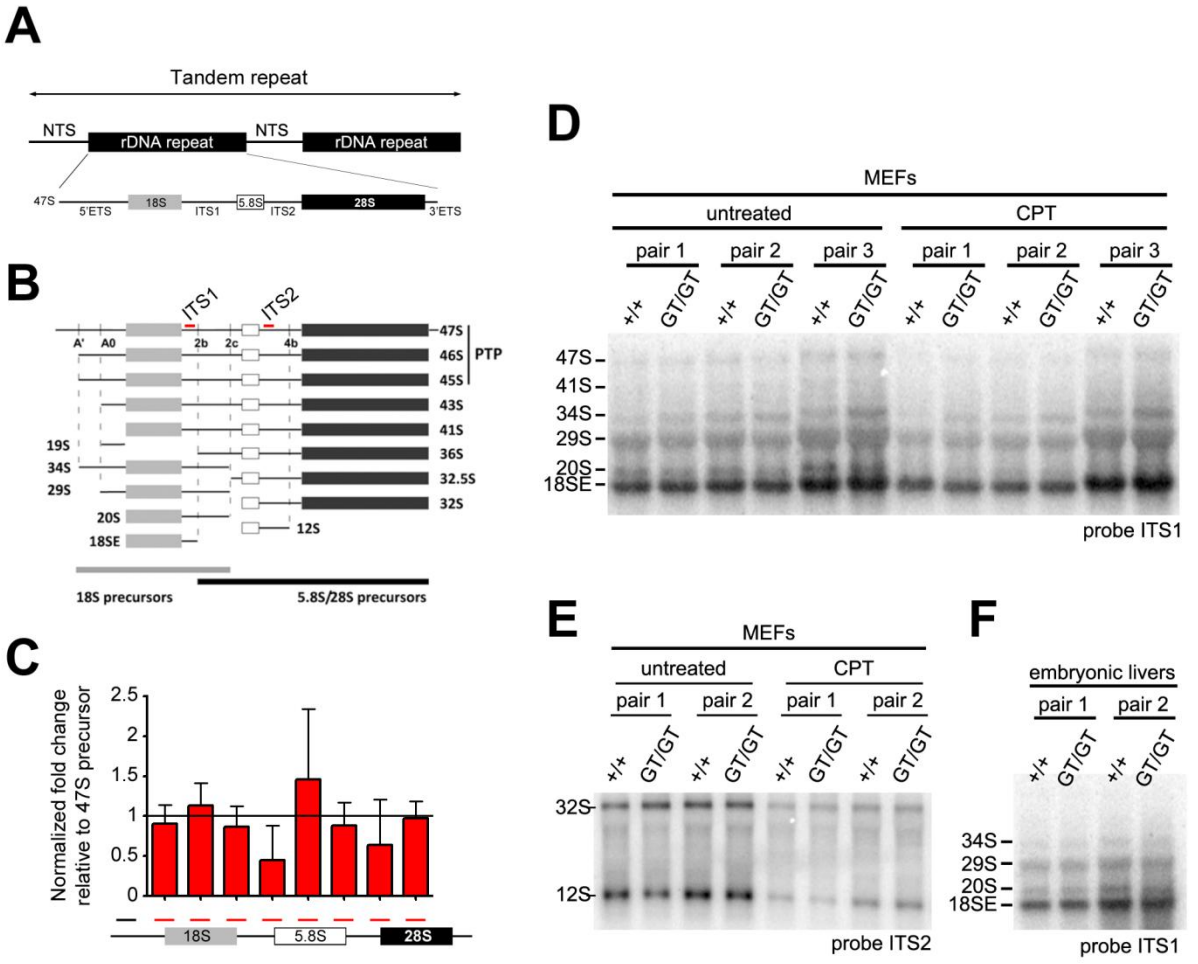

Figure 32
Biogenesis of rRNA is not affected in cells lacking EWS. (A) Schematic representation of the rDNA repetitive sequence and 47S repeating unit. NTS, non-transcribed sequence; ETS, external transcribed sequence; ITS, internal transcribed sequence. (B) Intermediate products of processing of the 47S precursor. Depending on the cleavage order at the different cleavage sites, different intermediates are generated that ultimately give rise to mature 18S, 5.8Sand 28S. Panel B adapted from (Wang Anikin and Pestov 2014). (C) Normalized fold change expression in *Ewsr1*$^{GT/GT}$ compared to *Ewsr1*$^{+/+}$, relativized to expression of the 47S precursor. (D and E) Northern blot of total RNA extracts of untreated or 3h 10μM CPT-treated, *Ewsr1*$^{+/+}$ and *Ewsr1*$^{GT/GT}$ MEF with probes hybridizing to ITS1 (D; probe ITS1, labeled in red in B) and to ITS2 (E; probe ITS2, labeled in red in B). (F) Northern blot of total RNA extracts of *Ewsr1*$^{+/+}$ and *Ewsr1*$^{GT/GT}$ embryonic livers with probe ITS1.

altered rRNA biogenesis. An aberrant accumulation of abortive rRNA intermediates might clog up the processing of RNA and subsequently facilitate R-loop accumulation.

A schematic representation of the rDNA complete repeating unit is depicted in Figure 32A. The transcribed 47S rRNA precursor is subjected to successive steps of cleavage giving rise to a variety of intermediate substrates and ultimately to the mature rRNA molecules 18S, 5.8S and 28S (Figure 32B). To assess rRNA biogenesis we used a set of primers mapping several regions of the 47S precursor (Figure 32C, scheme below the graph), including the 5' ETS as a measure of 47S precursor; 18S, 5.8S and 28S as a measure of mature rRNAs; and junctions between mature

rRNA sequences and contiguous ITSs to quantify the diverse intermediate products (Kwon et al., 2014). We performed quantitative RT-PCR and analyzed the relative abundances of mature rRNAs and intermediates with respect to 47S precursor (Figure 32C). However, we considered our data inconclusive because of a high variability across samples and experiment repetitions; in any case, we did not observe an overall defect across the distinct independent pairs of cells tested.

We decided to use a different approach to query the rRNA biogenesis function. Northern blotting of total RNA extracts enables the detection of distinct intermediates of rRNA biogenesis (O'Donohue et al., 2010; Wang et al., 2014). We used a probe to the ITS1, which hybridizes to all 18S precursors, and another one to ITS2, which hybridizes to all 5.8S/28S precursors (red labels at Figure 32B). No differences in rRNA intermediates were observed between *Ewsr1*$^{+/+}$ and *Ewsr1*$^{GT/GT}$ cells with the ITS1 or the ITS2 probe, and challenging cells with CPT did not result in any differences either (Figure 32D and E). Based on the high γH2AX rates observed at E18.5 embryonic livers (Figure 22E), we also tested embryonic liver RNA extracts, but again no significant differences were observed (Figure 32F). Hence, analysis of rRNA biogenesis, both by quantitative RT-PCR and by northern blotting, failed to detect alterations in rRNA biogenesis, suggesting that other causes could be responsible for R-loop accumulation in EWS-defective cells.

7.6. RNA nuclear export is impaired in *Ewsr1*$^{GT/GT}$ and EWS/FLI1-expressing cells

EWS is a substrate of PRMT1 (Araya et al., 2005), which also regulates CHTOP (Chromatin Target Of PRMT1). CHTOP is a component of the THO/TREX complex, with a role in mRNA nuclear export. Importantly, as mentioned at the introduction, mutations in the THO/TREX complex are responsible for R-loop accumulation and genome instability (Dominguez-Sanchez et al., 2011; Gomez-Gonzalez et al., 2011; Huertas and Aguilera, 2003). We speculated that EWS role in limiting R-loop accumulation might relate to nuclear export of RNA. Vanesa Lafarga at our lab contributed importantly to address this. To determine RNA export rates, we pulsed *Ewsr1*$^{+/+}$ and *Ewsr1*$^{GT/GT}$ MEF with EU (a ribonucleotide analog) to label nascent RNAs, and released them in fresh media for increasing time lapses (Figure 33A). Expectedly, labeled RNA molecules (particularly enriched at nucleoli) progressively migrated from the nucleus to the cytoplasm as evidenced by a nuclear signal decrease over time and a concomitant signal increase at the cytoplasm. Given that RNA degradation occurs only at the

cytoplasm and not at the nucleus, the decrease in nuclear EU signal can be interpreted as a surrogate indicator of RNA export. Strikingly, nuclear signal decrease was retarded in *Ewsr1*$^{GT/GT}$ cells, indicating an impaired export of newly synthesized RNA molecules (Figure 33B). Quantification of cells categorized as "EU-retaining" (black double-ended arrow in B) is plotted along time (Figure 33C). We repeated the assay for WT and EWS/FLI1-expressing MEF and we found a similar export retardation in EWS/FLI1-expressing MEF (Figure 33D). Representative pictures of *Ewsr1*$^{+/+}$ and *Ewsr1*$^{GT/GT}$ MEF at timepoints 0 and 240min after release are shown (Figure 33E). These results suggest that EWS might contribute to prevent R-loop accumulation by promoting RNA nuclear export, and again point to a putative dominant-negative effect of EWS/FLI1 over EWS.

Altogether, in section 7 we have demonstrated an R-loop accumulation in EWS-depleted and EWS/FLI1-expressing cells which recalls the R-loop accumulation detected in ES cell lines. We observed a concomitant retardation of RNA export, which might be responsible for R-loop accumulation. Increased genomic instability at NOR regions in EWS-depleted cells is a probable

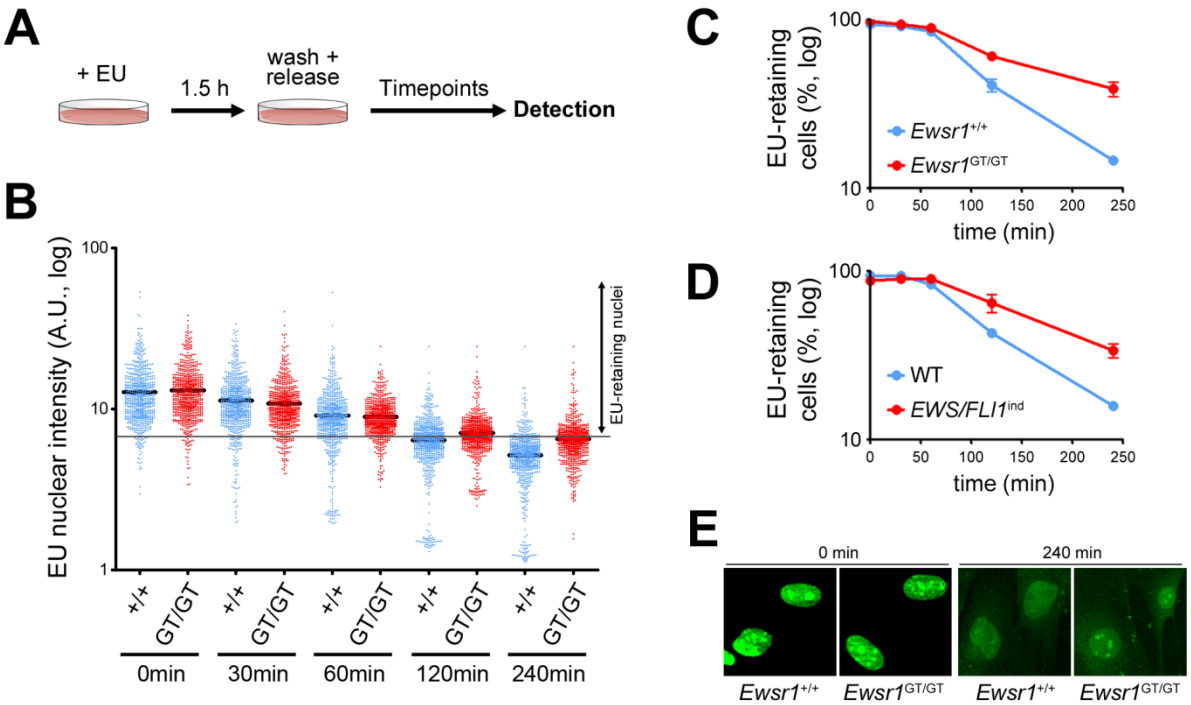

Figure 33
RNA transcripts are retained in the nucleus in EWS-depleted or EWS/FLI1-expressing cells. (A) Experimental pipeline is depicted. Cultured cells were pulsed with EU for 1.5h and subsequently washed and released in fresh media for different times. Cells were fixed and processed for HTM-mediated quantification of EU nuclear signal. (B) HTM analysis of nuclear retention of EU-labeled transcripts in *Ewsr1*$^{+/+}$ and *Ewsr1*$^{GT/GT}$ MEF. A threshold (grey horizontal line) was set to define subpopulations of EU-high nuclei. (C) Graphic representation of subpopulations of *Ewsr1*$^{+/+}$ and *Ewsr1*$^{GT/GT}$ EU-high nuclei in B. (D) Graphic representation of percentages of WT and EWS/FLI1-expressing EU-high nuclei. (E) Representative pictures of EU-labeled nuclei at timepoints 0 and 240min from experiment B. All experiments were performed by Vanesa Lafarga. Two independent MEF pairs were assayed in each experiment.

consequence of R-loops. These data suggests that R-loop accumulation is the cause of RS and genomic instability in Ewing sarcomas. In addition, parallel responses of EWS/FLI1-expressing cells and EWS-depleted cells suggest that EWS/FLI1 has a dominant-negative effect over EWS.

Regarding the clinical treatment of Ewing sarcoma, the identification of high RS levels in ES cells, as well as in EWS/FLI1-expressing and EWS-deficient cells, provides a rationale for the use of ATR inhibitors as a chemoterapeutic agent to treat Ewing sarcomas. Furthermore, we have proved the *in vivo* efficacy of this approach. Additionally, the findings described in this work provide a mechanistic explanation for the efficacy of currently used chemotherapies. CPT derivatives topotecan and irinotecan are used in the clinics and continue to be explored for improving the treatment of relapsed Ewing sarcoma (Kurucu et al., 2015), but the molecular basis of their toxicity to Ewing sarcoma remained unknown. Our study shows that the inability of EWS-deficient cells to limit R-loop accumulation might be responsible for sensitization to an agent that increases R-loop levels, such as CPT. Together, these findings might hopefully have a translation into the clinics and thus contribute to improve the prognosis of this pediatric cancer.

8. Consequences of *Ewsr1* deletion in adult mice

We next wondered whether RS is just a byproduct of the pathology of Ewing sarcomas - a feature that we indeed can exploit as an Achilles' heel to treat this cancer -, or it is rather an early event that constitutes a driving force for malignant transformation. Assuming the latter, RS derived from EWS deficiency might actively contribute to the development of Ewing sarcomas. Whereas EWS/FLI1oncogenic activity has been proven in a number of EWS/FLI1 transgenic mouse models (Ordonez et al., 2009), we wanted to assess the contribution of EWS to tumor suppression. On the other hand, as a proof of concept we were interested in exploring whether R-loop-driven genomic instability can fuel cancer, which has not been shown.

As shown in section 5 (Figure 22), constitutive deletion of *Ewsr1* is embryonic lethal. Therefore, to explore the impact of *Ewsr1* deletion in adult mice we used the conditional knockout version of our *Ewsr1* allele. We obtained that by breeding FLP transgenic mice into mice bearing the *Ewsr1*^{GT} allele (Figure 21). FLP-mediated recombination of the FRT sites converted the gene-trapped allele into a conditional allele (*Ewsr1*^{lox}) and restored gene activity.

8.1. Exploring a tumorigenic effect of *Ewsr1* deletion

Bmi1 is a known player in the self-renewal of adult stem cells (Lessard and Sauvageau, 2003; Leung et al., 2004; Molofsky et al., 2003). A CRE recombinase expressed under the control of the Bmi1 promoter (*Bmi1-CRE*^{ERT2}) proved to be a valuable tool for the development of ESFT-like tumors in a mouse model for conditional expression of EWS/ATF1 fusion protein (Straessler et al., 2013). Based on this we bred mice bearing *Bmi1-CRE*^{ERT2} to mice bearing the *Ewsr1*^{lox} allele and we generated a cohort of *Ewsr1*$^{+/+}$ :: Bmi1-Cre^{ERT2} and *Ewsr1*$^{lox/lox}$ :: Bmi1-Cre^{ERT2} mice in mixed litters. Mice were put on OHT-rich diet from the fourth week of age to induce CRE-mediated excision. However, at the moment of publication of the present work, *Ewsr1*$^{lox/lox}$ :: Bmi1-Cre^{ERT2} (*Ewsr1*$^{\Delta/\Delta}$, hereafter) have not shown an increased tumoral incidence, being 30 to 40 weeks old. In spite of this result, we cannot discard that EWS has a tumor suppressive role. Further study is needed in this regard; codepletion of p53 as a key tumor suppressor, or expression of known oncogenes such as Eμ-Myc, might preferentially favor tumorigenesis in a context of genomic instability such as in *Ewsr1*$^{\Delta/\Delta}$ mice. On the other hand, the Bmi1-expressing cell population might not be the right target to test the tumorigenic potential of *Ewsr1* deletion; in this sense, the use of a more ubiquitously expressed CRE recombinase would help highlight susceptibility to tumorigenesis in any tissue. There are ongoing experiments in these two directions that might help us address whether EWS has a tumor protective contribution, and whether R-loop-driven genomic instability can fuel tumorigenesis.

8.2. *Ewsr1*$^{\Delta/\Delta}$ mice develop an ALS-like disease

In contrast to tumorigenesis, *Ewsr1*$^{\Delta/\Delta}$ mice developed motor problems. As mice aged, *Ewsr1*$^{\Delta/\Delta}$ animals presented scoliosis with a variable degree of incidence and intensity (Figure 34A). Unlike kyphosis, which appears in mice during normal ageing, scoliosis is not a common feature in aged mice. We speculated that the underlying cause might relate to motor problems at the neuromuscular level. Postural compensation of asymmetrical motor problems on the limbs might at the long term result in spinal cord deformation and scoliosis. To investigate motor capacity in the mice, we studied hindlimb extension performance. The hindlimb extension reflex is the reflex by which mice extend their hindlimbs immediately upon being lifted by the tail. Hindlimb clasping and failure to extend upon lifting is indicative of abnormal motor function. We classified mice in three categories based on their extension capacity (full, partial or null; Figure 34B), and we also assessed symmetrical or asymmetrical performance. These parameters are commonly used for neurological scoring in mouse models of neurodegeneration (Acevedo-

Arozena et al., 2011) (Leitner et al., 2009). *Ewsr1*$^{\Delta/\Delta}$ mice showed a decreased capacity of extension compared to *Ewsr1*$^{+/+}$ mice (Figure 34C), as well as an increased asymmetry during performance (Figure 34D). Analysis of subpopulations revealed interesting data: extension defects aggravated upon ageing, consistent with a neurodegenerative defect, and were more pronounced in males than in females (Figure 34C). All of the above are reminiscent of amyotrophic lateral sclerosis (ALS), which is age-associated and has a greater incidence in males. Assymetry in *Ewsr1*$^{\Delta/\Delta}$ mice was also reminiscent of ALS, as motor defects in ALS typically initiate locally at one side of the body and later extend to the rest, and this was also aggravated in males (Figure 34D).

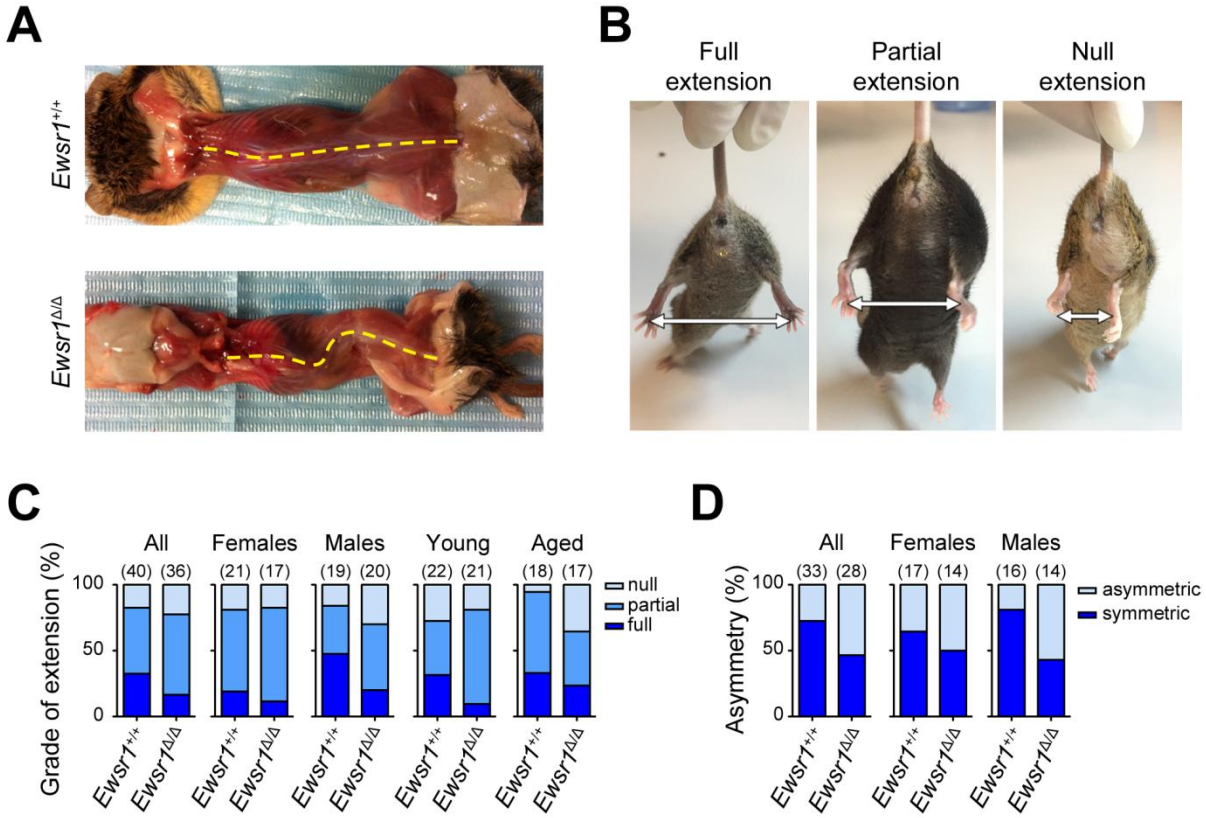

Figure 34
EWS-depleted mice have a reduced hind limb extension capacity and display an increased asymmetry during extension. (A) 53-week-old *Ewsr1*$^{+/+}$ and *Ewsr1*$^{\Delta/\Delta}$ littermates. *Ewsr1*$^{\Delta/\Delta}$ mouse presents scoliosis. Yellow dashed lines indicate spinal cord path. (B) Scoring of extension capacity during hind limb extension reflex. (C) Distributions of extension capacity groups within *Ewsr1*$^{+/+}$ and *Ewsr1*$^{\Delta/\Delta}$ mice. Panels correspond to general population, females, males, young (<=30 week-old) animals and aged (>30 week-old) animals, respectively. (D) Distributions of animals performing extension symmetrically or asymmetrically. Panels correspond to general population, females and males. Only animals with full or partial extension capacity were evaluated for symmetry/asymmetry. Numbers of animals in each group are indicated on top of the corresponding columns.

ALS (OMIM #105400) is a neurodegenerative disorder characterized by the death of motor neurons (MN) in the brain and spinal cord. It usually begins with asymmetric atrophy of limb muscles in mid-life, and muscular function is progressively impaired leading to paralysis and death (Boillee et al., 2006; Pasinelli and Brown, 2006). Up to 10% of ALS cases are familial (fALS) (Dion et al., 2009), usually autosomal dominant. Defects in several genes have been reported to cause ALS, SOD1 being the most prevalent cause in fALS (Rosen et al., 1993). Mutations in FUS and Senataxin are also causative of fALS (Chen et al., 2004; Kwiatkowski et al., 2009) and, intriguingly, sequentiation of the *EWSR1* gene in 817 individuals diagnosed with ALS revealed deleterious mutations at the RNA binding domains of EWS in 2 independent patients.

Several transgenic mouse models of SOD1 have been developed that recapitulate the disease (Bruijn et al., 1997; Gurney et al., 1994; Jonsson et al., 2004; Jonsson et al., 2006; Wong et al., 1995). A hallmark of ALS is the loss of MNs, a feature that is shared in ALS mouse models (Acevedo-Arozena et al., 2011; Pasinelli and Brown, 2006), and vacuolization at the neuronal bodies is also observed in both ALS patients and mice (Riancho et al., 2014; Vinsant et al., 2013; Wong et al., 1995). Based on this we explored the MN population at the spinal cords of aged *Ewsr1*$^{+/+}$ and *Ewsr1*$^{\Delta/\Delta}$ mice. Strikingly, MN counts were decreased in *Ewsr1*$^{\Delta/\Delta}$ mice (Figure 35A and B), and they presented a severe vacuolization as assessed by Cresyl violet staining (Figure 35C).

Whether the R-loop-limiting role of EWS is related to the ALS-like phenotype observed in *Ewsr1*$^{\Delta/\Delta}$ mice, and whether R-loops do actually accumulate in motor neurons remain open questions that need to be addressed. Still, these preliminary results suggest that EWS has a neuroprotective role, and that EWS deficiency in the adult Bmi1-positive stem cell compartment can trigger a progressive ALS in mice.

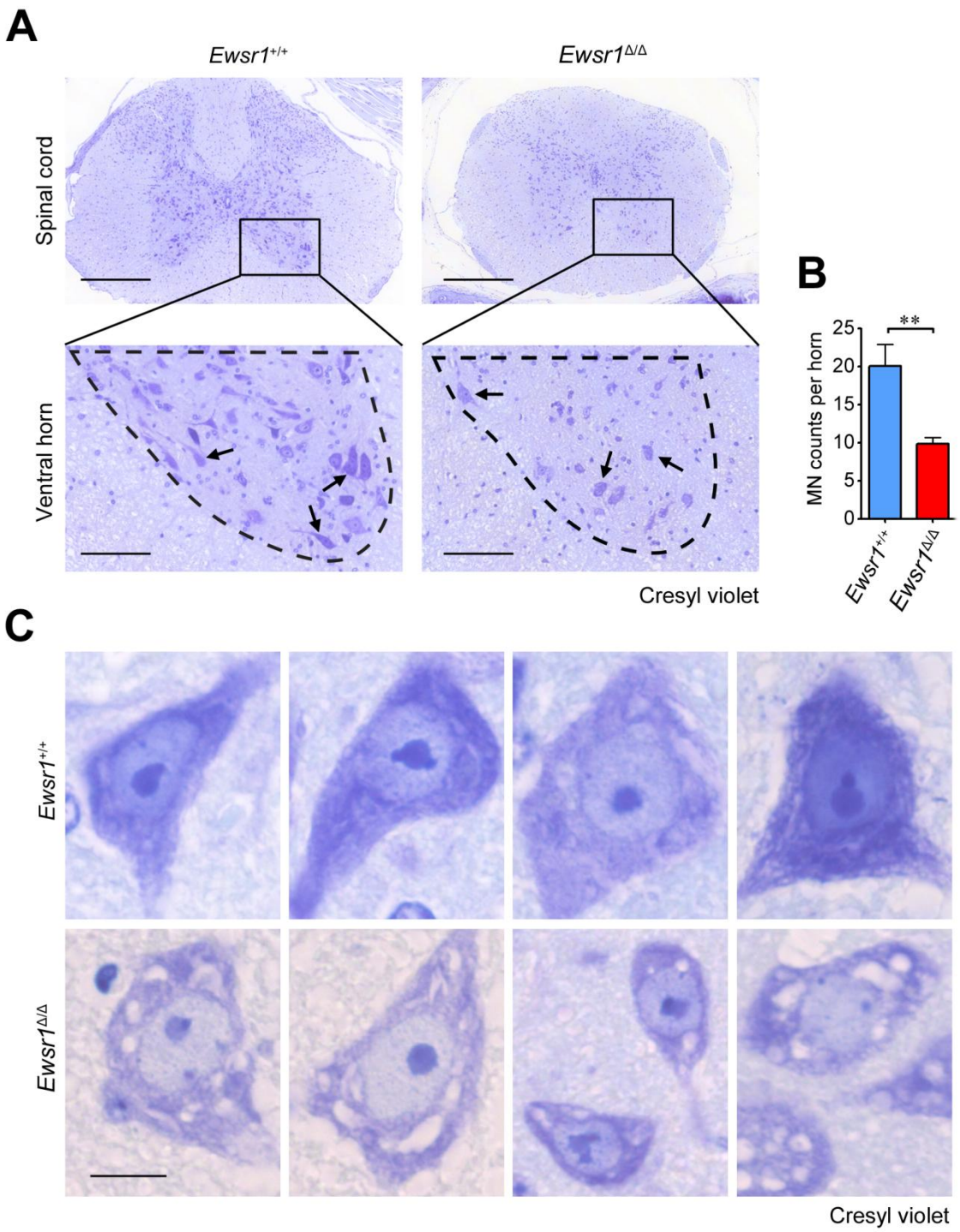

Figure 35
Motor neuron counts are reduced in aged *Ewsr1*$^{\Delta/\Delta}$ mice and present vacuolization at neuronal bodies. (A) Transversal sections of thoracic spinal cords of 53-week-old *Ewsr1*$^{+/+}$ and *Ewsr1*$^{\Delta/\Delta}$ mice. Insets show ventral horns (area delimited by dashed line) where motor neurons are identified by shape and size. Arrows point to some motor neurons. Scale bars, 100 µM (B) Quantification of motor neuron counts in aged *Ewsr1*$^{+/+}$ and *Ewsr1*$^{\Delta/\Delta}$ mice. n=2 mice per genotype. At least 3 ventral horns per mouse were analyzed. (C) Representative pictures of motor neurons. Scale bar, 16 µM.

DISCUSSION

PART I: Modest impact of FBH1 deficiency in mammals

The first objective of this PhD was to evaluate the *in vivo* contribution of FBH1 to maintenance of genome integrity. In this study we have developed a mouse strain for deletion of *Fbh1*. We have observed a moderate impact of *Fbh1* deletion on mouse weight and on RS-derived signaling, but embryonary development, viability and fertility were unaltered, and we failed to detect any other deficiency on the previously described roles of this helicase.

Consistent with other studies (Fugger et al., 2009) we detected attenuated signaling after RS at the cellular level, including a mild decrease in RPA phosphorylation and in γH2AX. However, we were unable to detect an altered cellular response, either in damage repair, cell cycle arrest/regulation or cellular viability (Figure 11). According to recent work (Fugger et al., 2013; Jeong et al., 2013b), FBH1 mediates apoptosis in the presence of excessive RS, and decreased signaling in FBH1-depleted cells results in deficient activation of pro-apoptotic pathways. Nonetheless, cell cycle profiles of *Fbh1*$^{GT/GT}$ cells revealed no increased survival rates, either in untreated cells or after inducing RS with HU or ATRi. One possible explanation is that apoptosis is only abrogated below a certain threshold of pro-apoptotic signaling, and *Fbh1* deletion reduces RS-derived signalling to a level that does not reach this threshold. Therefore, reduced signaling is observed but abrogation of apoptosis is not. Whether or not this is the case, remains an unanswered question. Remarkably, we bred the *Fbh1*^{GT} allele into ATR$^{S/S}$ mice, which suffer from RS and undergo cellular apoptosis during embryo development. Importantly, *Fbh1* deletion did not rescue any of the ATR$^{S/S}$ phenotypes; on the contrary, it further aggravated it (Figure 12). Therefore, both at the cellular and at the organism level, our results do not support the aforementioned model, by which FBH1 would promote apoptosis in cells accumulating excessive RS. We do not discard this model either; in ATR$^{S/S}$ mice, the absence of an orchestrated apoptosis in stressed cells upon *Fbh1* deletion might have effects that are even more detrimental at the organism level, and thus lead to a further aggravation of the ATR$^{S/S}$ phenotype, although these data are at this point preliminary and the hypothesis remains to be strengthened. Regardless of the precise function of FBH1, the proposed pro-apoptotic role suggests a tumor suppressor function, by which cells with genomic instability derived from

excessive RS are eliminated from the organism to prevent malignant transformation. This is supported by mutations or deletions detected at the *FBH1* gene in human melanoma cell lines (Jeong et al., 2013a). However, our colony of *Fbh1*$^{GT/GT}$ mice did not present an increased incidence of tumors, and thus does not support this hypothesis. Perhaps mutations linked to development of melanoma, such as loss of PTEN or expression of BRAF^{V600E} (Mehnert and Kluger, 2012), might increase the susceptibility of FBH1-deficient animals to develop cancer. The use of mouse models of melanoma might help address this issue at the organism level.

Mechanistically, several *in vitro* and cellular studies have shown that FBH1 negatively regulates the Rad51 nucleofilament by disrupting it through its helicase-translocase activity and by ubiquitylating it to prevent re-recruitment (Chu et al., 2015; Simandlova et al., 2013; Tsutsui et al., 2014). In these works, FBH1 depletion in cellular models resulted in retention of Rad51 in the chromatin fraction after sub cellular fractionation. However, in the present study, *Fbh1*$^{+/+}$ and *Fbh1*$^{GT/GT}$ cells did not show any difference in Rad51 binding to chromatin, either in basal conditions or after MMC treatment, and total Rad51 levels were unaltered (Figure 13). Consistently, we did not observe any phenotypes derived of excessive or unscheduled HR in *Fbh1*$^{GT/GT}$ cells, such as breakage or aberrations in metaphase chromosomes. This reinforces the idea that higher eukaryotes have evolved redundant mechanisms for HR regulation, making FBH1 dispensable for RS-derived HR (Fugger et al., 2009; Kohzaki et al., 2007).

FBH1 was proposed to be a functional homolog of the yeast canonical anti-recombinase Srs2. In this regard, Simandlova and colleagues found that mutant FBH1 cells were resistant to PARP1 inhibition. This argues in favor of an anti-recombinase role for FBH1, as deletion of pro-recombination factors such as BRCA1 generate hypersensitivity to PARP1 inhibition (Farmer et al., 2005). BRCA1 mutant mice have a strong phenotype with embryonic lethality and impaired HR in cell cultures. We aimed at obtaining genetic proof of the anti-recombinase activity of FBH1 by deleting *Fbh1* in BRCA1 mutant mice. The reasoning was that removing a negative regulator of HR might restore HR to some extent in those animals. However, deletinon of *Fbh1* in did not show any rescue of the BRCA1 mutant phenotype, indicating that FBH1 loss does not compensate for a low-recombinant phenotype (Figure 14). In line with this, *Fbh1* deletion did not have an impact on the efficiency of class-switch recombination, a physiological process in B cells that invokes NHEJ as opposed to HR (Bunting et al., 2010). Taken together, we could not demonstrate an anti-recombinase activity of FBH1 *in vivo*. Again, this might reflect a pathway redundancy existing in higher eukariotes.

To summarize, we found that FBH1 has a moderate role in signaling RS, although we could not detect any effects of *Fbh1* deletion in terms of genomic instability or tumorigenesis. An impact of FBH1 on regulation of HR was not detected, either at the cellular level or in animals with a genetic background involving limited HR. Whereas putative homolog Srs2 in yeasts limits HR and is critical for resistance to DNA damaging agents, it is possible that higher eukaryotes have evolved redundant mechanisms for regulating HR, so that in mammals FBH1 is dispensable for a proficient HR. In this regard several works propose RTEL1 helicase as another functional homolog of yeast anti-recombinase Srs2 (Barber et al., 2008). One possibility is that several proteins, including FBH1 and RTEL1, contribute to regulating HR and are sufficient to fulfill their function in the absence of functional partners. Alternatively, differences between the present model and previous approaches might explain the opposing observations. Many studies were performed with RNA interference of *Fbh1* which promotes depletion of the protein immediately before observation; instead, constitutive genetic deletion of *Fbh1* in mice might let the organism re-wire alternative pathways to compensate for the lack of FBH1. In this scenario, we might have underestimated the actual roles of FBH1 at the organism level; in any case, these roles are most probably non-essential and/or compensable.

The mouse strain described in this work might serve to further study genetic interactions between FBH1 and players of the HR and the RS-response pathways, and as a genetic model of FBH1 deficiency to unravel the molecular mechanisms of this elusive helicase.

PART II: New insights into Ewing sarcoma and EWS function

1. Exploiting tumor-associated RS for the treatment of Ewing sarcoma

RS is a relevant source of DNA damage and genomic instability (Lecona and Fernandez-Capetillo, 2014). Interestingly, Ewing sarcoma has a high rate of genomic rearrangements (Ferreira et al., 2008; Ohali et al., 2004) but is among the tumor types with lowest point mutation frequency (Alexandrov et al., 2013), which together is reminiscent of RS. In the present work we have detected increased levels of RS in Ewing sarcoma (Figure 15 and Figure 16). In our lab we previously showed that tumors with increased RS levels, such as Eu-myc lymphoma, H-Ras fibrosarcoma and MLL-ENL AML, are especially dependent on ATR activity and can be selectively targeted by inhibiting ATR, which drives the rapidly growing tumoral cells to unrestrained cell cycle progression and mitotic catastrophe (Murga et al., 2011; Schoppy et al., 2012). We have here shown that ES cells are hypersensitive to ATR inhibition (Figure 17), and that inhibiting ATR efficiently abrogates Ewing sarcoma xenograft growth (Figure 18). Remarkably, our ATRi is specifically toxic to ES cell lines at doses at which it is not toxic to control cell lines. In relation to other drugs, ATRi is almost 100-fold more toxic to ES cells than Olaparib and at least 10^4-fold more toxic tan TMZ (Figure 17C), two drugs that are being tested in combination in clinical trials as an alternative to current chemoterapeutics for the treatment of Ewing sarcomas (NCT01858168; https://clinicaltrials.gov/ct2/show/NCT01858168).

2. Understanding Ewing sarcoma: R-loops are responsible for RS

Multiple processes can contribute to increase RS in proliferating cells; one is the aberrant accumulation or persistency of R-loops. In this work we have determined an accumulation of R-loops in ES cell lines and in EWS-defective cells (Figure 29), revealing R-loops as the source of RS in this particular tumor type. Several links have been suggested between R-loops and cancer (reviewed in (Groh and Gromak, 2014); most remarkably, BRCA2 (a tumor suppressor that is frequently mutated in breast cancer) was found to be required for preventing R-loop

accumulation (Bhatia et al., 2014). Nonetheless, for the first time we are reporting the distinctive presence of R-loops in a particular type of cancer.

Our findings in this work provide a mechanistic explanation for the hypersensitivity of Ewing sarcomas to TopoI inhibitors, which remained not understood to date. CPT inhibits TopoI, an enzyme that relieves torsional stress during transcription, and mutation of top1 (yeast TopoI homolog) results in R-loop accumulation (El Hage et al., 2010). Work by Vanesa Lafarga at our lab has demonstrated that a deficiency in R-loop-suppressing mechanisms sensitizes cells to CPT and ATRi (unpublished data). We have detected a high sensitivity of EWS-deficient cells to CPT and, significantly, TopoI inhibitors topotecan and irinotecan are being explored for chemotherapy of Ewing sarcoma with promising results (Kurucu et al., 2015), although the basis of this sensitivity remained elusive. We here show that sensitivity of Ewing sarcomas to TopoI inhibitors is based on their inability to limit R-loop accumulation.

Whereas CPT generates a high burden of R-loop-derived RS, ATRi has an essentially different effect; it prevents a response to RS, thus aggravating its accumulation and impeding cell cycle checkpoint activation and arrest. Under these circumstances RS is extremely toxic, as cells have no emergency stop to prevent premature entry into mitosis. Under-replicated DNA causes segregation defects that lead cells to mitotic catastrophe. Based on this we suggest ATR inhibition as an alternative strategy to treat Ewing sarcomas, and we propose a combination of TopoI inhibitors with ATRi to induce RS-based synthetic lethality in Ewing sarcoma tumoral cells (Figure 36).

Of note, in regards to RS, we base our conclusions on the levels and staining pattern of γH2AX

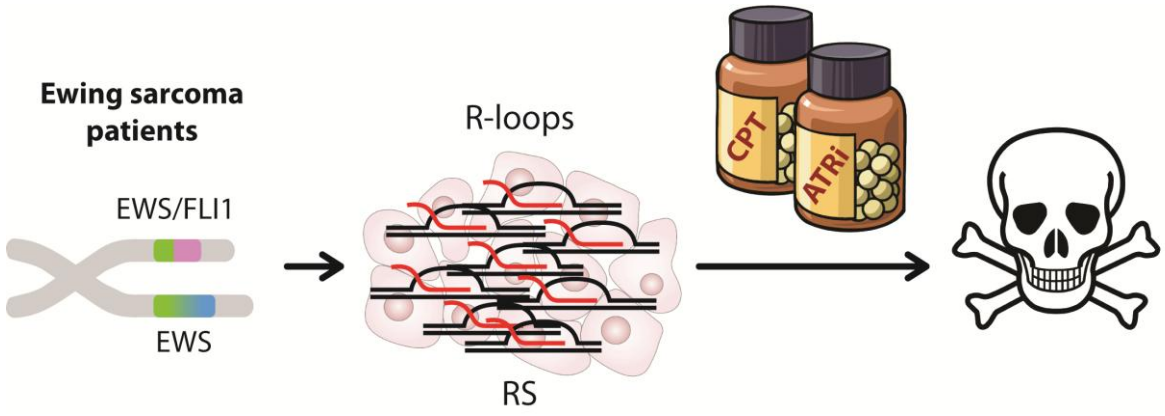

Figure 36
A synthetic lethal approach to target Ewing sarcomas based on the molecular mechanisms of this particular cancer type. Ewing sarcomas suffer from R-loop-derived RS. CPT or derivatives increase R-loop burden thereby impairing proper DNA replication. ATR inhibition pushes under-replicating cells to mitosis causing mitotic catastrophe and death.

found in ES cell lines and EWS/FLI1-expressing cells, as well as on the hypersensitivity to RS-inducing treatments. However, neither ES cell lines nor EWS/FLI1-expressing cells showed increased ssDNA or RPA foci (data not shown), which is a frequent outcome of fork stalling and a common readout of RS. For example, HU, a commonly used RS-inducing agent, promotes dNTP pool depletion leading to a blockade of the DNA polymerase and uncoupling of the helicase, which continues to unwind DNA ahead of the fork and generates extensive ssDNA threads (Byun et al., 2005). Nonetheless the absence of RPA foci at RS sites is not new. For instance, inter-strand crosslinks or DNA-protein adducts are physical barriers and can block replication fork progress whithout a concomitant helicase-polymerase uncoupling, and therefore do not lead to a significant ssDNA-RPA accumulation (Nam and Cortez, 2011). R-loops appear to be also physical obstacles to fork progression and may not allow uncoupling; therefore, uncoupling-derived ssDNA might not arise in this scenario, consistent with failure of ES cell lines EWS/FLI-expressing cells to show increased ssDNA in spite of RS evidence. In fact, this work highlights R-loops as an RPA-ssDNA-independent source of RS. It will be interesting to assess the means by which ATR is activated under these circumstances, which remains an open question. Furthermore, how common is R-loop-derived RS in physiological and pathological contexts, and what might be its contribution to pathogenesis needs to be addressed.

3. Contributions of EWS deletion and EWS/FLI1 expression in tumorigenesis: molecular dissection

Whereas the founding event leading to Ewing sarcoma is well established to be the translocation between *EWSR1* and *FLI1* genes, two direct consequences of the translocation can be identified: 1) the production of an EWS/FLI1 fusion product, and 2) the interruption of one *EWSR1* allele, and therefore loss of EWS activity. To dissect the contributions of each of these two conditions to R-loop accumulation and RS, we have benefited from a model for transgenic EWS/FLI1 expression (Lin et al., 2008) and a model for deletion of EWS (described in this work) (Figure 20).

EWS/FLI1 ectopic expression in cells induces R-loops and RS, consistent with R-loops and RS detected in ES cell lines, indicating that R-loops in ES cell lines are a consequence of the translocation. Strikingly, EWS-deficient embryos show hallmarks of RS, and embryo-derived EWS-deficient cells also accumulate R-loops and RS, analogously to EWS/FLI1-expressing cells, and suffer from genomic instability. Furthermore, EWS-deficient cells are hypersensitive to CPT, consistent with the increased sensitivity of Ewing sarcomas to TopoI inhibitors.

The fact that EWS deletion phenocopies the defects in EWS/FLI1-expressing cells and in Ewing sarcomas, suggests that expression of EWS/FLI1 promotes a loss of function of EWS. In Ewing sarcomas one *EWSR1* allele is involved in the founding translocation and, thus, expression of wild-type EWS from that allele is lost. However the other allele remains intact; in fact, EWS protein can be detected in ES cell lines in decreased amounts (Figure 16A). On the other hand, in the EWS/FLI1 model, the fusion protein is expressed from a transgene, and both *Ewsr1* alleles are intact. In both cases, loss of EWS activity might be explained through a putative dominant-negative effect of the fusion protein over EWS protein. Based on this, we propose that EWS works as an R-loop suppressor, and EWS/FLI1 has an indirect role in R-loop accumulation through inhibition of EWS activity (Figure 37). The parallel defects in both *Ewsr1*$^{GT/GT}$ cells and EWS/FLI1-expressing cells over R-loop accumulation, impaired RNA export and RS support the idea of an EWS loss-of-function common mechanism. Supporting this model, EWS and EWS/FLI1 were found to be co-interactors (Spahn et al., 2003). In any case, further research is needed in this regard. For example, it will be interesting to assess whether expression of EWS/FLI1 in EWS-deficient cells fails to further increase R-loops.

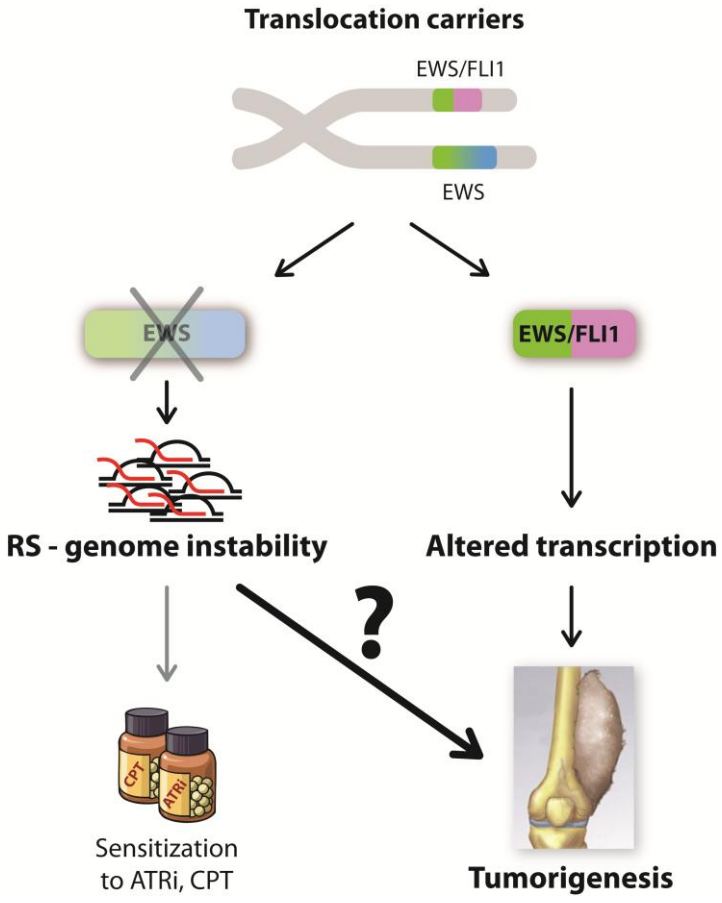

Figure 37
Molecular dissection of EWS and EWS/FLI1 contributions to tumorigenesis. EWS/FLI1 is a reported oncogene that alters the bone transcriptional pattern and leads to tumorigenesis. Concomitant loss of EWS activity in carriers of the EWS/FLI1 translocation results in R-loop-driven RS and genomic instability. Whether this has an active contribution to tumorigenesis, remains an open question.

We further wondered about the role of R-loops in Ewing sarcoma. We have demonstrated an association of R-loops and Ewing sarcoma, but it remains unclear whether R-loop accumulation is merely a bystander or rather an active driver of tumorigenesis. Our findings do not discard that R-loop accumulation and subsequent RS are a mere byproduct of Ewing sarcoma biology, which indeed we can exploit to specifically target and kill tumoral cells through ATR inhibition or other strategies. Conversely, we can envision a scenario in which R-loop-driven RS has an active role in driving genomic instability and contributes to tumorigenesis. In other words, we speculate on the potential tumor suppressor role of EWS, independently of the proven oncogenic activity of the fusion protein EWS/FLI1, and we wonder about the tumorigenic potential of R-loop-driven RS (Figure 37). The genomic instability accumulating in EWS-deficient cells (Figure 31) supports this idea.

However, deletion of EWS in the adult Bmi1-positive cell population has not lead to increased tumorigenesis. Because the cell of origin of Ewing sarcoma remains elusive (Lessnick and Ladanyi, 2012), the generation of appropriate mouse models is greatly hampered. In this sense, deletion of EWS in other cellular compartments on in the whole organism might highlight any tissue-specific susceptibility to tumorigenesis. On the other hand, concomitant deletion of a central tumor suppressor such as p53 might lower the threshold for malignant transformation and lead to a differential tumoral incidence in *Ewsr1*$^{\Delta/\Delta}$ mice. Alternatively, our hypothesis might be wrong, and R-loop-derived RS might just be a bystander in Ewing sarcoma with no contribution to tumorigenesis. Ongoing experiments in the lab in these directions might shed light on these issues.

4. EWS contribution to preventing neurodegeneration

Besides the molecular determinants of Ewing sarcoma and speculations on EWS contribution to suppressing tumorigenesis, we have identified a neurodegenerative disorder in adult, EWS-depleted mice that recapitulates several phenotypes of human ALS, including a decreased fitness in motor function and alterations in the MN population (Figure 34 and Figure 35). R-loops have been previously associated to ALS and other neurodegenerative disorders, and appear to be a central node linking a number of ALS-causing mutations (Salvi and Mekhail, 2015). Namely, mutations in SETX, a helicase that unwinds RNA:DNA hybrids and prevents R-loop accumulation, cause ALS (Chen et al., 2004). Actually in the lab we have observed that SETX knockdown leads to increased R-loops and sensitivity to TopoI inhibition (unpublished data). Mutations in ATXN2, with a described role in suppressing R-loops in yeast (Elden et al., 2010),

are also linked to ALS. Hexanucleotide repeat expansion occurring at C9ORF72 gene mediates accumulation of R-loops and is responsible for ALS and FTD, a neurodegenerative disease with molecular similarities to ALS (Haeusler et al., 2014; Wang et al., 2015). Furthermore, mutations in FUS (a member of the FET family) and in TDP43 (a structurally related protein) are causative of ALS. Although R-loop involvement in these cases has not been established, mutations in FUS and TDP43 are responsible for nuclear protein depletion and engagement in cytoplasmic RNP aggregates such as stress granules (Alami et al., 2014; Kwiatkowski et al., 2009; Sreedharan et al., 2008; Takanashi and Yamaguchi, 2014). Remarkably, wild-type EWS and TAF15 have also been reported to engage in such aggregates in tissue samples from FTD patients (Mackenzie and Neumann, 2012). Strikingly, deleterious mutations on *EWSR1* were recently identified in two patients with ALS (Couthouis et al., 2012). For the first time we report EWS deficiency as responsible for a phenotype reminiscent of ALS. To our knowledge, EWS is unique in that it both limits R-loops and incorporates into aberrant cytoplasmic aggregates, two main molecular hallmarks of ALS. This model highlights the role of EWS in RNA metabolism and provides a link to neurodegenerative processes. Importantly, the EWS conditional knockout mouse described in this work might serve as a genetic model for ALS.

5. A mechanism for EWS protein

We were especially interested in understanding the mechanisms of EWS in R-loop biology and its implication in the pathogenesis of diseases as diverse as Ewing sarcoma and ALS. What is the molecular function of this elusive protein? Is one unique function of EWS responsible for preventing such diverse pathologies? Or are independent deficiencies whithin the protein responsible for each of the pathologies? Four lines of evidence help answer these questions.

5.1. EWS is an R-loop suppressor

In the present work we have identified a novel role for EWS in preventing R-loops and subsequent genomic instability. Consistently, EWS binds DNA G-quadruplexes (Takahama et al., 2011), structures that might help stabilize R-loops on the complementary strand (Hamperl and Cimprich, 2014). Furthermore, genomic instability, which is one consequence of R-loop

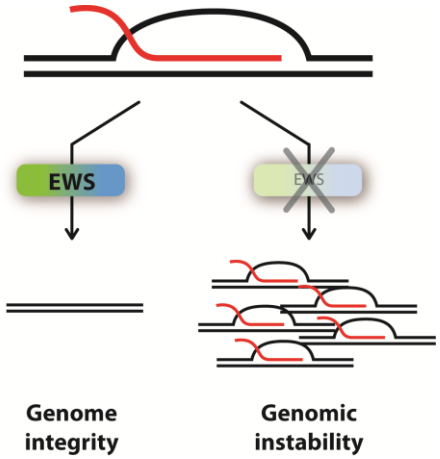

Figure 38
EWS is an R-loop suppressor. In an EWS-proficient context R-loops are efficiently removed and genome integrity is preserved. In an EWS-deficient context R-loops persist and accumulate, leading to RS and genomic instability.

accumulation, has also been described in mice deficient for FET family partner FUS (Hicks et al., 2000). EWS functional deficiency has an impact on the development of ALS, and possibly on cancer. The reduced RNA export rate observed in EWS-deficient cells (Figure 33) suggests that the R-loop-suppressive role of EWS is linked to the RNA export process.

5.2. EWS is recruited to particular genomic sites

Under certain circumstances EWS is recruited to DSB. All three FET proteins, which share a high degree of homology, are recruited to laser microirradiation sites in a PARP1- and PAR-dependent manner (Britton et al., 2014; Mastrocola et al., 2013; Rulten et al., 2014) suggesting a role in the response to DNA damage. FET proteins contain several RGG domains at their C-terminal region (Figure 9). Whereas RGG domains were initially postulated to represent RNA binding motifs (Kiledjian and Dreyfuss, 1992), they might alternatively be responsible for recruitment to PAR chains synthesized at DSBs, based on PAR structural similarity to RNA. This would imply that the C-terminus is required for protein mobilization. Interestingly, the two EWS deleterious mutations detected in ALS patients are located at the RGG domains (Couthouis et al., 2012).

EWS appears to have a distinct role at nucleoli. Immunofluorescent staining of U2OS cells showed nuclear staining with enhanced nucleolar localization in around 15% of cells (data not shown). Instead, in primary MEF, EWS is constitutively nuclear and excluded from nucleoli, and is recruited to nucleoli after UV irradiation (Paronetto et al., 2011) and after TopoI inhibition by CPT treatment (Figure 28). UV generates thymidin dimers and bulky adducts, whereas TopoI relieves torsional stress during transcription. Both conditions necessarily lead to transcription-replication or pure transcriptional conflicts (Figure 27), and with a special incidence where

transcription is more active: namely, at nucleoli. Whereas Paronetto and colleagues proposed that EWS was sequestered at the nucleoli as a strategy to prevent interruption of alternative splicing events in response to UV damage (Paronetto et al., 2011), we think EWS is has an active role in nucleoli in preventing R-loop accumulation. Consistent with this, EWS was found to be required for resistance to CPT in a genome wide sensitivity screen (O'Connell et al., 2010). Remarkably, BRCA1 and BARD1, which form a stable heterodimer required for regulation of RS-derived recombinatorial repair (Wu et al., 1996), were also top hits in that screen, and EWS has been found to interact with BARD1 (Spahn et al., 2002). This provides further evidence of the involvement of EWS in genome surveillance.

5.3. Self-aggregating properties of EWS

FET proteins and other hnRNPs undergo self-aggregation *in vitro* (Kato et al., 2012). The process is mediated by a low complexity (LC) domain, which in EWS (and in FET proteins) is located at the N-terminus, within the SYGQ-rich region (Figure 39A). LC domains, present in numerous proteins, have been described to undergo a concentration-dependent and RNA-dependent phase transition to a hydrogel-like state (Kato et al., 2012). Hydrogels are composed of uniformly polymerized amyloid-like fibers and can accommodate heterotypic polymerization in a dynamic manner. These observations might underlie a physiological organizing principle for the formation of membrane-less cellular structures. Both FET protein recruitment to laser microirradiation sites (Britton et al., 2014; Mastrocola et al., 2013; Rulten et al., 2014) and CPT-induced recruitment of EWS to nucleoli might represent physiological responses involving self-aggregation into hydrogels. Remarkably, the two *EWSR1* independent mutations detected in ALS patients alter EWS localization in motor neurons, exhibiting enhanced aggregation propensity (Couthouis et al., 2012). Importantly, ALS-linked mutant variants of FUS and EWS showed RNA-dependent engagement in cytoplasmic aggregates (Bentmann et al., 2013; Couthouis et al., 2012) and tissue sections from FTD patients present cytosolic aggregates or stress granules containing all three FET proteins and other hnRNPs (Bosco et al., 2010; Kwiatkowski et al., 2009; Mackenzie and Neumann, 2012; Takanashi and Yamaguchi, 2014). We speculate that mutations that alter the nuclear localization and/or the determinants for self-aggregation might result in enhanced/aberrant aggregation in the cytoplasm.

5.4. A model for EWS mechanism

Altogether, EWS mobilization to sites with genomic alterations (G-quadrulexes, DNA breaks, R-loops) is dependent on its C-terminal nucleic acid binding domains, while polymerization into aggregates is mediated by its N-terminal LC sequences. EWS has been thoroughly described as being involved in transcription and RNA processing, and there has been increasing evidence of its role as a genome caretaker, although a connection between these two functions was missing.

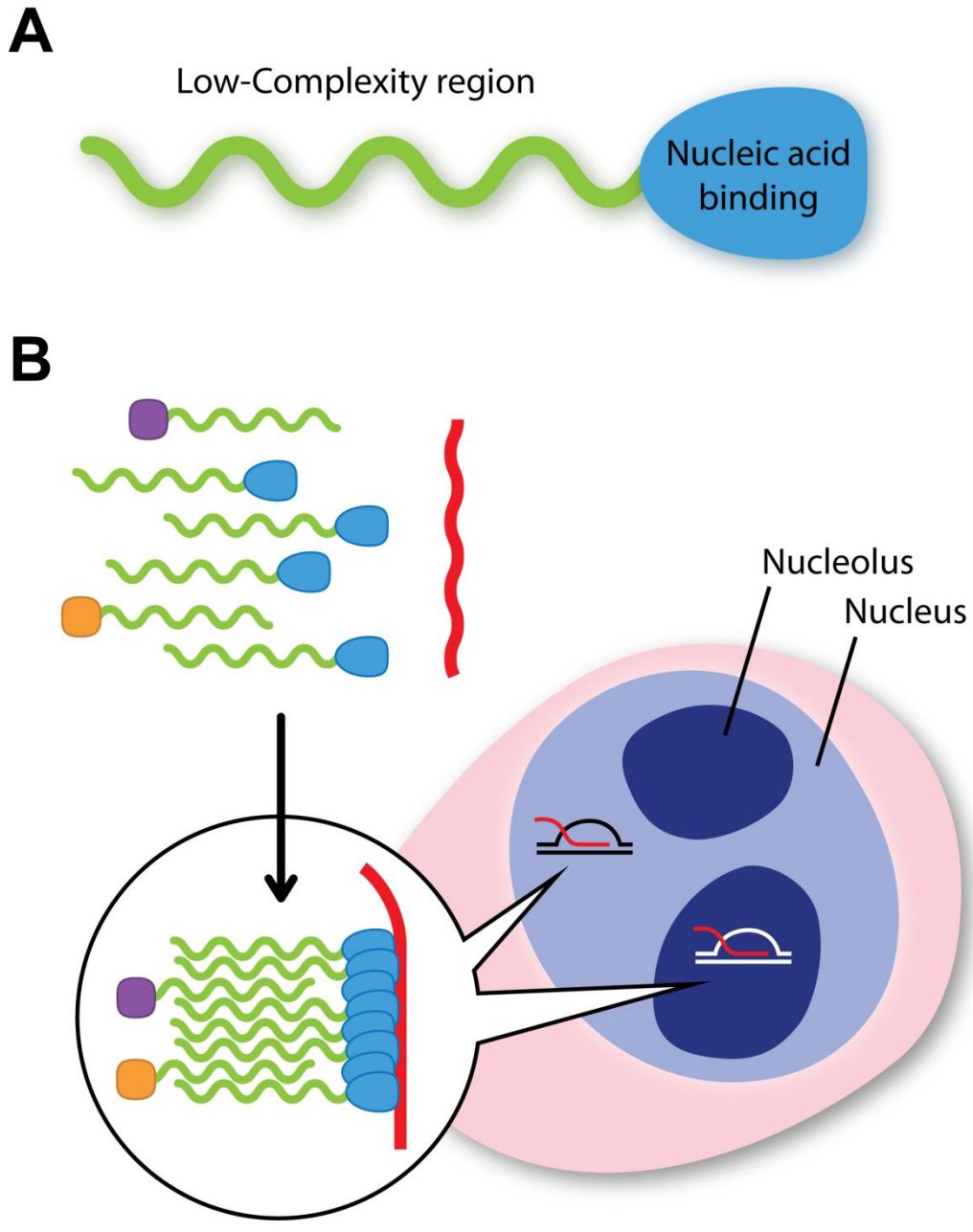

Figure 39
A model for aggregation-mediated EWS activity. (A) The SYGQ repeats at the N-terminal region of EWS constitute low-complexity sequences, which are intrinsically unstructured. (B) LC domains undergo a concentration-dependent phase transition to a hydrogel-like state which is dependent on the presence of RNA. EWS polymerization promotes incorporation into hydrogels of other LC-containing proteins (purple and orange) which might exert functions at the site of polymerization, such as DNA damage repair or R-loop removal.

Based on our results and the literature briefly reviewed above, we propose a model that conciliates the two faces of this protein. EWS is recruited to potentially hazardous nucleic acid substrates, including G-quadruplexes and DNA breaks, but most remarkably to R-loops, tightly linked to RNA metabolism. This leads to a local concentration increase that favours polymerization into a hydrogel, which further recruits other LC-containing proteins to form a dynamic platform for orchestration of early events in response to R-loop accumulation (Figure 39B). However, the precise molecular mechanism by which EWS resolves R-loops or prevents

its formation remains elusive and requires further investigation. Impaired RNA export in EWS-deficient cells suggests that the mechanism is related to nuclear export of transcripts. In this regard, EWS chromatin immunoprecipitation might clarify whether a direct interaction between EWS and R-loops or R-loop-prone genomic regions exist, and thus provide further insight into its molecular mechanism.

In the light of this model, deleterious EWS mutations might facilitate aberrant aggregation at the cytoplasm into stress granules, composed of RNA and proteins (Bentmann et al., 2012; Bosco et al., 2010). The presence of diverse protein aggregates in degenerating neurons has been thoroughly described (Bosco et al., 2010; Kwiatkowski et al., 2009; Mackenzie and Neumann, 2012; Takanashi and Yamaguchi, 2014), and the active – or passive – involvement of these aggregates in pathogenesis is a subject of debate. A hypothetical gain of function of aberrant FET protein aggregates might alter cytosolic RNA metabolism, which might have a cumulative effect eventually driving cellular degeneration and ALS pathogenesis (Baron et al., 2013). Conversely, following a loss-of-function model, FET protein cytosolic aggregates might essentially act to sequester additional LC-containing genome safeguarding proteins, thereby depleting the nucleus of functional units. Subsequent accumulation of R-loops and DNA damage would clog up the DNA-RNA-protein information flow of the cell, as supported by impaired RNA nuclear export in EWS-deficient cells (Figure 33). In the long term, this would contribute to a deficient cellular function and neurodegeneration (Figure 40). Genomic instability in FUS-KO and EWS-KO mouse models, and ALS-like phenotypes in adult EWS-KO mice support a loss-of-function mechanism rather than a gain-of-function of toxic, cytosolic protein aggregates, although these two possibilities are not mutually exclusive.

In the context of translocations involving FET proteins, the LC domain of the FET protein is fused to the DNA binding domain of a transcription factor. The fusion protein lacks the C-terminus of nucleic acid binding domains, which is replaced by the DNA-binding domain of a transcription factor (FLI1). This modification might lead to a number of consequences. First,

loss of the C-terminal region might prevent recruitment to C-terminal-dependent nucleic acid substrates such as R-loops. Second, and by the same reason, EWS interactors that depend on its C-terminus might be lost. Third, the fusion protein might be targeted to sites that differ from the original localization of EWS. Namely, the DNA binding domain contributed by FLI1 might localize the fusion protein to promoters specific to the transcription factor. Mislocalization and hydrogel polymerization in unscheduled sites might lead to sequestration of functional EWS and interactors, thereby depleting the cell of EWS and other genome safeguarding proteins. A similar effect was reported for RNAPII. It was shown that RNAPII interacted with LC-containing protein aggregates through its C-terminal domain (CTD). Based on this, it was proposed that

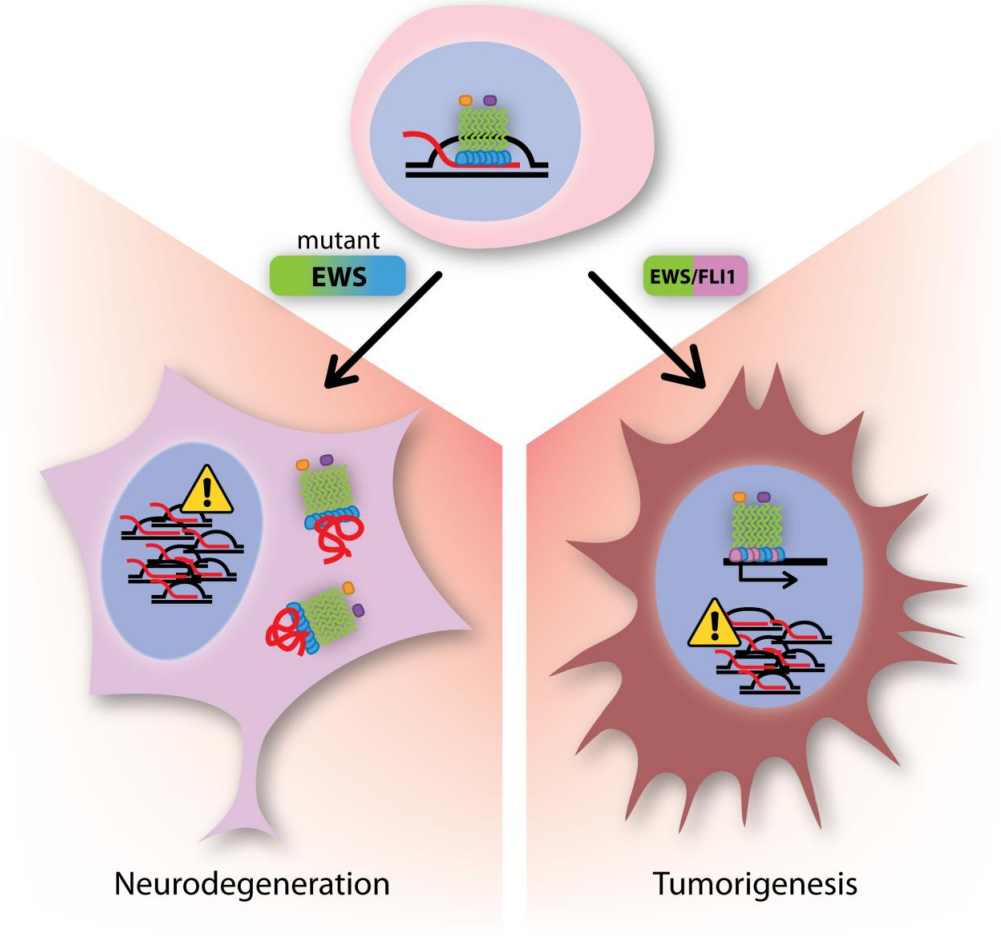

Figure 40
A model for pathogenesis derived from EWS deficiency. Key mutations in EWS result in impaired recruitment to target sites and/or aberrant polymerization at unscheduled sites, thereby depleting the nucleus from EWS activity. This results into R-loop accumulation, which in the long term impacts on neuronal function and leads to neurodegeneration. EWS/FLI1 is targeted to FLI1 promoters or unscheduled genomic regions where it promotes hydrogel polymerization. EWS/FLI1 aberrant hydrogels sequester endogenous EWS molecules at unscheduled sites, thereby depleting the cell of EWS activity. R-loops accumulating in this context generate RS and genomic instability which might contribute to tumorigenesis.

localization and polymerization of EWS/FLI1 to FLI1 promoters leads to recruitment of RNAPII, which triggers unscheduled transcription favouring tumoral transformation (Kwon et al., 2013), which might explain the oncogenic mechanism of EWS/FLI1. Based on this polymerization-sequestration effect, we hypothesize that polymerization of the fusion protein in

hydrogels at unscheduled sites might result in sequestration of functional EWS protein. This could explain the dominant-negative effect of EWS/FLI1 over EWS proposed throughout this work. In proliferating cells, depletion of functional EWS might lead to R-loop accumulation and increased RS levels, favouring tumoral transformation (Figure 40). Both mechanisms - gain of function of EWS/FLI1 and loss of function of EWS - are not mutually exclusive and might both contribute to tumorigenesis.

6. A novel physiological role for R-loops?

For the NOR-specific metaphase breakage analysis presented in this work we have used S9.6, an RNA:DNA hybrid-specific antibody as a tool to label NOR regions and analyse NOR breakage. Nonetheless, the presence of R-loops in metaphases (Figure 30) is *per se* a novelty: R-loops have not been described to persist throughout mitosis before. The presence of RNAPI and UBF in NORs on metaphase chromosomes was reported in some early works (Roussel et al., 1996; Weisenberger and Scheer, 1995). In those works they proposed that the persistence of transcriptional machinery attached to metaphasic NORs served to restart rRNA transcription immediately after chromosomal segregation, at telophase. Our observation that RNA:DNA hybrids persist on NORs supports this hypothesis and suggests that rRNA transcription is frozen at the elongation or termination level, and transcripts retained at their loci. Consistent with this, R-loops are thought to slow down or block transcription at the elongation/termination (Aguilera and Garcia-Muse, 2012). We can speculate on alternative functions for metaphasic NOR-associated R-loops. A very detailed work by Heliot and colleagues on the 3D organization of metaphasic NORs described these structures as 60-80 nM fibers emanating from the chromosomal axis and coiled around it (Heliot et al., 1997). The presence of DNA within these fibers was validated, and we now know that they also contain an RNA fraction that forms RNA:DNA hybrids. Interestingly, on our S9.6-stained metaphase spreads we sometimes observed some of the NOR-bearing chromosomes lying together and precisely aligned along their NORs (data not shown). This, together with the idea of chromatin fibers emanating from the chromosome and coiled around to form the structure of the NOR, suggests a possible structural role of NORs during metaphase. Intertwined NOR fibers might facilitate

interchromosomal organization during mitosis. Furthermore, and on a purely speculative basis, the intertwined RNA component at metaphasic NORs might serve as a security lock preventing premature segregation, or instead as a segregation sensor. Further work is needed in regards to determine a role for R-loops during mitosis.

To sum up, we have identified R-loops as the molecular basis of the vulnerability of Ewing sarcoma to TopoI inhibitors and to RS-inducing agents, and we provide a rationale for the use of ATR inhibitors for the treatment of Ewing sarcomas. We have determined a role for EWS protein in suppressing R-loop accumulation, which contributes to the maintenance of genome integrity. In Ewing sarcomas, loss of EWS activity might be responsible for R-loop accumulation, although the hypothesis of a dominant-negative effect of EWS/FLI1 over EWS remains to be strengthened. Whereas R-loop accumulation in Ewing sarcomas constitutes a vulnerability that can be exploited for treatment, the possible contribution of R-loop-derived genomic instability to tumorigenesis is still unanswered. An unexpected ALS-like phenotype in mice with EWS deletion in the adult stem cell compartment has highlighted the role of EWS in R-loop metabolism and has provided further insight in the ethiology of neurodegenerative diseases such as ALS or FTD. Whereas a gain-of-function model of mutant proteins has been widely attributed to the ethiology of these pathologies, our knockout mouse model rather supports a loss of function of R-loop-processing factors as the cause of disease. Finally, the detection of R-loops on metaphasic chromosomes opens a new field of study for R-loop biology.

CONCLUSIONS

PART I

1. FBH1 contributes to the signaling of RS, but has no impact on RS-driven toxicity.
2. FBH1 does not regulate Rad51 *in vivo* nor it rescues the viability of HR-deficient cells.
3. FBH1 is largely dispensable for mouse health.

PART II

4. Ewing sarcomas suffer from increased RS and are hypersensitive to ATR inhibition.
5. EWS protein limits RS and genomic instability, and its deletion sensitizes to ATR inhibition *in vivo*.
6. EWS protein prevents R-loop accumulation.
7. EWS favours nuclear export of RNA molecules.
8. Constitutive EWS deletion in mice leads to anemia and embryonic lethality.
9. EWS deletion in adult stem cells does not promote tumorigenesis in mice.
10. EWS deletion in adult stem cells leads to an ALS-like phenotype in mice.

CONCLUSIONES

PARTE I

1. FBH1 contribuye a la señalización del RS pero no tiene un impacto en la toxicidad derivada del RS.

2. FBH1 no regula a Rad51 in vivo ni rescata la viabilidad de células deficientes en HR.

3. FBH1 es prescindible para la salud de los ratones.

PARTE II

4. Los sarcomas de Ewing presentan altos niveles de RS y son hipersensitivos a la inhibición de ATR.

5. La protein EWS limita el RS y la inestabilidad genómica, y su deleción sensibiliza a la inhibición de ATR *in vivo*.

6. La proteína EWS previene la acumulación de bucles-R.

7. La proteína EWS promueve la exportación nuclear de moléculas de RNA.

8. La deleción constitutive de EWS en ratones produce anemia y letalidad embrionaria.

9. La deleción de EWS en células madre adultas no promueve tumorigénesis en ratones.

10. La deleción de EWS en células madre adultas da lugar a un fenotipo similar a esclerosis lateral amiotrófica en ratones.

BIBLIOGRAPHY

Acevedo-Arozena, A., B. Kalmar, S. Essa, T. Ricketts, P. Joyce, R. Kent, C. Rowe, A. Parker, A. Gray, M. Hafezparast, J.R. Thorpe, L. Greensmith, and E.M. Fisher. 2011. A comprehensive assessment of the SOD1G93A low-copy transgenic mouse, which models human amyotrophic lateral sclerosis. *Dis Model Mech*. 4:686-700.

Agarwal, S., A.A. Tafel, and R. Kanaar. 2006. DNA double-strand break repair and chromosome translocations. *DNA Repair (Amst)*. 5:1075-81.

Aguilera, A., and T. Garcia-Muse. 2012. R loops: from transcription byproducts to threats to genome stability. *Mol Cell*. 46:115-24.

Alami, N.H., R.B. Smith, M.A. Carrasco, L.A. Williams, C.S. Winborn, S.S. Han, E. Kiskinis, B. Winborn, B.D. Freibaum, A. Kanagaraj, A.J. Clare, N.M. Badders, B. Bilican, E. Chaum, S. Chandran, C.E. Shaw, K.C. Eggan, T. Maniatis, and J.P. Taylor. 2014. Axonal transport of TDP-43 mRNA granules is impaired by ALS-causing mutations. *Neuron*. 81:536-43.

Alexandrov, L.B., S. Nik-Zainal, D.C. Wedge, S.A. Aparicio, S. Behjati, A.V. Biankin, G.R. Bignell, N. Bolli, A. Borg, A.L. Borresen-Dale, S. Boyault, B. Burkhardt, A.P. Butler, C. Caldas, H.R. Davies, C. Desmedt, R. Eils, J.E. Eyfjord, J.A. Foekens, M. Greaves, F. Hosoda, B. Hutter, T. Ilicic, S. Imbeaud, M. Imielinski, N. Jager, D.T. Jones, D. Jones, S. Knappskog, M. Kool, S.R. Lakhani, C. Lopez-Otin, S. Martin, N.C. Munshi, H. Nakamura, P.A. Northcott, M. Pajic, E. Papaemmanuil, A. Paradiso, J.V. Pearson, X.S. Puente, K. Raine, M. Ramakrishna, A.L. Richardson, J. Richter, P. Rosenstiel, M. Schlesner, T.N. Schumacher, P.N. Span, J.W. Teague, Y. Totoki, A.N. Tutt, R. Valdes-Mas, M.M. van Buuren, L. van 't Veer, A. Vincent-Salomon, N. Waddell, L.R. Yates, I. Australian Pancreatic Cancer Genome, I.B.C. Consortium, I.M.-S. Consortium, I. PedBrain, J. Zucman-Rossi, P.A. Futreal, U. McDermott, P. Lichter, M. Meyerson, S.M. Grimmond, R. Siebert, E. Campo, T. Shibata, S.M. Pfister, P.J. Campbell, and M.R. Stratton. 2013. Signatures of mutational processes in human cancer. *Nature*. 500:415-21.

Alzu, A., R. Bermejo, M. Begnis, C. Lucca, D. Piccini, W. Carotenuto, M. Saponaro, A. Brambati, A. Cocito, M. Foiani, and G. Liberi. 2012. Senataxin associates with replication forks to protect fork integrity across RNA-polymerase-II-transcribed genes. *Cell*. 151:835-46.

Andersen, S.L., D.T. Bergstralh, K.P. Kohl, J.R. LaRocque, C.B. Moore, and J. Sekelsky. 2009. Drosophila MUS312 and the vertebrate ortholog BTBD12 interact with DNA structure-specific endonucleases in DNA repair and recombination. *Mol Cell*. 35:128-35.

Andersson, M.K., A. Stahlberg, Y. Arvidsson, A. Olofsson, H. Semb, G. Stenman, O. Nilsson, and P. Aman. 2008. The multifunctional FUS, EWS and TAF15 proto-oncoproteins show cell type-specific expression patterns and involvement in cell spreading and stress response. *BMC Cell Biol*. 9:37.

Araya, N., H. Hiraga, K. Kako, Y. Arao, S. Kato, and A. Fukamizu. 2005. Transcriptional down-regulation through nuclear exclusion of EWS methylated by PRMT1. *Biochem Biophys Res Commun*. 329:653-60.

Araya, N., K. Hirota, Y. Shimamoto, M. Miyagishi, E. Yoshida, J. Ishida, S. Kaneko, M. Kaneko, T. Nakajima, and A. Fukamizu. 2003. Cooperative interaction of EWS with CREB-binding protein selectively activates hepatocyte nuclear factor 4-mediated transcription. *J Biol Chem*. 278:5427-32.

Arlt, M.F., J.G. Mulle, V.M. Schaibley, R.L. Ragland, S.G. Durkin, S.T. Warren, and T.W. Glover. 2009. Replication stress induces genome-wide copy number changes in human cells that resemble polymorphic and pathogenic variants. *Am J Hum Genet*. 84:339-50.

Babu, K.A., and R.S. Verma. 1985. Structural and functional aspects of nucleolar organizer regions (NORs) of human chromosomes. *Int Rev Cytol.* 94:151-76.

Bailly, R.A., R. Bosselut, J. Zucman, F. Cormier, O. Delattre, M. Roussel, G. Thomas, and J. Ghysdael. 1994. DNA-binding and transcriptional activation properties of the EWS-FLI-1 fusion protein resulting from the t(11;22) translocation in Ewing sarcoma. *Mol Cell Biol.* 14:3230-41.

Balamuth, N.J., and R.B. Womer. 2010. Ewing's sarcoma. *Lancet Oncol.* 11:184-92.

Barber, L.J., J.L. Youds, J.D. Ward, M.J. McIlwraith, N.J. O'Neil, M.I. Petalcorin, J.S. Martin, S.J. Collis, S.B. Cantor, M. Auclair, H. Tissenbaum, S.C. West, A.M. Rose, and S.J. Boulton. 2008. RTEL1 maintains genomic stability by suppressing homologous recombination. *Cell.* 135:261-71.

Barlow, J.H., R.B. Faryabi, E. Callen, N. Wong, A. Malhowski, H.T. Chen, G. Gutierrez-Cruz, H.W. Sun, P. McKinnon, G. Wright, R. Casellas, D.F. Robbiani, L. Staudt, O. Fernandez-Capetillo, and A. Nussenzweig. 2013. Identification of early replicating fragile sites that contribute to genome instability. *Cell.* 152:620-32.

Baron, D.M., L.J. Kaushansky, C.L. Ward, R.R. Sama, R.J. Chian, K.J. Boggio, A.J. Quaresma, J.A. Nickerson, and D.A. Bosco. 2013. Amyotrophic lateral sclerosis-linked FUS/TLS alters stress granule assembly and dynamics. *Mol Neurodegener.* 8:30.

Barretina, J., G. Caponigro, N. Stransky, K. Venkatesan, A.A. Margolin, S. Kim, C.J. Wilson, J. Lehar, G.V. Kryukov, D. Sonkin, A. Reddy, M. Liu, L. Murray, M.F. Berger, J.E. Monahan, P. Morais, J. Meltzer, A. Korejwa, J. Jane-Valbuena, F.A. Mapa, J. Thibault, E. Bric-Furlong, P. Raman, A. Shipway, I.H. Engels, J. Cheng, G.K. Yu, J. Yu, P. Aspesi, Jr., M. de Silva, K. Jagtap, M.D. Jones, L. Wang, C. Hatton, E. Palescandolo, S. Gupta, S. Mahan, C. Sougnez, R.C. Onofrio, T. Liefeld, L. MacConaill, W. Winckler, M. Reich, N. Li, J.P. Mesirov, S.B. Gabriel, G. Getz, K. Ardlie, V. Chan, V.E. Myer, B.L. Weber, J. Porter, M. Warmuth, P. Finan, J.L. Harris, M. Meyerson, T.R. Golub, M.P. Morrissey, W.R. Sellers, R. Schlegel, and L.A. Garraway. 2012. The Cancer Cell Line Encyclopedia enables predictive modelling of anticancer drug sensitivity. *Nature.* 483:603-7.

Bartek, J., M. Mistrik, and J. Bartkova. 2012. Thresholds of replication stress signaling in cancer development and treatment. *Nat Struct Mol Biol.* 19:5-7.

Bartkova, J., N. Rezaei, M. Liontos, P. Karakaidos, D. Kletsas, N. Issaeva, L.V. Vassiliou, E. Kolettas, K. Niforou, V.C. Zoumpourlis, M. Takaoka, H. Nakagawa, F. Tort, K. Fugger, F. Johansson, M. Sehested, C.L. Andersen, L. Dyrskjot, T. Orntoft, J. Lukas, C. Kittas, T. Helleday, T.D. Halazonetis, J. Bartek, and V.G. Gorgoulis. 2006. Oncogene-induced senescence is part of the tumorigenesis barrier imposed by DNA damage checkpoints. *Nature.* 444:633-7.

Beck, H., V. Nahse-Kumpf, M.S. Larsen, K.A. O'Hanlon, S. Patzke, C. Holmberg, J. Mejlvang, A. Groth, O. Nielsen, R.G. Syljuasen, and C.S. Sorensen. 2012. Cyclin-dependent kinase suppression by WEE1 kinase protects the genome through control of replication initiation and nucleotide consumption. *Mol Cell Biol.* 32:4226-36.

Bentmann, E., C. Haass, and D. Dormann. 2013. Stress granules in neurodegeneration--lessons learnt from TAR DNA binding protein of 43 kDa and fused in sarcoma. *FEBS J.* 280:4348-70.

Bentmann, E., M. Neumann, S. Tahirovic, R. Rodde, D. Dormann, and C. Haass. 2012. Requirements for stress granule recruitment of fused in sarcoma (FUS) and TAR DNA-binding protein of 43 kDa (TDP-43). *J Biol Chem.* 287:23079-94.

Bermejo, R., M.S. Lai, and M. Foiani. 2012. Preventing replication stress to maintain genome stability: resolving conflicts between replication and transcription. *Mol Cell.* 45:710-8.

Bertolotti, A., Y. Lutz, D.J. Heard, P. Chambon, and L. Tora. 1996. hTAF(II)68, a novel RNA/ssDNA-binding protein with homology to the pro-oncoproteins TLS/FUS and EWS is associated with both TFIID and RNA polymerase II. *Embo j.* 15:5022-31.

Bertolotti, A., T. Melot, J. Acker, M. Vigneron, O. Delattre, and L. Tora. 1998. EWS, but not EWS-FLI-1, is associated with both TFIID and RNA polymerase II: interactions between two members of the TET family, EWS and hTAFII68, and subunits of TFIID and RNA polymerase II complexes. *Mol Cell Biol.* 18:1489-97.

Bester, A.C., M. Roniger, Y.S. Oren, M.M. Im, D. Sarni, M. Chaoat, A. Bensimon, G. Zamir, D.S. Shewach, and B. Kerem. 2011. Nucleotide deficiency promotes genomic instability in early stages of cancer development. *Cell.* 145:435-46.

Betous, R., A.C. Mason, R.P. Rambo, C.E. Bansbach, A. Badu-Nkansah, B.M. Sirbu, B.F. Eichman, and D. Cortez. 2012. SMARCAL1 catalyzes fork regression and Holliday junction migration to maintain genome stability during DNA replication. *Genes Dev.* 26:151-62.

Bhatia, V., S.I. Barroso, M.L. Garcia-Rubio, E. Tumini, E. Herrera-Moyano, and A. Aguilera. 2014. BRCA2 prevents R-loop accumulation and associates with TREX-2 mRNA export factor PCID2. *Nature.* 511:362-5.

Bochman, M.L., K. Paeschke, and V.A. Zakian. 2012. DNA secondary structures: stability and function of G-quadruplex structures. *Nat Rev Genet.* 13:770-80.

Boillee, S., C. Vande Velde, and D.W. Cleveland. 2006. ALS: a disease of motor neurons and their nonneuronal neighbors. *Neuron.* 52:39-59.

Bolderson, E., N. Tomimatsu, D.J. Richard, D. Boucher, R. Kumar, T.K. Pandita, S. Burma, and K.K. Khanna. 2010. Phosphorylation of Exo1 modulates homologous recombination repair of DNA double-strand breaks. *Nucleic Acids Res.* 38:1821-31.

Bosco, D.A., N. Lemay, H.K. Ko, H. Zhou, C. Burke, T.J. Kwiatkowski, Jr., P. Sapp, D. McKenna-Yasek, R.H. Brown, Jr., and L.J. Hayward. 2010. Mutant FUS proteins that cause amyotrophic lateral sclerosis incorporate into stress granules. *Hum Mol Genet.* 19:4160-75.

Boule, J.B., and V.A. Zakian. 2007. The yeast Pif1p DNA helicase preferentially unwinds RNA DNA substrates. *Nucleic Acids Res.* 35:5809-18.

Bouwman, P., A. Aly, J.M. Escandell, M. Pieterse, J. Bartkova, H. van der Gulden, S. Hiddingh, M. Thanasoula, A. Kulkarni, Q. Yang, B.G. Haffty, J. Tommiska, C. Blomqvist, R. Drapkin, D.J. Adams, H. Nevanlinna, J. Bartek, M. Tarsounas, S. Ganesan, and J. Jonkers. 2010. 53BP1 loss rescues BRCA1 deficiency and is associated with triple-negative and BRCA-mutated breast cancers. *Nat Struct Mol Biol.* 17:688-95.

Braun, B.S., R. Frieden, S.L. Lessnick, W.A. May, and C.T. Denny. 1995. Identification of target genes for the Ewing's sarcoma EWS/FLI fusion protein by representational difference analysis. *Mol Cell Biol.* 15:4623-30.

Brenner, J.C., F.Y. Feng, S. Han, S. Patel, S.V. Goyal, L.M. Bou-Maroun, M. Liu, R. Lonigro, J.R. Prensner, S.A. Tomlins, and A.M. Chinnaiyan. 2012. PARP-1 inhibition as a targeted strategy to treat Ewing's sarcoma. *Cancer Res.* 72:1608-13.

Britton, S., E. Dernoncourt, C. Delteil, C. Froment, O. Schiltz, B. Salles, P. Frit, and P. Calsou. 2014. DNA damage triggers SAF-A and RNA biogenesis factors exclusion from chromatin coupled to R-loops removal. *Nucleic Acids Res.* 42:9047-62.

Brooks, P.J., and J.A. Theruvathu. 2005. DNA adducts from acetaldehyde: implications for alcohol-related carcinogenesis. *Alcohol.* 35:187-93.

Bruijn, L.I., M.W. Becher, M.K. Lee, K.L. Anderson, N.A. Jenkins, N.G. Copeland, S.S. Sisodia, J.D. Rothstein, D.R. Borchelt, D.L. Price, and D.W. Cleveland. 1997. ALS-linked SOD1 mutant G85R mediates damage to astrocytes and promotes rapidly progressive disease with SOD1-containing inclusions. *Neuron.* 18:327-38.

Bunting, S.F., E. Callen, N. Wong, H.T. Chen, F. Polato, A. Gunn, A. Bothmer, N. Feldhahn, O. Fernandez-Capetillo, L. Cao, X. Xu, C.X. Deng, T. Finkel, M. Nussenzweig, J.M. Stark, and A. Nussenzweig. 2010. 53BP1 inhibits homologous recombination in Brca1-deficient cells by blocking resection of DNA breaks. *Cell.* 141:243-54.

Burrell, R.A., S.E. McClelland, D. Endesfelder, P. Groth, M.C. Weller, N. Shaikh, E. Domingo, N. Kanu, S.M. Dewhurst, E. Gronroos, S.K. Chew, A.J. Rowan, A. Schenk, M. Sheffer, M. Howell, M. Kschischo, A. Behrens, T. Helleday, J. Bartek, I.P. Tomlinson, and C. Swanton. 2013. Replication stress links structural and numerical cancer chromosomal instability. *Nature*. 494:492-6.

Butler, D.K. 1992. Ribosomal DNA is a site of chromosome breakage in aneuploid strains of Neurospora. *Genetics*. 131:581-92.

Byun, T.S., M. Pacek, M.C. Yee, J.C. Walter, and K.A. Cimprich. 2005. Functional uncoupling of MCM helicase and DNA polymerase activities activates the ATR-dependent checkpoint. *Genes Dev*. 19:1040-52.

Cao, L., X. Xu, S.F. Bunting, J. Liu, R.H. Wang, L.L. Cao, J.J. Wu, T.N. Peng, J. Chen, A. Nussenzweig, C.X. Deng, and T. Finkel. 2009. A selective requirement for 53BP1 in the biological response to genomic instability induced by Brca1 deficiency. *Mol Cell*. 35:534-41.

Celeste, A., O. Fernandez-Capetillo, M.J. Kruhlak, D.R. Pilch, D.W. Staudt, A. Lee, R.F. Bonner, W.M. Bonner, and A. Nussenzweig. 2003. Histone H2AX phosphorylation is dispensable for the initial recognition of DNA breaks. *Nat Cell Biol*. 5:675-9.

Chakraborty, P., and F. Grosse. 2011. Human DHX9 helicase preferentially unwinds RNA-containing displacement loops (R-loops) and G-quadruplexes. *DNA Repair (Amst)*. 10:654-65.

Chapman, J.R., M.R. Taylor, and S.J. Boulton. 2012. Playing the end game: DNA double-strand break repair pathway choice. *Mol Cell*. 47:497-510.

Chaudhuri, J., and F.W. Alt. 2004. Class-switch recombination: interplay of transcription, DNA deamination and DNA repair. *Nat Rev Immunol*. 4:541-52.

Chen, Y.Z., C.L. Bennett, H.M. Huynh, I.P. Blair, I. Puls, J. Irobi, I. Dierick, A. Abel, M.L. Kennerson, B.A. Rabin, G.A. Nicholson, M. Auer-Grumbach, K. Wagner, P. De Jonghe, J.W. Griffin, K.H. Fischbeck, V. Timmerman, D.R. Cornblath, and P.F. Chance. 2004. DNA/RNA helicase gene mutations in a form of juvenile amyotrophic lateral sclerosis (ALS4). *Am J Hum Genet*. 74:1128-35.

Chiolo, I., M. Saponaro, A. Baryshnikova, J.H. Kim, Y.S. Seo, and G. Liberi. 2007. The human F-Box DNA helicase FBH1 faces Saccharomyces cerevisiae Srs2 and postreplication repair pathway roles. *Mol Cell Biol*. 27:7439-50.

Chu, W.K., M.J. Payne, P. Beli, K. Hanada, C. Choudhary, and I.D. Hickson. 2015. FBH1 influences DNA replication fork stability and homologous recombination through ubiquitylation of RAD51. *Nat Commun*. 6:5931.

Ciccia, A., and S.J. Elledge. 2010. The DNA damage response: making it safe to play with knives. *Mol Cell*. 40:179-204.

Ciccia, A., N. McDonald, and S.C. West. 2008. Structural and functional relationships of the XPF/MUS81 family of proteins. *Annu Rev Biochem*. 77:259-87.

Cimprich, K.A., and D. Cortez. 2008. ATR: an essential regulator of genome integrity. *Nat Rev Mol Cell Biol*. 9:616-27.

Clauson, C., O.D. Scharer, and L. Niedernhofer. 2013. Advances in understanding the complex mechanisms of DNA interstrand cross-link repair. *Cold Spring Harb Perspect Biol*. 5:a012732.

Costantino, L., S.K. Sotiriou, J.K. Rantala, S. Magin, E. Mladenov, T. Helleday, J.E. Haber, G. Iliakis, O.P. Kallioniemi, and T.D. Halazonetis. 2014. Break-induced replication repair of damaged forks induces genomic duplications in human cells. *Science*. 343:88-91.

Cotta-Ramusino, C., D. Fachinetti, C. Lucca, Y. Doksani, M. Lopes, J. Sogo, and M. Foiani. 2005. Exo1 processes stalled replication forks and counteracts fork reversal in checkpoint-defective cells. *Mol Cell*. 17:153-9.

Couch, F.B., C.E. Bansbach, R. Driscoll, J.W. Luzwick, G.G. Glick, R. Betous, C.M. Carroll, S.Y. Jung, J. Qin, K.A. Cimprich, and D. Cortez. 2013. ATR phosphorylates SMARCAL1 to prevent replication fork collapse. *Genes Dev.* 27:1610-23.

Couthouis, J., M.P. Hart, R. Erion, O.D. King, Z. Diaz, T. Nakaya, F. Ibrahim, H.J. Kim, J. Mojsilovic-Petrovic, S. Panossian, C.E. Kim, E.C. Frackelton, J.A. Solski, K.L. Williams, D. Clay-Falcone, L. Elman, L. McCluskey, R. Greene, H. Hakonarson, R.G. Kalb, V.M. Lee, J.Q. Trojanowski, G.A. Nicholson, I.P. Blair, N.M. Bonini, V.M. Van Deerlin, Z. Mourelatos, J. Shorter, and A.D. Gitler. 2012. Evaluating the role of the FUS/TLS-related gene EWSR1 in amyotrophic lateral sclerosis. *Hum Mol Genet.* 21:2899-911.

Croteau, D.L., V. Popuri, P.L. Opresko, and V.A. Bohr. 2014. Human RecQ helicases in DNA repair, recombination, and replication. *Annu Rev Biochem.* 83:519-52.

Dalgaard, J.Z. 2012. Causes and consequences of ribonucleotide incorporation into nuclear DNA. *Trends Genet.* 28:592-7.

Dauphinot, L., C. De Oliveira, T. Melot, N. Sevenet, V. Thomas, B.E. Weissman, and O. Delattre. 2001. Analysis of the expression of cell cycle regulators in Ewing cell lines: EWS-FLI-1 modulates p57KIP2and c-Myc expression. *Oncogene.* 20:3258-65.

Debatisse, M., B. Le Tallec, A. Letessier, B. Dutrillaux, and O. Brison. 2012. Common fragile sites: mechanisms of instability revisited. *Trends Genet.* 28:22-32.

Dereli-Oz, A., G. Versini, and T.D. Halazonetis. 2011. Studies of genomic copy number changes in human cancers reveal signatures of DNA replication stress. *Mol Oncol.* 5:308-14.

Di Micco, R., M. Fumagalli, A. Cicalese, S. Piccinin, P. Gasparini, C. Luise, C. Schurra, M. Garre, P.G. Nuciforo, A. Bensimon, R. Maestro, P.G. Pelicci, and F. d'Adda di Fagagna. 2006. Oncogene-induced senescence is a DNA damage response triggered by DNA hyper-replication. *Nature.* 444:638-42.

Dion, P.A., H. Daoud, and G.A. Rouleau. 2009. Genetics of motor neuron disorders: new insights into pathogenic mechanisms. *Nat Rev Genet.* 10:769-82.

Dominguez-Sanchez, M.S., S. Barroso, B. Gomez-Gonzalez, R. Luna, and A. Aguilera. 2011. Genome instability and transcription elongation impairment in human cells depleted of THO/TREX. *PLoS Genet.* 7:e1002386.

Eguren, M., M. Alvarez-Fernandez, F. Garcia, A.J. Lopez-Contreras, K. Fujimitsu, H. Yaguchi, J.L. Luque-Garcia, O. Fernandez-Capetillo, J. Munoz, H. Yamano, and M. Malumbres. 2014. A synthetic lethal interaction between APC/C and topoisomerase poisons uncovered by proteomic screens. *Cell Rep.* 6:670-83.

Ekholm-Reed, S., J. Mendez, D. Tedesco, A. Zetterberg, B. Stillman, and S.I. Reed. 2004. Deregulation of cyclin E in human cells interferes with prereplication complex assembly. *J Cell Biol.* 165:789-800.

El Hage, A., S.L. French, A.L. Beyer, and D. Tollervey. 2010. Loss of Topoisomerase I leads to R-loop-mediated transcriptional blocks during ribosomal RNA synthesis. *Genes Dev.* 24:1546-58.

Elden, A.C., H.J. Kim, M.P. Hart, A.S. Chen-Plotkin, B.S. Johnson, X. Fang, M. Armakola, F. Geser, R. Greene, M.M. Lu, A. Padmanabhan, D. Clay-Falcone, L. McCluskey, L. Elman, D. Juhr, P.J. Gruber, U. Rub, G. Auburger, J.Q. Trojanowski, V.M. Lee, V.M. Van Deerlin, N.M. Bonini, and A.D. Gitler. 2010. Ataxin-2 intermediate-length polyglutamine expansions are associated with increased risk for ALS. *Nature.* 466:1069-75.

Elvers, I., F. Johansson, P. Groth, K. Erixon, and T. Helleday. 2011. UV stalled replication forks restart by re-priming in human fibroblasts. *Nucleic Acids Res.* 39:7049-57.

Farmer, H., N. McCabe, C.J. Lord, A.N. Tutt, D.A. Johnson, T.B. Richardson, M. Santarosa, K.J. Dillon, I. Hickson, C. Knights, N.M. Martin, S.P. Jackson, G.C. Smith, and A. Ashworth. 2005. Targeting the DNA repair defect in BRCA mutant cells as a therapeutic strategy. *Nature.* 434:917-21.

Fekairi, S., S. Scaglione, C. Chahwan, E.R. Taylor, A. Tissier, S. Coulon, M.Q. Dong, C. Ruse, J.R. Yates, 3rd, P. Russell, R.P. Fuchs, C.H. McGowan, and P.H. Gaillard. 2009. Human SLX4 is a Holliday junction resolvase subunit that binds multiple DNA repair/recombination endonucleases. *Cell.* 138:78-89.

Fernandez-Capetillo, O., H.T. Chen, A. Celeste, I. Ward, P.J. Romanienko, J.C. Morales, K. Naka, Z. Xia, R.D. Camerini-Otero, N. Motoyama, P.B. Carpenter, W.M. Bonner, J. Chen, and A. Nussenzweig. 2002. DNA damage-induced G2-M checkpoint activation by histone H2AX and 53BP1. *Nat Cell Biol.* 4:993-7.

Ferreira, B.I., J. Alonso, J. Carrillo, F. Acquadro, C. Largo, J. Suela, M.R. Teixeira, N. Cerveira, A. Molares, G. Gomez-Lopez, A. Pestana, A. Sastre, P. Garcia-Miguel, and J.C. Cigudosa. 2008. Array CGH and gene-expression profiling reveals distinct genomic instability patterns associated with DNA repair and cell-cycle checkpoint pathways in Ewing's sarcoma. *Oncogene.* 27:2084-90.

Fugger, K., W.K. Chu, P. Haahr, A.N. Kousholt, H. Beck, M.J. Payne, K. Hanada, I.D. Hickson, and C.S. Sorensen. 2013. FBH1 co-operates with MUS81 in inducing DNA double-strand breaks and cell death following replication stress. *Nat Commun.* 4:1423.

Fugger, K., M. Mistrik, J.R. Danielsen, C. Dinant, J. Falck, J. Bartek, J. Lukas, and N. Mailand. 2009. Human Fbh1 helicase contributes to genome maintenance via pro- and anti-recombinase activities. *J Cell Biol.* 186:655-63.

Fujimura, Y., H. Siddique, L. Lee, V.N. Rao, and E.S. Reddy. 2001. EWS-ATF-1 chimeric protein in soft tissue clear cell sarcoma associates with CREB-binding protein and interferes with p53-mediated trans-activation function. *Oncogene.* 20:6653-9.

Fukuma, M., H. Okita, J. Hata, and A. Umezawa. 2003. Upregulation of Id2, an oncogenic helix-loop-helix protein, is mediated by the chimeric EWS/ets protein in Ewing sarcoma. *Oncogene.* 22:1-9.

Gagou, M.E., P. Zuazua-Villar, and M. Meuth. 2010. Enhanced H2AX phosphorylation, DNA replication fork arrest, and cell death in the absence of Chk1. *Mol Biol Cell.* 21:739-52.

Garnett, M.J., E.J. Edelman, S.J. Heidorn, C.D. Greenman, A. Dastur, K.W. Lau, P. Greninger, I.R. Thompson, X. Luo, J. Soares, Q. Liu, F. Iorio, D. Surdez, L. Chen, R.J. Milano, G.R. Bignell, A.T. Tam, H. Davies, J.A. Stevenson, S. Barthorpe, S.R. Lutz, F. Kogera, K. Lawrence, A. McLaren-Douglas, X. Mitropoulos, T. Mironenko, H. Thi, L. Richardson, W. Zhou, F. Jewitt, T. Zhang, P. O'Brien, J.L. Boisvert, S. Price, W. Hur, W. Yang, X. Deng, A. Butler, H.G. Choi, J.W. Chang, J. Baselga, I. Stamenkovic, J.A. Engelman, S.V. Sharma, O. Delattre, J. Saez-Rodriguez, N.S. Gray, J. Settleman, P.A. Futreal, D.A. Haber, M.R. Stratton, S. Ramaswamy, U. McDermott, and C.H. Benes. 2012. Systematic identification of genomic markers of drug sensitivity in cancer cells. *Nature.* 483:570-5.

Gascoyne, D.M., G.R. Thomas, and D.S. Latchman. 2004. The effects of Brn-3a on neuronal differentiation and apoptosis are differentially modulated by EWS and its oncogenic derivative EWS/Fli-1. *Oncogene.* 23:3830-40.

Ge, X.Q., D.A. Jackson, and J.J. Blow. 2007. Dormant origins licensed by excess Mcm2-7 are required for human cells to survive replicative stress. *Genes Dev.* 21:3331-41.

Ginno, P.A., P.L. Lott, H.C. Christensen, I. Korf, and F. Chedin. 2012. R-loop formation is a distinctive characteristic of unmethylated human CpG island promoters. *Mol Cell.* 45:814-25.

Gomez-Gonzalez, B., M. Garcia-Rubio, R. Bermejo, H. Gaillard, K. Shirahige, A. Marin, M. Foiani, and A. Aguilera. 2011. Genome-wide function of THO/TREX in active genes prevents R-loop-dependent replication obstacles. *Embo j.* 30:3106-19.

Goodpasture, C., and S.E. Bloom. 1975. Visualization of nucleolar organizer regions im mammalian chromosomes using silver staining. *Chromosoma.* 53:37-50.

Groh, M., and N. Gromak. 2014. Out of balance: R-loops in human disease. *PLoS Genet.* 10:e1004630.

Gurney, M.E., H. Pu, A.Y. Chiu, M.C. Dal Canto, C.Y. Polchow, D.D. Alexander, J. Caliendo, A. Hentati, Y.W. Kwon, H.X. Deng, and et al. 1994. Motor neuron degeneration in mice that express a human Cu,Zn superoxide dismutase mutation. *Science*. 264:1772-5.

Haeusler, A.R., C.J. Donnelly, G. Periz, E.A. Simko, P.G. Shaw, M.S. Kim, N.J. Maragakis, J.C. Troncoso, A. Pandey, R. Sattler, J.D. Rothstein, and J. Wang. 2014. C9orf72 nucleotide repeat structures initiate molecular cascades of disease. *Nature*. 507:195-200.

Halazonetis, T.D., V.G. Gorgoulis, and J. Bartek. 2008. An oncogene-induced DNA damage model for cancer development. *Science*. 319:1352-5.

Hamperl, S., and K.A. Cimprich. 2014. The contribution of co-transcriptional RNA:DNA hybrid structures to DNA damage and genome instability. *DNA Repair (Amst)*. 19:84-94.

Harper, J.W., and S.J. Elledge. 2007. The DNA damage response: ten years after. *Mol Cell*. 28:739-45.

Hartlerode, A.J., and R. Scully. 2009. Mechanisms of double-strand break repair in somatic mammalian cells. *Biochem J*. 423:157-68.

Heliot, L., H. Kaplan, L. Lucas, C. Klein, A. Beorchia, M. Doco-Fenzy, M. Menager, M. Thiry, M.F. O'Donohue, and D. Ploton. 1997. Electron tomography of metaphase nucleolar organizer regions: evidence for a twisted-loop organization. *Mol Biol Cell*. 8:2199-216.

Hicks, G.G., N. Singh, A. Nashabi, S. Mai, G. Bozek, L. Klewes, D. Arapovic, E.K. White, M.J. Koury, E.M. Oltz, L. Van Kaer, and H.E. Ruley. 2000. Fus deficiency in mice results in defective B-lymphocyte development and activation, high levels of chromosomal instability and perinatal death. *Nat Genet*. 24:175-9.

Hoeijmakers, J.H. 2009. DNA damage, aging, and cancer. *N Engl J Med*. 361:1475-85.

Hu, J., L. Sun, F. Shen, Y. Chen, Y. Hua, Y. Liu, M. Zhang, Y. Hu, Q. Wang, W. Xu, F. Sun, J. Ji, J.M. Murray, A.M. Carr, and D. Kong. 2012. The intra-S phase checkpoint targets Dna2 to prevent stalled replication forks from reversing. *Cell*. 149:1221-32.

Huang, M., H. Li, L. Zhang, F. Gao, P. Wang, Y. Hu, S. Yan, L. Zhao, Q. Zhang, J. Tan, X. Liu, S. He, and L. Li. 2012. Plant 45S rDNA clusters are fragile sites and their instability is associated with epigenetic alterations. *PLoS One*. 7:e35139.

Huen, M.S., S.M. Sy, and J. Chen. 2010. BRCA1 and its toolbox for the maintenance of genome integrity. *Nat Rev Mol Cell Biol*. 11:138-48.

Huertas, P., and A. Aguilera. 2003. Cotranscriptionally formed DNA:RNA hybrids mediate transcription elongation impairment and transcription-associated recombination. *Mol Cell*. 12:711-21.

Huey, E.D., R. Ferrari, J.H. Moreno, C. Jensen, C.M. Morris, F. Potocnik, R.N. Kalaria, M. Tierney, E.M. Wassermann, J. Hardy, J. Grafman, and P. Momeni. 2012. FUS and TDP43 genetic variability in FTD and CBS. *Neurobiol Aging*. 33:1016 e9-17.

Ibarra, A., E. Schwob, and J. Mendez. 2008. Excess MCM proteins protect human cells from replicative stress by licensing backup origins of replication. *Proc Natl Acad Sci U S A*. 105:8956-61.

Ip, S.C., U. Rass, M.G. Blanco, H.R. Flynn, J.M. Skehel, and S.C. West. 2008. Identification of Holliday junction resolvases from humans and yeast. *Nature*. 456:357-61.

Jackson, S.P., and J. Bartek. 2009. The DNA-damage response in human biology and disease. *Nature*. 461:1071-8.

Jeong, Y.T., L. Cermak, M.V. Guijarro, E. Hernando, and M. Pagano. 2013a. FBH1 protects melanocytes from transformation and is deregulated in melanomas. *Cell Cycle*. 12:1128-32.

Jeong, Y.T., M. Rossi, L. Cermak, A. Saraf, L. Florens, M.P. Washburn, P. Sung, C.L. Schildkraut, and M. Pagano. 2013b. FBH1 promotes DNA double-strand breakage and apoptosis in response to DNA replication stress. *J Cell Biol*. 200:141-9.

Jiricny, J. 2006. The multifaceted mismatch-repair system. *Nat Rev Mol Cell Biol*. 7:335-46.

Jones, R.M., O. Mortusewicz, I. Afzal, M. Lorvellec, P. Garcia, T. Helleday, and E. Petermann. 2013. Increased replication initiation and conflicts with transcription underlie Cyclin E-induced replication stress. *Oncogene*. 32:3744-53.

Jonsson, P.A., K. Ernhill, P.M. Andersen, D. Bergemalm, T. Brannstrom, O. Gredal, P. Nilsson, and S.L. Marklund. 2004. Minute quantities of misfolded mutant superoxide dismutase-1 cause amyotrophic lateral sclerosis. *Brain*. 127:73-88.

Jonsson, P.A., K.S. Graffmo, T. Brannstrom, P. Nilsson, P.M. Andersen, and S.L. Marklund. 2006. Motor neuron disease in mice expressing the wild type-like D90A mutant superoxide dismutase-1. *J Neuropathol Exp Neurol*. 65:1126-36.

Kanaar, R., and C. Wyman. 2008. DNA repair by the MRN complex: break it to make it. *Cell*. 135:14-6.

Kato, M., T.W. Han, S. Xie, K. Shi, X. Du, L.C. Wu, H. Mirzaei, E.J. Goldsmith, J. Longgood, J. Pei, N.V. Grishin, D.E. Frantz, J.W. Schneider, S. Chen, L. Li, M.R. Sawaya, D. Eisenberg, R. Tycko, and S.L. McKnight. 2012. Cell-free formation of RNA granules: low complexity sequence domains form dynamic fibers within hydrogels. *Cell*. 149:753-67.

Kauer, M., J. Ban, R. Kofler, B. Walker, S. Davis, P. Meltzer, and H. Kovar. 2009. A molecular function map of Ewing's sarcoma. *PLoS One*. 4:e5415.

Keeney, S., and M.J. Neale. 2006. Initiation of meiotic recombination by formation of DNA double-strand breaks: mechanism and regulation. *Biochem Soc Trans*. 34:523-5.

Kiledjian, M., and G. Dreyfuss. 1992. Primary structure and binding activity of the hnRNP U protein: binding RNA through RGG box. *Embo j*. 11:2655-64.

Kim, H.D., J. Choe, and Y.S. Seo. 1999. The sen1(+) gene of Schizosaccharomyces pombe, a homologue of budding yeast SEN1, encodes an RNA and DNA helicase. *Biochemistry*. 38:14697-710.

Kim, J., J.H. Kim, S.H. Lee, D.H. Kim, H.Y. Kang, S.H. Bae, Z.Q. Pan, and Y.S. Seo. 2002. The novel human DNA helicase hFBH1 is an F-box protein. *J Biol Chem*. 277:24530-7.

Kim, J.C., and S.M. Mirkin. 2013. The balancing act of DNA repeat expansions. *Curr Opin Genet Dev*. 23:280-8.

Kim, J.H., J. Kim, D.H. Kim, G.H. Ryu, S.H. Bae, and Y.S. Seo. 2004. SCFhFBH1 can act as helicase and E3 ubiquitin ligase. *Nucleic Acids Res*. 32:2287-97.

Kohzaki, M., A. Hatanaka, E. Sonoda, M. Yamazoe, K. Kikuchi, N. Vu Trung, D. Szuts, J.E. Sale, H. Shinagawa, M. Watanabe, and S. Takeda. 2007. Cooperative roles of vertebrate Fbh1 and Blm DNA helicases in avoidance of crossovers during recombination initiated by replication fork collapse. *Mol Cell Biol*. 27:2812-20.

Kurucu, N., N. Sari, and I.E. Ilhan. 2015. Irinotecan and temozolamide treatment for relapsed Ewing sarcoma: a single-center experience and review of the literature. *Pediatr Hematol Oncol*. 32:50-9.

Kwiatkowski, T.J., Jr., D.A. Bosco, A.L. Leclerc, E. Tamrazian, C.R. Vanderburg, C. Russ, A. Davis, J. Gilchrist, E.J. Kasarskis, T. Munsat, P. Valdmanis, G.A. Rouleau, B.A. Hosler, P. Cortelli, P.J. de Jong, Y. Yoshinaga, J.L. Haines, M.A. Pericak-Vance, J. Yan, N. Ticozzi, T. Siddique, D. McKenna-Yasek, P.C. Sapp, H.R. Horvitz, J.E. Landers, and R.H. Brown, Jr. 2009. Mutations in the FUS/TLS gene on chromosome 16 cause familial amyotrophic lateral sclerosis. *Science*. 323:1205-8.

Kwon, I., M. Kato, S. Xiang, L. Wu, P. Theodoropoulos, H. Mirzaei, T. Han, S. Xie, J.L. Corden, and S.L. McKnight. 2013. Phosphorylation-regulated binding of RNA polymerase II to fibrous polymers of low-complexity domains. *Cell*. 155:1049-60.

Kwon, I., S. Xiang, M. Kato, L. Wu, P. Theodoropoulos, T. Wang, J. Kim, J. Yun, Y. Xie, and S.L. McKnight. 2014. Poly-dipeptides encoded by the C9orf72 repeats bind nucleoli, impede RNA biogenesis, and kill cells. *Science*. 345:1139-45.

Labelle, Y., J. Zucman, G. Stenman, L.G. Kindblom, J. Knight, C. Turc-Carel, B. Dockhorn-Dworniczak, N. Mandahl, C. Desmaze, M. Peter, and et al. 1995. Oncogenic conversion of a novel orphan nuclear receptor by chromosome translocation. *Hum Mol Genet.* 4:2219-26.

Ladanyi, M., and W. Gerald. 1994. Fusion of the EWS and WT1 genes in the desmoplastic small round cell tumor. *Cancer Res.* 54:2837-40.

Lambert, S., and A.M. Carr. 2013. Impediments to replication fork movement: stabilisation, reactivation and genome instability. *Chromosoma.* 122:33-45.

Laulier, C., A. Cheng, N. Huang, and J.M. Stark. 2010. Mammalian Fbh1 is important to restore normal mitotic progression following decatenation stress. *DNA Repair (Amst).* 9:708-17.

Le Tallec, B., G.A. Millot, M.E. Blin, O. Brison, B. Dutrillaux, and M. Debatisse. 2013. Common fragile site profiling in epithelial and erythroid cells reveals that most recurrent cancer deletions lie in fragile sites hosting large genes. *Cell Rep.* 4:420-8.

Lecona, E., and O. Fernandez-Capetillo. 2014. Replication stress and cancer: it takes two to tango. *Exp Cell Res.* 329:26-34.

Lee, J., B.K. Rhee, G.Y. Bae, Y.M. Han, and J. Kim. 2005. Stimulation of Oct-4 activity by Ewing's sarcoma protein. *Stem Cells.* 23:738-51.

Leitner, M., S. Menzies, and C. Lutz. 2009. Working with ALS Mice. Guidelines for preclinical testing & colony management. The Jackson Laboratory.

Lessard, J., and G. Sauvageau. 2003. Bmi-1 determines the proliferative capacity of normal and leukaemic stem cells. *Nature.* 423:255-60.

Lessnick, S.L., and M. Ladanyi. 2012. Molecular pathogenesis of Ewing sarcoma: new therapeutic and transcriptional targets. *Annu Rev Pathol.* 7:145-59.

Leung, C., M. Lingbeek, O. Shakhova, J. Liu, E. Tanger, P. Saremaslani, M. Van Lohuizen, and S. Marino. 2004. Bmi1 is essential for cerebellar development and is overexpressed in human medulloblastomas. *Nature.* 428:337-41.

Li, H., W. Watford, C. Li, A. Parmelee, M.A. Bryant, C. Deng, J. O'Shea, and S.B. Lee. 2007. Ewing sarcoma gene EWS is essential for meiosis and B lymphocyte development. *J Clin Invest.* 117:1314-23.

Li, X., and J.L. Manley. 2005a. Inactivation of the SR protein splicing factor ASF/SF2 results in genomic instability. *Cell.* 122:365-78.

Li, X., and J.L. Manley. 2005b. New talents for an old acquaintance: the SR protein splicing factor ASF/SF2 functions in the maintenance of genome stability. *Cell Cycle.* 4:1706-8.

Lin, P.P., M.K. Pandey, F. Jin, S. Xiong, M. Deavers, J.M. Parant, and G. Lozano. 2008. EWS-FLI1 induces developmental abnormalities and accelerates sarcoma formation in a transgenic mouse model. *Cancer Res.* 68:8968-75.

Lindahl, T., and D.E. Barnes. 2000. Repair of endogenous DNA damage. *Cold Spring Harb Symp Quant Biol.* 65:127-33.

Liu, J., T. Doty, B. Gibson, and W.D. Heyer. 2010. Human BRCA2 protein promotes RAD51 filament formation on RPA-covered single-stranded DNA. *Nat Struct Mol Biol.* 17:1260-2.

Llorente, B., C.E. Smith, and L.S. Symington. 2008. Break-induced replication: what is it and what is it for? *Cell Cycle.* 7:859-64.

Lopes, M., M. Foiani, and J.M. Sogo. 2006. Multiple mechanisms control chromosome integrity after replication fork uncoupling and restart at irreparable UV lesions. *Mol Cell.* 21:15-27.

Lopez-Contreras, A.J., and O. Fernandez-Capetillo. 2010. The ATR barrier to replication-born DNA damage. *DNA Repair (Amst).* 9:1249-55.

Lopez-Contreras, A.J., P. Gutierrez-Martinez, J. Specks, S. Rodrigo-Perez, and O. Fernandez-Capetillo. 2012. An extra allele of Chk1 limits oncogene-induced replicative stress and promotes transformation. *J Exp Med.* 209:455-61.

Lopez-Contreras, A.J., J. Specks, J.H. Barlow, C. Ambrogio, C. Desler, S. Vikingsson, S. Rodrigo-Perez, H. Green, L.J. Rasmussen, M. Murga, A. Nussenzweig, and O.

Fernandez-Capetillo. 2015. Increased Rrm2 gene dosage reduces fragile site breakage and prolongs survival of ATR mutant mice. *Genes Dev.* 29:690-5.

Lorenz, A., F. Osman, V. Folkyte, S. Sofueva, and M.C. Whitby. 2009. Fbh1 limits Rad51-dependent recombination at blocked replication forks. *Mol Cell Biol.* 29:4742-56.

Lukas, J., C. Lukas, and J. Bartek. 2011. More than just a focus: The chromatin response to DNA damage and its role in genome integrity maintenance. *Nat Cell Biol.* 13:1161-9.

Mackenzie, I.R., and M. Neumann. 2012. FET proteins in frontotemporal dementia and amyotrophic lateral sclerosis. *Brain Res.* 1462:40-3.

Mahaney, B.L., K. Meek, and S.P. Lees-Miller. 2009. Repair of ionizing radiation-induced DNA double-strand breaks by non-homologous end-joining. *Biochem J.* 417:639-50.

Mailand, N., I. Gibbs-Seymour, and S. Bekker-Jensen. 2013. Regulation of PCNA-protein interactions for genome stability. *Nat Rev Mol Cell Biol.* 14:269-82.

Market, E., and F.N. Papavasiliou. 2003. V(D)J recombination and the evolution of the adaptive immune system. *PLoS Biol.* 1:E16.

Mastrocola, A.S., S.H. Kim, A.T. Trinh, L.A. Rodenkirch, and R.S. Tibbetts. 2013. The RNA-binding protein fused in sarcoma (FUS) functions downstream of poly(ADP-ribose) polymerase (PARP) in response to DNA damage. *J Biol Chem.* 288:24731-41.

May, W.A., A. Arvand, A.D. Thompson, B.S. Braun, M. Wright, and C.T. Denny. 1997. EWS/FLI1-induced manic fringe renders NIH 3T3 cells tumorigenic. *Nat Genet.* 17:495-7.

May, W.A., M.L. Gishizky, S.L. Lessnick, L.B. Lunsford, B.C. Lewis, O. Delattre, J. Zucman, G. Thomas, and C.T. Denny. 1993a. Ewing sarcoma 11;22 translocation produces a chimeric transcription factor that requires the DNA-binding domain encoded by FLI1 for transformation. *Proc Natl Acad Sci U S A.* 90:5752-6.

May, W.A., S.L. Lessnick, B.S. Braun, M. Klemsz, B.C. Lewis, L.B. Lunsford, R. Hromas, and C.T. Denny. 1993b. The Ewing's sarcoma EWS/FLI-1 fusion gene encodes a more potent transcriptional activator and is a more powerful transforming gene than FLI-1. *Mol Cell Biol.* 13:7393-8.

Meek, K., V. Dang, and S.P. Lees-Miller. 2008. DNA-PK: the means to justify the ends? *Adv Immunol.* 99:33-58.

Mehnert, J.M., and H.M. Kluger. 2012. Driver mutations in melanoma: lessons learned from bench-to-bedside studies. *Curr Oncol Rep.* 14:449-57.

Michaud, S., and R. Reed. 1993. A functional association between the 5' and 3' splice site is established in the earliest prespliceosome complex (E) in mammals. *Genes Dev.* 7:1008-20.

Molofsky, A.V., R. Pardal, T. Iwashita, I.K. Park, M.F. Clarke, and S.J. Morrison. 2003. Bmi-1 dependence distinguishes neural stem cell self-renewal from progenitor proliferation. *Nature.* 425:962-7.

Morishita, T., F. Furukawa, C. Sakaguchi, T. Toda, A.M. Carr, H. Iwasaki, and H. Shinagawa. 2005. Role of the Schizosaccharomyces pombe F-Box DNA helicase in processing recombination intermediates. *Mol Cell Biol.* 25:8074-83.

Moynahan, M.E., J.W. Chiu, B.H. Koller, and M. Jasin. 1999. Brca1 controls homology-directed DNA repair. *Mol Cell.* 4:511-8.

Munoz, I.M., K. Hain, A.C. Declais, M. Gardiner, G.W. Toh, L. Sanchez-Pulido, J.M. Heuckmann, R. Toth, T. Macartney, B. Eppink, R. Kanaar, C.P. Ponting, D.M. Lilley, and J. Rouse. 2009. Coordination of structure-specific nucleases by human SLX4/BTBD12 is required for DNA repair. *Mol Cell.* 35:116-27.

Murga, M., S. Bunting, M.F. Montana, R. Soria, F. Mulero, M. Canamero, Y. Lee, P.J. McKinnon, A. Nussenzweig, and O. Fernandez-Capetillo. 2009. A mouse model of ATR-Seckel shows embryonic replicative stress and accelerated aging. *Nat Genet.* 41:891-8.

Murga, M., S. Campaner, A.J. Lopez-Contreras, L.I. Toledo, R. Soria, M.F. Montana, L. D'Artista, T. Schleker, C. Guerra, E. Garcia, M. Barbacid, M. Hidalgo, B. Amati, and O. Fernandez-Capetillo. 2011. Exploiting oncogene-induced replicative stress for the selective killing of Myc-driven tumors. *Nat Struct Mol Biol.* 18:1331-5.

Nakatani, F., K. Tanaka, R. Sakimura, Y. Matsumoto, T. Matsunobu, X. Li, M. Hanada, T. Okada, and Y. Iwamoto. 2003. Identification of p21WAF1/CIP1 as a direct target of EWS-Fli1 oncogenic fusion protein. *J Biol Chem.* 278:15105-15.

Nam, E.A., and D. Cortez. 2011. ATR signalling: more than meeting at the fork. *Biochem J.* 436:527-36.

Neumann, M., E. Bentmann, D. Dormann, A. Jawaid, M. DeJesus-Hernandez, O. Ansorge, S. Roeber, H.A. Kretzschmar, D.G. Munoz, H. Kusaka, O. Yokota, L.C. Ang, J. Bilbao, R. Rademakers, C. Haass, and I.R. Mackenzie. 2011. FET proteins TAF15 and EWS are selective markers that distinguish FTLD with FUS pathology from amyotrophic lateral sclerosis with FUS mutations. *Brain.* 134:2595-609.

Nick McElhinny, S.A., D. Kumar, A.B. Clark, D.L. Watt, B.E. Watts, E.B. Lundstrom, E. Johansson, A. Chabes, and T.A. Kunkel. 2010. Genome instability due to ribonucleotide incorporation into DNA. *Nat Chem Biol.* 6:774-81.

O'Connell, B.C., B. Adamson, J.R. Lydeard, M.E. Sowa, A. Ciccia, A.L. Bredemeyer, M. Schlabach, S.P. Gygi, S.J. Elledge, and J.W. Harper. 2010. A genome-wide camptothecin sensitivity screen identifies a mammalian MMS22L-NFKBIL2 complex required for genomic stability. *Mol Cell.* 40:645-57.

O'Donohue, M.F., V. Choesmel, M. Faubladier, G. Fichant, and P.E. Gleizes. 2010. Functional dichotomy of ribosomal proteins during the synthesis of mammalian 40S ribosomal subunits. *J Cell Biol.* 190:853-66.

Ohali, A., S. Avigad, I.J. Cohen, I. Meller, Y. Kollender, J. Issakov, Y. Goshen, I. Yaniv, and R. Zaizov. 2004. High frequency of genomic instability in Ewing family of tumors. *Cancer Genet Cytogenet.* 150:50-6.

Ordonez, J.L., D. Osuna, D. Herrero, E. de Alava, and J. Madoz-Gurpide. 2009. Advances in Ewing's sarcoma research: where are we now and what lies ahead? *Cancer Res.* 69:7140-50.

Osman, F., J. Dixon, A.R. Barr, and M.C. Whitby. 2005. The F-Box DNA helicase Fbh1 prevents Rhp51-dependent recombination without mediator proteins. *Mol Cell Biol.* 25:8084-96.

Pahlich, S., L. Quero, B. Roschitzki, R.P. Leemann-Zakaryan, and H. Gehring. 2009. Analysis of Ewing sarcoma (EWS)-binding proteins: interaction with hnRNP M, U, and RNA-helicases p68/72 within protein-RNA complexes. *J Proteome Res.* 8:4455-65.

Panagopoulos, I., M. Hoglund, F. Mertens, N. Mandahl, F. Mitelman, and P. Aman. 1996. Fusion of the EWS and CHOP genes in myxoid liposarcoma. *Oncogene.* 12:489-94.

Park, J.S., E. Choi, S.H. Lee, C. Lee, and Y.S. Seo. 1997. A DNA helicase from Schizosaccharomyces pombe stimulated by single-stranded DNA-binding protein at low ATP concentration. *J Biol Chem.* 272:18910-9.

Paronetto, M.P. 2013. Ewing sarcoma protein: a key player in human cancer. *Int J Cell Biol.* 2013:642853.

Paronetto, M.P., I. Bernardis, E. Volpe, E. Bechara, E. Sebestyen, E. Eyras, and J. Valcarcel. 2014. Regulation of FAS exon definition and apoptosis by the Ewing sarcoma protein. *Cell Rep.* 7:1211-26.

Paronetto, M.P., B. Minana, and J. Valcarcel. 2011. The Ewing sarcoma protein regulates DNA damage-induced alternative splicing. *Mol Cell.* 43:353-68.

Pasinelli, P., and R.H. Brown. 2006. Molecular biology of amyotrophic lateral sclerosis: insights from genetics. *Nat Rev Neurosci.* 7:710-23.

Patton, E.E., A.R. Willems, and M. Tyers. 1998. Combinatorial control in ubiquitin-dependent proteolysis: don't Skp the F-box hypothesis. *Trends Genet.* 14:236-43.

Paulsen, R.D., D.V. Soni, R. Wollman, A.T. Hahn, M.C. Yee, A. Guan, J.A. Hesley, S.C. Miller, E.F. Cromwell, D.E. Solow-Cordero, T. Meyer, and K.A. Cimprich. 2009. A genome-wide siRNA screen reveals diverse cellular processes and pathways that mediate genome stability. *Mol Cell.* 35:228-39.

Petermann, E., and T. Helleday. 2010. Pathways of mammalian replication fork restart. *Nat Rev Mol Cell Biol.* 11:683-7.

Pohjoismaki, J.L., J.B. Holmes, S.R. Wood, M.Y. Yang, T. Yasukawa, A. Reyes, L.J. Bailey, T.J. Cluett, S. Goffart, S. Willcox, R.E. Rigby, A.P. Jackson, J.N. Spelbrink, J.D. Griffith, R.J. Crouch, H.T. Jacobs, and I.J. Holt. 2010. Mammalian mitochondrial DNA replication intermediates are essentially duplex but contain extensive tracts of RNA/DNA hybrid. *J Mol Biol.* 397:1144-55.

Riancho, J., M. Ruiz-Soto, N.T. Villagra, J. Berciano, M.T. Berciano, and M. Lafarga. 2014. Compensatory Motor Neuron Response to Chromatolysis in the Murine hSOD1(G93A) Model of Amyotrophic Lateral Sclerosis. *Front Cell Neurosci.* 8:346.

Riggi, N., M.L. Suva, D. Suva, L. Cironi, P. Provero, S. Tercier, J.M. Joseph, J.C. Stehle, K. Baumer, V. Kindler, and I. Stamenkovic. 2008. EWS-FLI-1 expression triggers a Ewing's sarcoma initiation program in primary human mesenchymal stem cells. *Cancer Res.* 68:2176-85.

Rogakou, E.P., D.R. Pilch, A.H. Orr, V.S. Ivanova, and W.M. Bonner. 1998. DNA double-stranded breaks induce histone H2AX phosphorylation on serine 139. *J Biol Chem.* 273:5858-68.

Roseaulin, L., Y. Yamada, Y. Tsutsui, P. Russell, H. Iwasaki, and B. Arcangioli. 2008. Mus81 is essential for sister chromatid recombination at broken replication forks. *Embo j.* 27:1378-87.

Rosen, D.R., T. Siddique, D. Patterson, D.A. Figlewicz, P. Sapp, A. Hentati, D. Donaldson, J. Goto, J.P. O'Regan, H.X. Deng, and et al. 1993. Mutations in Cu/Zn superoxide dismutase gene are associated with familial amyotrophic lateral sclerosis. *Nature.* 362:59-62.

Rossow, K.L., and R. Janknecht. 2001. The Ewing's sarcoma gene product functions as a transcriptional activator. *Cancer Res.* 61:2690-5.

Roussel, P., C. Andre, L. Comai, and D. Hernandez-Verdun. 1996. The rDNA transcription machinery is assembled during mitosis in active NORs and absent in inactive NORs. *J Cell Biol.* 133:235-46.

Rulten, S.L., A. Rotheray, R.L. Green, G.J. Grundy, D.A. Moore, F. Gomez-Herreros, M. Hafezparast, and K.W. Caldecott. 2014. PARP-1 dependent recruitment of the amyotrophic lateral sclerosis-associated protein FUS/TLS to sites of oxidative DNA damage. *Nucleic Acids Res.* 42:307-14.

Salvi, J.S., and K. Mekhail. 2015. R-loops highlight the nucleus in ALS. *Nucleus*:0.

Sarmento, L.M., V. Povoa, R. Nascimento, G. Real, I. Antunes, L.R. Martins, C. Moita, P.M. Alves, M. Abecasis, L.F. Moita, R.M. Parkhouse, J.P. Meijerink, and J.T. Barata. 2014. CHK1 overexpression in T-cell acute lymphoblastic leukemia is essential for proliferation and survival by preventing excessive replication stress. *Oncogene.* 0.

Schoppy, D.W., R.L. Ragland, O. Gilad, N. Shastri, A.A. Peters, M. Murga, O. Fernandez-Capetillo, J.A. Diehl, and E.J. Brown. 2012. Oncogenic stress sensitizes murine cancers to hypomorphic suppression of ATR. *J Clin Invest.* 122:241-52.

Schreiber, V., F. Dantzer, J.C. Ame, and G. de Murcia. 2006. Poly(ADP-ribose): novel functions for an old molecule. *Nat Rev Mol Cell Biol.* 7:517-28.

Schulze, J., A.J. Lopez-Contreras, O. Uluckan, O. Grana-Castro, O. Fernandez-Capetillo, and E.F. Wagner. 2014. Fos-dependent induction of Chk1 protects osteoblasts from replication stress. *Cell Cycle.* 13:1980-6.

Shima, N., A. Alcaraz, I. Liachko, T.R. Buske, C.A. Andrews, R.J. Munroe, S.A. Hartford, B.K. Tye, and J.C. Schimenti. 2007. A viable allele of Mcm4 causes chromosome instability and mammary adenocarcinomas in mice. *Nat Genet*. 39:93-8.

Simandlova, J., J. Zagelbaum, M.J. Payne, W.K. Chu, I. Shevelev, K. Hanada, S. Chatterjee, D.A. Reid, Y. Liu, P. Janscak, E. Rothenberg, and I.D. Hickson. 2013. FBH1 helicase disrupts RAD51 filaments in vitro and modulates homologous recombination in mammalian cells. *J Biol Chem*. 288:34168-80.

Sogo, J.M., M. Lopes, and M. Foiani. 2002. Fork reversal and ssDNA accumulation at stalled replication forks owing to checkpoint defects. *Science*. 297:599-602.

Spahn, L., R. Petermann, C. Siligan, J.A. Schmid, D.N. Aryee, and H. Kovar. 2002. Interaction of the EWS NH2 terminus with BARD1 links the Ewing's sarcoma gene to a common tumor suppressor pathway. *Cancer Res*. 62:4583-7.

Spahn, L., C. Siligan, R. Bachmaier, J.A. Schmid, D.N. Aryee, and H. Kovar. 2003. Homotypic and heterotypic interactions of EWS, FLI1 and their oncogenic fusion protein. *Oncogene*. 22:6819-29.

Sreedharan, J., I.P. Blair, V.B. Tripathi, X. Hu, C. Vance, B. Rogelj, S. Ackerley, J.C. Durnall, K.L. Williams, E. Buratti, F. Baralle, J. de Belleroche, J.D. Mitchell, P.N. Leigh, A. Al-Chalabi, C.C. Miller, G. Nicholson, and C.E. Shaw. 2008. TDP-43 mutations in familial and sporadic amyotrophic lateral sclerosis. *Science*. 319:1668-72.

Srinivasan, S.V., D. Dominguez-Sola, L.C. Wang, O. Hyrien, and J. Gautier. 2013. Cdc45 is a critical effector of myc-dependent DNA replication stress. *Cell Rep*. 3:1629-39.

Stavnezer, J., J.E. Guikema, and C.E. Schrader. 2008. Mechanism and regulation of class switch recombination. *Annu Rev Immunol*. 26:261-92.

Straessler, K.M., K.B. Jones, H. Hu, H. Jin, M. van de Rijn, and M.R. Capecchi. 2013. Modeling clear cell sarcomagenesis in the mouse: cell of origin differentiation state impacts tumor characteristics. *Cancer Cell*. 23:215-27.

Sun, W., A. Lorenz, F. Osman, and M.C. Whitby. 2011. A failure of meiotic chromosome segregation in a fbh1Delta mutant correlates with persistent Rad51-DNA associations. *Nucleic Acids Res*. 39:1718-31.

Svendsen, J.M., A. Smogorzewska, M.E. Sowa, B.C. O'Connell, S.P. Gygi, S.J. Elledge, and J.W. Harper. 2009. Mammalian BTBD12/SLX4 assembles a Holliday junction resolvase and is required for DNA repair. *Cell*. 138:63-77.

Syljuasen, R.G., C.S. Sorensen, L.T. Hansen, K. Fugger, C. Lundin, F. Johansson, T. Helleday, M. Sehested, J. Lukas, and J. Bartek. 2005. Inhibition of human Chk1 causes increased initiation of DNA replication, phosphorylation of ATR targets, and DNA breakage. *Mol Cell Biol*. 25:3553-62.

Takahama, K., K. Kino, S. Arai, R. Kurokawa, and T. Oyoshi. 2011. Identification of Ewing's sarcoma protein as a G-quadruplex DNA- and RNA-binding protein. *FEBS J*. 278:988-98.

Takanashi, K., and A. Yamaguchi. 2014. Aggregation of ALS-linked FUS mutant sequesters RNA binding proteins and impairs RNA granules formation. *Biochem Biophys Res Commun*. 452:600-7.

Thomas, G.R., and D.S. Latchman. 2002. The pro-oncoprotein EWS (Ewing's Sarcoma protein) interacts with the Brn-3a POU transcription factor and inhibits its ability to activate transcription. *Cancer Biol Ther*. 1:428-32.

Thompson, A.D., B.S. Braun, A. Arvand, S.D. Stewart, W.A. May, E. Chen, J. Korenberg, and C. Denny. 1996. EAT-2 is a novel SH2 domain containing protein that is up regulated by Ewing's sarcoma EWS/FLI1 fusion gene. *Oncogene*. 13:2649-58.

Toledo, L.I., M. Murga, R. Zur, R. Soria, A. Rodriguez, S. Martinez, J. Oyarzabal, J. Pastor, J.R. Bischoff, and O. Fernandez-Capetillo. 2011. A cell-based screen identifies ATR

inhibitors with synthetic lethal properties for cancer-associated mutations. *Nat Struct Mol Biol*. 18:721-7.

Tsutsui, Y., Y. Kurokawa, K. Ito, M.S. Siddique, Y. Kawano, F. Yamao, and H. Iwasaki. 2014. Multiple regulation of Rad51-mediated homologous recombination by fission yeast Fbh1. *PLoS Genet*. 10:e1004542.

Tuduri, S., L. Crabbe, C. Conti, H. Tourriere, H. Holtgreve-Grez, A. Jauch, V. Pantesco, J. De Vos, A. Thomas, C. Theillet, Y. Pommier, J. Tazi, A. Coquelle, and P. Pasero. 2009. Topoisomerase I suppresses genomic instability by preventing interference between replication and transcription. *Nat Cell Biol*. 11:1315-24.

Vinsant, S., C. Mansfield, R. Jimenez-Moreno, V. Del Gaizo Moore, M. Yoshikawa, T.G. Hampton, D. Prevette, J. Caress, R.W. Oppenheim, and C. Milligan. 2013. Characterization of early pathogenesis in the SOD1(G93A) mouse model of ALS: part II, results and discussion. *Brain Behav*. 3:431-57.

Wai, D.H., K.L. Schaefer, A. Schramm, E. Korsching, F. Van Valen, T. Ozaki, W. Boecker, L. Schweigerer, B. Dockhorn-Dworniczak, and C. Poremba. 2002. Expression analysis of pediatric solid tumor cell lines using oligonucleotide microarrays. *Int J Oncol*. 20:441-51.

Wang, J., A.R. Haeusler, and E.A. Simko. 2015. Emerging role of RNA*DNA hybrids in C9orf72-linked neurodegeneration. *Cell Cycle*. 14:526-32.

Wang, M., L. Anikin, and D.G. Pestov. 2014. Two orthogonal cleavages separate subunit RNAs in mouse ribosome biogenesis. *Nucleic Acids Res*. 42:11180-91.

Weisenberger, D., and U. Scheer. 1995. A possible mechanism for the inhibition of ribosomal RNA gene transcription during mitosis. *J Cell Biol*. 129:561-75.

West, S.C. 2003. Molecular views of recombination proteins and their control. *Nat Rev Mol Cell Biol*. 4:435-45.

Williams, R.S., J.S. Williams, and J.A. Tainer. 2007. Mre11-Rad50-Nbs1 is a keystone complex connecting DNA repair machinery, double-strand break signaling, and the chromatin template. *Biochem Cell Biol*. 85:509-20.

Wisniewski, J.R., A. Zougman, N. Nagaraj, and M. Mann. 2009. Universal sample preparation method for proteome analysis. *Nat Methods*. 6:359-62.

Wold, M.S. 1997. Replication protein A: a heterotrimeric, single-stranded DNA-binding protein required for eukaryotic DNA metabolism. *Annu Rev Biochem*. 66:61-92.

Wong, P.C., C.A. Pardo, D.R. Borchelt, M.K. Lee, N.G. Copeland, N.A. Jenkins, S.S. Sisodia, D.W. Cleveland, and D.L. Price. 1995. An adverse property of a familial ALS-linked SOD1 mutation causes motor neuron disease characterized by vacuolar degeneration of mitochondria. *Neuron*. 14:1105-16.

Wongsurawat, T., P. Jenjaroenpun, C.K. Kwoh, and V. Kuznetsov. 2012. Quantitative model of R-loop forming structures reveals a novel level of RNA-DNA interactome complexity. *Nucleic Acids Res*. 40:e16.

Wu, L.C., Z.W. Wang, J.T. Tsan, M.A. Spillman, A. Phung, X.L. Xu, M.C. Yang, L.Y. Hwang, A.M. Bowcock, and R. Baer. 1996. Identification of a RING protein that can interact in vivo with the BRCA1 gene product. *Nat Genet*. 14:430-40.

Xu, B., and D.A. Clayton. 1996. RNA-DNA hybrid formation at the human mitochondrial heavy-strand origin ceases at replication start sites: an implication for RNA-DNA hybrids serving as primers. *Embo j*. 15:3135-43.

Xu, X., K.U. Wagner, D. Larson, Z. Weaver, C. Li, T. Ried, L. Hennighausen, A. Wynshaw-Boris, and C.X. Deng. 1999. Conditional mutation of Brca1 in mammary epithelial cells results in blunted ductal morphogenesis and tumour formation. *Nat Genet*. 22:37-43.

Yang, L., H.A. Chansky, and D.D. Hickstein. 2000. EWS.Fli-1 fusion protein interacts with hyperphosphorylated RNA polymerase II and interferes with serine-arginine protein-mediated RNA splicing. *J Biol Chem*. 275:37612-8.

You, Z., and J.M. Bailis. 2010. DNA damage and decisions: CtIP coordinates DNA repair and cell cycle checkpoints. *Trends Cell Biol.* 20:402-9.

Yuce, O., and S.C. West. 2013. Senataxin, defective in the neurodegenerative disorder ataxia with oculomotor apraxia 2, lies at the interface of transcription and the DNA damage response. *Mol Cell Biol.* 33:406-17.

Yun, M.H., and K. Hiom. 2009. CtIP-BRCA1 modulates the choice of DNA double-strand-break repair pathway throughout the cell cycle. *Nature.* 459:460-3.

Zeman, M.K., and K.A. Cimprich. 2014. Causes and consequences of replication stress. *Nat Cell Biol.* 16:2-9.

Zou, L., and S.J. Elledge. 2003. Sensing DNA damage through ATRIP recognition of RPA-ssDNA complexes. *Science.* 300:1542-8.

Zucman, J., O. Delattre, C. Desmaze, A.L. Epstein, G. Stenman, F. Speleman, C.D. Fletchers, A. Aurias, and G. Thomas. 1993. EWS and ATF-1 gene fusion induced by t(12;22) translocation in malignant melanoma of soft parts. *Nat Genet.* 4:341-5.